

## Abstract

Plastic deformations and fragmentation of deformed actin and cofilactin filaments

Anthony Christopher Schramm

2019

The assembly of actin filaments generates forces that are necessary for cell movement. Actin filaments must be mechanically stable in order to sustain these forces. However, filaments must also be broken down and recycled in order to maintain a population of monomers available for continued actin polymerization and network restructuring. The interplay between force and actin severing proteins such as cofilin accelerates the disassembly of actin filament structures and networks. In this dissertation, a mesoscopic length-scale model is presented to determine how cofilin-mediated mechanical and structural changes affect fragmentation and the development of strain within actin filaments. Modeled filaments are shown to have similar bending and twisting rigidities to *in vitro* measurements, and they fragment at comparable bending angles. It is shown that the incorporation of structural weaknesses at actin-cofilactin boundaries invokes greater localization of strain at these boundaries than previous continuum-mechanics studies. Filament twist is predicted to have a large effect on cofilin occupancy due to an accumulation of strain in cofilin-actin bonds, but bending is unlikely to have a large effect. Bending and twisting (but not extending) actin filaments imparts an uneven distribution of strain on protein interfaces, which leads to partial interface rupture prior to complete filament fragmentation. These results suggest a common mechanism of fragmentation where partial interface disruption at the D-loop can facilitate filament fragmentation.

Plastic deformations and fragmentation of deformed actin and cofilactin filaments

A Dissertation  
Presented to the Faculty of the Graduate School  
of  
Yale University  
in Candidacy for the Degree of  
Doctor of Philosophy

by  
Anthony Christopher Schramm

Dissertation Director: Enrique M. De La Cruz

December 2019

© 2019 by Anthony Christopher Schramm

All rights reserved.

# Contents

Acknowledgements.....	vi
Chapter 1: Introduction.....	1
1.1 Structure and properties of actin.....	1
1.2 Regulation of actin filament assembly.....	5
1.3 Regulation of actin filament disassembly.....	7
1.4 Cofilin-mediated actin filament severing.....	9
1.5 Forces on actin filaments.....	12
1.6 Overview.....	19
Chapter 2: Mesoscopic Model of Actin and Cofilactin Filaments.....	20
2.1 INTRODUCTION.....	20
2.2 MODEL CONSTRUCTION.....	22
Application of external load.....	28
Severing parameters and transition state energies.....	29
Implementation of filament fragmentation.....	32
Summary of simulation flow.....	36
2.3 FILAMENT MECHANICAL PROPERTIES.....	39
Chapter 3: The Effect of Cofilin on Strained Actin Filaments.....	42
3.1 INTRODUCTION.....	43
3.2 RESULTS.....	44
Strain energy of buckled filaments.....	44
Strain energy of twisted filaments.....	46
Strain energy of partially decorated filaments.....	48
Fragmentation of buckled filaments.....	51
3.3 DISCUSSION.....	53
Filament severing mechanisms.....	53
Influence of filament shape deformations on cofilin binding.....	54
Limitations of the model and analysis.....	56
Chapter 4: Fragmentation of Actin Filaments Under Strain.....	58
4.1 INTRODUCTION.....	59
4.2 RESULTS.....	61
Fragmentation of compressed/bent filaments.....	61
Fragmentation of extended and twisted filaments.....	67
Critical bending angle of filament fragmentation.....	74

4.3 DISCUSSION .....	76
Filament fragmentation angles .....	76
Actin-cofilactin boundaries are brittle and fragment at low bending angles .....	77
Plastic deformation precedes fragmentation of compressed filaments .....	78
High filament curvature partially disrupts long-axis actin subunit contacts and could potentially enhance cofilin binding kinetics .....	80
Partial rupture of protein interfaces may be a general mechanism to disrupt stable protein-protein interactions.....	82
Effect of filament length .....	83
Effect of bond density .....	83
Effect of actin-cofilactin boundary placement.....	90
Effect of cofilin gap size .....	90
CHAPTER 5: Summary and Conclusions .....	92
REFERENCES .....	97

## Acknowledgements

I am incredibly grateful for my time at Yale. This opportunity has given me the time and space for professional and personal growth. I met a lot of friends that I will have for life, and I will never forget my experiences here.

It was wonderful working with all of the members of the De La Cruz lab. My conversations with these people ranged from sarcastic, and often pointless, arguments over coffee, to genuine and enlightening discussions about scientific concepts. These people kept me coming back day after day.

Jean-Louis Martiel was completely instrumental to all of this work. He provided the initial framework for the computational model and continued to work with me to make improvements to the code and provide feedback.

The members of my thesis committee, Julien Berro, Paul Forscher, and Charles Sindelar, always made themselves available for questions, and they have sparked numerous discussions both within and outside my committee meetings. These conversations led to many new experiments, and their enthusiasm for all of the minutia of my work helped me craft concise, clear arguments.

I would like to thank my advisor, Enrique De La Cruz for his support throughout my PhD. His understanding of my needs as a student and as a person were unmatched. His flexibility allowed me to finish what I started.

I would also like to thank my family. They have crafted who am I as a person. My parents have supported me throughout all of my education and I have no doubt that without them, I would not be where I am today. My fiancée, Alona, has supported me

through the last years of my time at Yale and continues to do so, and for that I am very grateful.

# Chapter 1: Introduction

## 1.1 Structure and properties of actin

The protein actin is a critical component in a plethora of cellular processes, including cytokinesis, cell motility, cytokinesis, cargo trafficking, cellular adhesion, and cell shape maintenance (Rottner, Faix, Bogdan, Linder, & Kerkhoff, 2017). Accordingly, it is one of the most common proteins in eukaryotic organisms and is highly conserved across species (Dominguez & Holmes, 2011). The actin cytoskeleton is dynamic and is constantly regulated by a host of accessory proteins. Broadly, these proteins include myosin, which exerts forces on actin filaments, proteins that control the assembly of actin filaments and structures, and other proteins which act to break down filaments (Pollard, 2016).

The actin monomer is a 42 kDa globular protein, and has 4 subdomains (Figure 1.1A). Actin monomers polymerize into double-stranded, polarized helical filaments, and these filaments are a crucial part of the cytoskeleton (Huxley, 1963). The filaments are right-handed, with a helical pitch of 72 nm over 26 subunits. The kinetics of assembly and disassembly at the barbed end are 1-2 orders of magnitude higher than at the pointed end (Fujiwara, Vavylonis, & Pollard, 2007). Actin can polymerize spontaneously after reaching a critical nucleus size of three to four subunits, but this nucleation step is much slower than the elongation of existing filaments (Cooper, Walker, & Pollard, 1983).

Actin binds ATP in a cleft between subdomains 2 and 3. The nucleotide state of actin (ATP, ADP-Pi, or ADP-bound) strongly influences the on/off-rates of subunits to the ends of filaments, with the affinity of ATP actin being higher than that of ADP-bound

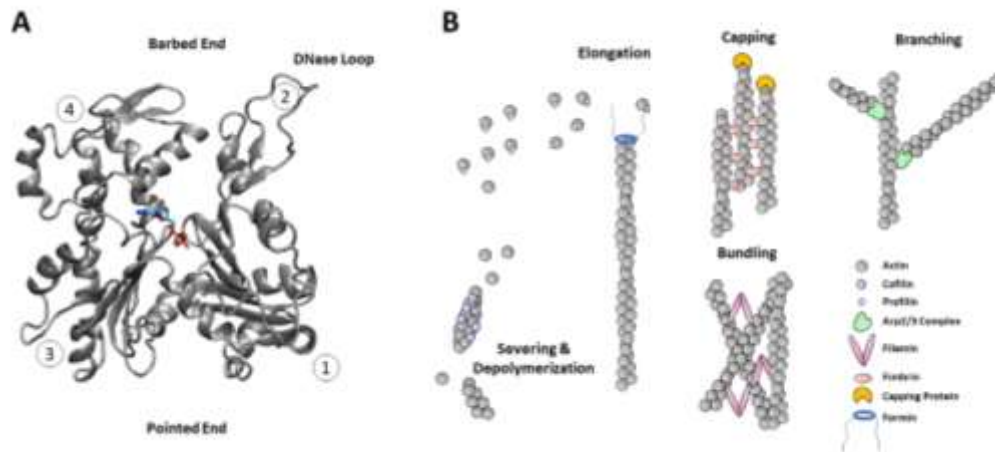


FIGURE 1.1 The structure and functions of actin. A) Ribbon structure of an actin molecule showing the locations of subdomains 1, 2, 3, and 4. The ATP nucleotide, barbed and pointed ends, and DNase loop are also labeled. B) Some of the actin structures of actin and various actin binding proteins that participate in these functions and structures.

actin (Fujiwara et al., 2007). Actin is an intrinsic ATPase, and the rate of ATP hydrolysis in monomeric form is slow ( $7 \times 10^{-6} \text{ sec}^{-1}$ ) (Rould, Wan, Joel, Lowey, & Trybus, 2006). However, upon polymerization the rate of hydrolysis accelerates by four orders of magnitude to  $0.3 \text{ sec}^{-1}$  (Blanchoin & Pollard, 2002). ADP and inorganic phosphate remain bound and the subsequent phosphate release is much slower than hydrolysis, with a 6-minute half-time. ADP-actin depolymerizes faster than ADP-Pi or ATP-actin (Carrier & Pantaloni, 1986). In most near-physiological conditions these processes lead to filaments with a short ATP-actin cap on barbed ends, with a significant stretch of ADP-Pi actin, and ADP-actin pointed ends (Vavylonis, Yang, & O'Shaughnessy, 2005). In the presence of ATP, the depolymerized subunits exchange to ATP actin and are able to rebind actin filaments. At certain solution concentrations of actin (between the critical concentrations of barbed and pointed ends) this can lead to a process called treadmilling, where the ATP-actin is incorporated with the barbed end at the same rate as ADP-actin is depolymerizing from the pointed end (Wegner, 1976). The differential between ATP- and ADP- affinity for filament ends is one means of producing mechanical work from the chemical energy of ATP hydrolysis (Mogilner & Oster, 2003).

Solution salts have been shown to greatly influence the polymerization and mechanical properties of actin filaments. Salt lowers the critical concentration ( $C_c$ ) of actin filaments, which is due to both specific binding sites (Frieden, 1983) and charge screening behavior for actin monomers (Rouayrenc & Travers, 1981). There are both high- and low-affinity binding sites present within filaments. A tightly bound divalent cation ( $\text{Mg}^{2+}$  or  $\text{Ca}^{2+}$ ) is required for the binding and hydrolysis of the bound ATP molecule to actin monomers. Additionally, there exists another high affinity binding site

within actin filaments between adjacent subunits deemed the “polymerization site” (Kang et al., 2012). Mutation of a coordinating residue in this latter site greatly increases the critical concentration of actin filaments for yeast actin (Kang et al., 2012). Divalent cation binding can affect filament aggregation, likely due to both screening of the negative surface charges on actin filaments (Tang & Janmey, 1996) as well as specific binding sites on the sides of filaments (Castaneda et al., 2018).

One low-affinity cation binding site of structural importance has been deemed the “stiffness site” due to its role in modulating actin filament mechanics (Kang et al., 2012). The “stiffness” site is located between subdomain 2 and subdomain 1 of the adjacent subunit, and coordinated by acidic residues on both subunits. Increasing the concentration of solution ions increases the stiffness of mammalian skeletal actin filaments and the effect of different ions suggests that  $Mg^{2+}$  is the physiologically relevant cation bound to this site. Molecular dynamics modeling suggests that this cation is coordinated by residues on both subunits. This interaction likely stabilizes interactions of the DNase I binding loop (D-loop) with the adjacent subunit. While this binding site is present in mammalian skeletal actin, it is missing in yeast actin, which may be why the yeast actin filament is more flexible. The flexibility of yeast actin filaments does not have a large dependence on the concentration of magnesium ions. However, conferring the proposed stiffness site by the A167E mutation in yeast actin introduces a correlation between salt concentration and filament stiffness. This mutation also allows human cofilin 1 to rescue a yeast cofilin knockout mutation (Kang et al., 2014).

## 1.2 Regulation of actin filament assembly

Actin assembly must be regulated to prevent the spontaneous formation of unproductive filaments and to form the structures necessary to carry out the roles I have discussed in the preceding section. A variety of structures and functions requires a variety of actin binding partners (Figure 1.1B). Here I discuss the means of controlling the monomeric actin population, the actin nucleators, and the actin crosslinkers required for these processes in more detail.

A pool of actin monomers must be present to allow for immediate polymerization where necessary. Profilin binds the majority of monomeric actin in cells. Profilin binding does not prevent elongation of barbed ends, but it prevents the spontaneous nucleation of new filaments due to steric clashes of profilin-bound actin (Courtemanche & Pollard, 2013). Profilin binding is also able to increase the exchange of ADP for ATP in actin monomers (Witke, 2004). This is necessary for making the monomers fully available for polymerization. Capping protein also works to control filament growth by binding the more dynamic barbed end of filaments to prevent addition of subunits to the ends of filaments (Wear, Yamashita, Kim, Maeda, & Cooper, 2003). The location of actin polymerization can be controlled by spatially localizing where capping protein is or is not bound.

Filaments are often organized into higher-order assemblies of bundles and crosslinked networks, which diversifies the roles it can play. Broadly, these structures take the form of actin bundles or branched/crosslinked actin networks, and many consist of a combination of both. Actin filaments are rigid on the sub-micron length scale, but filament bundles are more mechanically stable and can maintain structural rigidity over

the entire length of a cell. Filopodia, for example, use bundled actin filaments to sense the environment at long distances from the cell (Mattila & Lappalainen, 2008). Branched and crosslinked actin networks can widely spread actin filament ends, which can be useful for spreading the force of polymerization over a large area of the cell membrane, or to rigidify a meshwork of filaments. The architecture of these structures is critical to carry out actin's many functions, so the cell has many ways of controlling the spatial and temporal organization of assemblies.

Nucleation of new filaments is controlled by other accessory proteins. The formin family of proteins nucleates actin filaments by staying associated with the barbed end of actin filaments during filament growth (Breitsprecher & Goode, 2013). While in most conditions this does not accelerate the filament growth rate, it both localizes the location of filament growth (if formin is localized) and prevents the capping protein binding (Mizuno & Watanabe, 2012). The Arp2/3 complex nucleates new actin filaments from the side of existing filaments, creating new filaments that grow at angles to the original filaments. Arp2/3 complex binding is controlled by filament shape and additional activators (Risca et al., 2012).

Actin crosslinkers join existing filaments together to form larger networks. The geometry and binding properties of crosslinkers can control the organization of actin filaments. Proteins such as fascin organize filaments into polar, parallel bundles, such as those found in filopodia (Vignjevic et al., 2006). Filopodia are narrow extensions extending past lamellipodia, and are involved in chemotropic sensing and cell movement (Mattila & Lappalainen, 2008). Bundling filaments in this context increases the rigidity of these structures and coordinates the formin-mediated polymerization direction at the

filopodial tip. These structures can maintain a coherent direction for much longer than the persistence length of individual filaments. Fimbrin is another actin bundling protein that creates very compact, parallel bundles (Bretscher, 1981). Alpha-actinin also bundles actin filaments and is unique in the fact that it contains a single actin binding domain and must dimerize to efficiently bundle actin. It plays a critical role in the actin organization within skeletal muscle cells (Sjoblom, Salmazo, & Djinovic-Carugo, 2008). Other proteins such as filamin organize the cytoskeleton into orthogonal networks, which can form a network that protects the cell from shear forces (Razinia, Makela, Ylanne, & Calderwood, 2012).

### 1.3 Regulation of actin filament disassembly

Actin filaments must be recycled in order to maintain a pool of actin monomer available for further polymerization. This process involves a combination of removing crosslinkers, severing, and depolymerizing filaments. All three processes must occur in tandem in order to facilitate the fast turnover of actin filament structures seen *in vivo*.

Glia maturation factor (GMF) is a member of the ADF-H family of proteins. The primary role of GMF is thought to be the removal of the Arp2/3 complex and the associated daughter filament from the mother filament. GMF binds directly to the Arp2/3 complex, which can both prevent the nucleation facilitate the removal of branched actin filaments (Boczkowska, Rebowski, & Dominguez, 2013). This role is further supported by studies of Gmf1 in budding yeast, which show that Gmf1 localizes to endocytic patches (Goode, Eskin, & Wendland, 2015). Additionally, deletion of the GMF1 gene prolongs the lifetime of these patches (Gandhi et al., 2010).

Gelsolin is 6-domain protein that has a  $\text{Ca}^{2+}$ -dependent severing mechanism. Gelsolin tightly binds actin filaments, which disrupts hydrophobic contacts of adjacent monomers.

a very efficient severer, and requires  $\text{Ca}^{2+}$  to bind, sever, and cap actin filaments. Upon severing the filament, gelsolin also remains bound to the barbed end, preventing further polymerization of filaments (McGough, Chiu, & Way, 1998). Interactions between gelsolin-capped actin filaments and phosphoinositides have been shown to reverse gelsolin capping, suggesting that interactions with the cell membrane can play a critical role in the reversal of this mechanism (Janmey & Stossel, 1989).

The MICAL family of Redox enzymes destabilize actin enzymatically. Mical uses NADPH cofactor to stereospecifically oxidize residues M44 and M47 of actin, but only in polymerized form (Hung, Pak, & Terman, 2011). Oxidized actin monomers are less able to form filaments, and any filaments that are formed undergo accelerated depolymerization (Grintsevich et al., 2017). These residues are in the D-loop of actin, and this oxidation changes methionine from a hydrophobic to hydrophilic residue, disrupting the existing contacts between the D-loop and subdomain 1 of adjacent monomers (Grintsevich et al., 2017). The oxidation of monomers can be reversed by methionine-R-sulfoxide reductase B1 (MsrB1) to reverse the effects of Mical (Lee et al., 2013).

The ADF/cofilin family of proteins can either depolymerize or fragment actin filaments, depending on the isoform and solution pH. Unicellular organisms typically have one isoform of this family, while multicellular organisms often express several. In mammals, there are three isoforms: cofilin 1, cofilin 2, and actin depolymerizing factor (ADF) (Bamburg, McGough, & Ono, 1999). These isoforms are differentially expressed across cell types.

## 1.4 Cofilin-mediated actin filament severing

Cofilin binding leads to a filament that is more compliant in bending and twisting (McCullough, Blanchoin, Martiel, & De la Cruz, 2008). Additionally, cofilin binding changes the twist of filamentous actin from -169 degrees/subunit to -162 degrees/subunit, resulting in a filament that appears more twisted (McGough, Pope, Chiu, & Weeds, 1997). It also changes the tilt between the inner and outer domains of actin monomers within the filament, making the configuration more similar to G-actin. For human, cofilin, where the stiffness site is predicted to exist (Kang et al., 2012), binding is coupled with the release of a single cation (Kang et al., 2014). In this case, it is likely that the change in mechanical properties is due to the release of the stiffness cation and the associated configurational changes to the D-loop of subdomain 2.

Molecular dynamics simulations have shown similar changes in actin-actin contacts upon cofilin binding. The comparison of MD simulations between bare actin and cofilin-decorated actin shows how long-axis actin-actin contacts redistribute upon cofilin binding. Not only are there fewer contacts overall for the cofilactin filament, but the contacts distribute more towards the filament central axis (Fan et al., 2013). Molecularly, this results from cofilin restructuring the D-loop so that it no longer makes contacts with the adjacent subunit. These simulations show that cofilin decreases the persistence length of actin filaments from 9.0  $\mu\text{m}$  to 2.2  $\mu\text{m}$ . These structural changes have recently been confirmed by recent cryo-EM structural analysis (Tanaka et al., 2018).

Cofilin binds actin filaments cooperatively, meaning cofilin is more likely to bind near existing bound cofilin than elsewhere on the actin filament. This interaction has been modeled as binding to a one-dimensional lattice with nearest-neighbor cooperativity.

Traditionally, this approach has been used to describe DNA binding (McGhee & von Hippel, 1974), but unlike most of these cases where cooperativity arises from ligand-ligand interactions (Lohman & Mascotti, 1992), cofilin binding cooperativity arises through structural changes in actin, since bound cofilin molecules do not contact each other (V. E. Galkin et al., 2011).

The exact extent of cooperativity is not entirely clear, and some confusion is brought about by the use of different cofilin isoforms. The proposed distance over which cofilin binding is enhanced adjacent to existing cofilin clusters ranges from 2 nm (only the adjacent site) (De La Cruz & Sept, 2010) to more than 65 nm (24 subunits) (Hayakawa, Sakakibara, Sokabe, & Tatsumi, 2014). The degree of cooperativity also varies widely, from 2.3 (Hayakawa et al., 2014) to several orders of magnitude higher than this (Wioland et al., 2017).

Cofilin severs actin filaments at boundaries between bare and cofilin decorated actin. It has been shown that equilibrium filament lengths are at a minimum at half binding density, further suggesting that fragmentation scales with the number of boundaries (which are maximal at half occupancy) (McCullough et al., 2011). Furthermore, preferential severing at actin-cofilactin boundaries has been observed *in vitro* experiments for freely fluctuating actin filaments (McCullough et al., 2011; Suarez et al., 2011).

One proposed reason for boundary fragmentation is due to structural weaknesses at actin-cofilactin boundaries. It has been proposed that cooperative binding originates from propagation of a cofilactin-like structure into the bare region adjacent to bound cofilin (Umeki, Hirose, & Uyeda, 2016). Structural data shows that these structural changes only

propagate a few subunits into the bare region (Huehn et al., 2018). If the same actin-actin longitudinal contacts are lost at the boundary as are lost within cofilactin, but without the extra stability of cofilin-actin contacts, this could explain why fragmentation occurs most frequently at or near boundaries. Aip1 has been shown to enhance cofilin-mediated fragmentation, but whether this is simply because it increases the number of boundaries is unknown (Chen, Courtemanche, & Pollard, 2015).

The structural and mechanical changes that cofilin binding imparts plays a role in its severing mechanism. A partially decorated filament will have regions of bare actin and regions of cofilin-decorated actin. The filament will thus be mechanically heterogenous due to cofilin's effect on filament mechanics. In other words, portions of the filament will be five times more flexible than others (McCullough et al., 2008). Continuum mechanics simulations of partially-decorated filaments show that these discontinuities in filament mechanics lead to localization of strain energy at the boundaries of these regions (De La Cruz, Martiel, & Blanchoin, 2015).

The purpose and advantage of cooperativity for the function of cofilin is not fully understood. Higher levels of cooperativity decrease the number of actin-cofilactin boundaries (Elam et al., 2017). For this reason, a cooperative cofilin should decrease the rate of severing, all else being equal. Some groups have shown evidence that there is a minimum cofilin cluster size for fragmentation (Gressin, Guillotin, Guerin, Blanchoin, & Michelot, 2015), which would give a possible benefit for high cooperativity in the limit of low cofilin concentration. Aip1 can also act to fragment fully cofilin-decorated filaments, so in this case high cooperativity would be less detrimental (Chen et al., 2015).

Of course, cofilin binding must be regulated to ensure that it severs filaments only where it is required. Cofilin senses the nucleotide state of actin, and preferentially binds ADP-actin filaments over ATP or ADP-P<sub>i</sub> filaments (Blanchoin & Pollard, 1999). While ATP hydrolysis is fast, phosphate release is slow, and inhibits cofilin binding (Muhlrad, Pavlov, Peyser, & Reisler, 2006). However, cofilin binding allosterically increases rate of phosphate release up to ten subunits away (Prochniewicz, Janson, Thomas, & De La Cruz, 2005; Suarez et al., 2011). Because of the different binding kinetics of each end, this has the effect of severing and depolymerizing the older filament segments towards the pointed end and preserving newly polymerized filaments.

Cofilin is phosphorylated at serine 3 by LIM-kinase 1 (Yang et al., 1998) and LIM-kinase 2 via the Rac-LIMK1-cofilin and Rho/Cdc42-LIMK2-cofilin pathways. Phosphorylation has been shown to inhibit cofilin (and other ADF family proteins) binding to actin filaments (Agnew, Minamide, & Bamburg, 1995; Arber et al., 1998; Moriyama, Iida, & Yahara, 1996). The phosphomimetic mutation of serine 3 to aspartic acid (S3D) has been used to measure the effects of cofilin phosphorylation, but the extent to which this approximates actual phospho-cofilin are unknown (Pope, Gonsior, Yeoh, McGough, & Weeds, 2000).

## 1.5 Forces on actin filaments

It is important to understand how filaments respond to all of the forces they are subject to in cells, and how their response changes when part of bundles or networks. Actin filaments buckle or bend in response to compressive or oblique forces. These forces may arise from thermal motion, the collective action of myosin motors, or from the force of polymerization against cellular structures.

To get an understanding of how actin filaments react to forces, it is informative to first approximate the filaments as rigid rods. The torque ( $F \cdot X$ ), or bending moment  $M$ , required to bend a slender rod (with width much smaller than its length) is:

$$M = EI \frac{1}{R} \quad (1.1)$$

where  $R$  is the resulting radius of curvature and  $EI$  is the flexural rigidity (Landau, Lifshits, Kosevich, & Pitaevskiĭ, 1986). The flexural rigidity is the product of the Young's modulus,  $E$ , and the second moment of inertia of the filament cross-section,  $I$ . The Young's modulus is determined only by the material properties, but the second moment of inertia is dictated by the rod cross-section (circular, ellipsoidal, etc.). Actin can be considered to have a mostly circular cross-section, but a slightly ellipsoidal shape (McCullough et al., 2008) may have implications in the development of strain within bent filaments.

The beam equation described above can be applied to determine the torque required to bend a filament to a particular shape. The filament can be broken up into short segments where Equation 1.2 holds.

$$\frac{d\theta}{ds}(s) = \frac{1}{EI} M(s) \quad (1.2)$$

If the tangent angle is small, Equation 1.1 simplifies to:

$$\frac{d^2y}{dx^2} = \frac{M(x)}{EI} \quad (1.3)$$

This equation can then be applied to various boundary conditions. For the experiments carried out in this dissertation, the most relevant boundary conditions are cantilever

bending, and the buckling force for filament compression with freely-rotating or fixed-angle ends (Figure 1.2).

The force required to impose cantilever bending on a rigid rod can be used to relate the stiffness of the rod to the force required to bend it. This can be used to calculate the stiffness of simulated actin filaments.

The most commonly reported metric to measure the stiffness of biological filaments is the persistence length. The persistence length can be thought of as the distance over which the filament behaves as a rigid rod. The persistence length of a filament that is bending in two dimensions can be measured by the cosine correlation function,

$$\langle \cos[\theta(s) - \theta(0)] \rangle = \exp\left(\frac{-s}{L_p}\right) \quad (1.4)$$

which describes how the average cosine of the difference in tangent angle between two points a distance  $s$  apart decays, and how that depends on the persistence length  $L_p$  of the filament (Howard, 2001). Intuitively, the persistence length of a filament is related to its flexural rigidity (a stiffer filament will have a longer persistence length). Using the Principle of Equipartition of Energy, it can be shown that this relation is:

$$L_p = \frac{EI}{k_B T} \quad (1.5)$$

where  $k_B$  is Boltzmann's constant and  $T$  is the temperature in Kelvin (Howard, 2001).

Bare actin filaments have a bending persistence length of 9.8  $\mu\text{m}$  (McCullough et al., 2008), but this reported number can vary by a factor of 2-3 depending on whether the filament is bound by the actin-stabilizing peptide phalloidin (Isambert et al., 1995). This means that unlike microtubules, which have a persistence length of 5200  $\mu\text{m}$ , actin

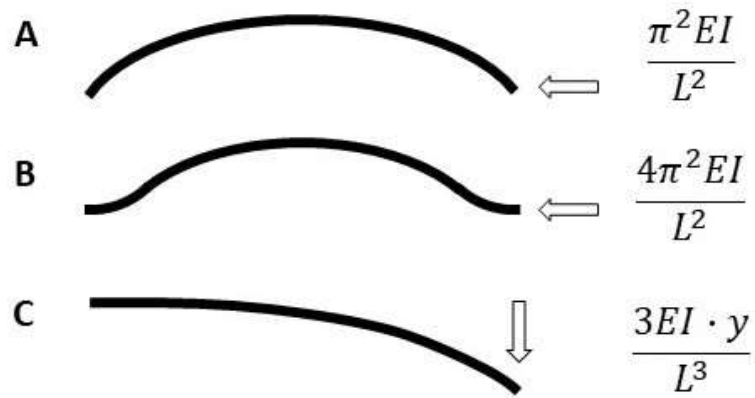


FIGURE 1.2 Forces required to deform rigid rods. A) Buckling shape and force for a rod with freely-rotating ends. B) Buckling shape and force for a rod with fixed-angle ends. C) Force required to bend filaments at small deflections.  $E$  is the Young's modulus,  $I$  is the second moment of inertia,  $L$  is the filament contour length,  $y$  is the deflection distance. Note that the buckling force is the force required to buckle filaments from straight to buckled, and is only applicable to the moment of buckling.

filaments are not completely rigid over the length scale of the cell (Gittes, Mickey, Nettleton, & Howard, 1993).

Actin is even more flexible in twisting than in bending, with a twisting persistence length of 0.15 to 0.4  $\mu\text{m}$  (Prochniewicz et al., 2005). Thus, even though torsional stresses of the filament are less obvious and apparent, it becomes important to understand how torsional strain affects actin filaments and ABPs. The torsional rigidity has been measured in several ways, and the result differs greatly. For one experiment, filaments were attached to a fluorescently labeled bead, and the variance in the rotation angle of the bead was measured. The authors found a torsional rigidity ( $\kappa$ ) of  $(8.0 \pm 1.2) \times 10^{-26} \text{ Nm}^2$  (Tsuda, Yasutake, Ishijima, & Yanagida, 1996). A second method labeled actin filaments with a phosphorescent marker to measure the transient phosphorescence anisotropy of filaments. These authors reported a torsional rigidity of  $2.3 \times 10^{-27} \text{ Nm}^2$  (Prochniewicz et al., 2005). Due to the helicity of actin filaments, the bending of a filament also induces a slight twist, and vice versa (De La Cruz, Roland, McCullough, Blanchoin, & Martiel, 2010). While these values vary by an order of magnitude, it is clear that actin filaments are much more flexible in twisting than bending.

Actin filaments appear to be resistant to fragmentation by tension. Long actin filaments *in vitro* respond to tension as an entropic spring (De La Cruz & Gardel, 2015). Accordingly, filament tension changes filament shape, as the mean end-to-end length increases. However, the force required to rupture a single actin filament has been reported to be  $\sim 400 \text{ pN}$  (Tsuda et al., 1996).

There is plenty of evidence suggesting that many actin interactions are force sensitive *in vivo*. Aside from the force-dependent interactions that are described above, forces have

also been shown to play a role in the regulation of actin assemblies *in vivo*. For example, the inhibition of myosin II by blebbistatin in the growth cone-like *Aplysia* bag cell neuron decreases the effectiveness of fragmentation and recycling of actin filament bundles (Medeiros, Burnette, & Forscher, 2006). Treatment of fibroblasts with blebbistatin also alters the concentration of actin at focal adhesions, suggesting that their attachment to integrin is force-sensitive in the cell (Hayakawa, Tatsumi, & Sokabe, 2008).

More quantitative measurements of the effect of force (and filament shape change) on actin-ABP binding interactions have been made, in many cases following the evidence posed by these *in vivo* experiments. The effect of force on these interactions depends on the specific binding protein in question. The Arp2/3 complex, for example, preferentially binds to the outside edge of bent actin filaments (Risca et al., 2012). This is proposed to help maintain a directionality of actin network growth towards the direction of opposing force (the cell membrane). Some proteins, such as vinculin, display catch-bond behavior with actin, which may be due to changes of the actin structure under tension, or possibly changes in the ABP structure (Huang, Bax, Buckley, Weis, & Dunn, 2017). This type of behavior could help reinforce actively loaded focal adhesions. Tension also appears to prevent fragmentation by cofilin (Hayakawa, Tatsumi, & Sokabe, 2011). Torsion generated by formin has been shown to hinder actin filament fragmentation by cofilin (Mizuno, Tanaka, Yamashiro, Narita, & Watanabe, 2018), but the mechanism for this (inhibition of binding or severing) is unknown. This regulation of cofilin severing could be useful in preventing fragmentation of actin filaments in regions of active filament growth. Constraining filaments by crosslinking them or attaching them to the surface, in

contrast, has been shown to enhance severing by cofilin (Wioland, Jegou, & Romet-Lemonne, 2019a).

There have been several experiments to try to link these single-molecule measurements with *in vivo* observations by reconstituting *in vitro* actin assemblies. Many of these experiments involve the creation of branched actin networks capable of exerting force across boundaries. The concentrations of Arp2/3 complex, capping protein, actin, and ADF/cofilin have been shown to have dramatic effects on the properties of these networks (Manhart et al., 2019). Forces resisting the growth of these networks increases their density at the expense of network growth rate, which suggests that these networks self-regulate to adapt to their environment (Bieling et al., 2016).

Studies of purified components are critical for understanding the molecular response of individual proteins. The simplification of these *in vitro* studies makes the determination of fundamental filament properties possible. The forces on actin filaments and the resulting filament shape changes affect the rate of filament fragmentation. The fragmentation rate of freely-fluctuating bare actin filaments has been estimated to be  $7 \times 10^{-7} \text{ s}^{-1}$  (Kinosian, Selden, Estes, & Gershman, 1993). This does not occur randomly, however, but occurs when filaments are sufficiently bent by thermal motion and reach a critical bending curvature (McCullough et al., 2011). Similarly, compression from myosin can accelerate fragmentation of membrane-bound actin filaments (Vogel, Petrusek, Heinemann, & Schwille, 2013).

Computational and mathematical studies of actin have furthered progress in the field by using the parameters found by “wet-lab” studies to make further predictions. Models can bypass the technical limitations of single-molecule experiments by allowing for

measurements that are more precise than experimentally feasible (e.g. due to the diffraction limit of light microscopy experiments) and allowing for the complete control of experimental conditions (e.g. binding properties, protein concentrations, etc.). This control can show how changes in an experimental system can affect measurable quantities and emergent behaviors.

Mathematical models have been used to show how cofilin fragmentation may play a necessary role in the quick disassembly of endocytic patches in fission yeast (Berro, Sirotkin, & Pollard, 2010). Models of individual filaments have made predictions about how mechanical deformations may affect ATP hydrolysis, and how strain can play a role in the cooperativity of ABP binding (Yogurtcu, Kim, & Sun, 2012).

## 1.6 Overview

In chapter 2 I will introduce the model that I have developed in my dissertation use in the subsequent chapters. Chapter 3 discusses which interfaces are most strained under compression or twist. I also discuss how this strain localization is affected by the presence of cofilin and some implications for filament fragmentation. In chapter 4 I discuss how strain localizes within actin-actin interfaces and implement filament fragmentation. In chapter 5 I summarize the results.

## Chapter 2: Mesoscopic Model of Actin and Cofilactin Filaments

### 2.1 INTRODUCTION

Computational models of cellular processes can be invaluable in furthering the progress of a field. The *in silico* approach can be used to make measurements that are technically challenging or otherwise impossible to probe otherwise. The precise control of experimental variables in a computational model can help to determine the sensitivity of an experiment to parameters such as molecular concentration. A precise control of other outside factors can also help to differentiate between signal and noise in a measurement.

Atomistic simulations have been useful in making predictions about actin and actin filament structural features prior to recent advances in structure determinations, and some of these predictions and observations are still yet to be validated. For example, more flexible regions of actin filaments, such as the D-loop, are hard to see in actin filament structures, but molecular dynamics simulations can give a better idea how they interact with the rest of the filament. However, the timescales available to these all-atom approaches still do not allow for the application of force to monitor structural changes for filament rupture in large assemblies of proteins, like actin filaments.

Continuum mechanics approaches have been used with great success, but they lack many molecular details that have been shown to be important at the length scale of individual proteins. Often, continuum mechanics models of actin filaments are used as a part of larger-scale simulations of actin filament networks, where the reduced computational complexity is necessary. Continuum mechanics simulations have been used to predict the acceleration of filament fragmentation due to mechanical

deformations and cofilin decoration, but little can be understood about this process at the interface level.

For these reasons, I have developed a mesoscopic model of actin/cofilin-decorated actin (cofilactin) filaments to study how forces and filament shape deformations can accelerate fragmentation of bare actin or cofilin-mediated fragmentation. This mesoscopic model discards all atomistic information of individual proteins, and instead models each subunit as a rigid body with the rough dimensions of the molecule. Filaments are constructed to match actin and cofilactin filament width, helicity, and rise per molecule according to cryo-electron microscopy derived structures of filaments. Instead of connecting proteins with a single bond that resists extension, twist, and bending, this model has many bonds that connect any two interacting proteins over a defined interface area. Each individual bond is modeled as a harmonic potential that resists extension and compression, but is free to twist or bend. Deformations are applied to any subset of proteins, and the strain energy of bonds after these deformations are analyzed. The simulations are carried out in the absence of thermal motion, both to simplify the computational complexity and to isolate the effects of the deformation itself.

This model fills a gap in the existing exploration of actin filament via computational models. While the number of variables in the simulation is greatly reduced in comparison to all-atom molecular dynamics simulations, it retains a considerable amount of information about the interactions between two proteins. Instead of reducing these interactions to a single bond, spatial information about the interface is retained. The bending and twisting resistance of these interfaces arises from the spring stiffness and contact area of each interface, which better describes the origin of the effect. Lastly, this

method gives more information about the spatial distribution of strain across filaments, and it gives us a more intuitive way to model how these interfaces might break down as they are deformed.

This model is useful for exploring how equilibrium filament shape changes can lead to strain localization at the filament and interface level. I use this information to make predictions about how compressive, torsional, and extensional deformations affect filament fragmentation and the binding stability of actin accessory proteins such as cofilin. I explore how the decoration of cofilin affects this behavior. Lastly, I incorporate partial bond rupture into the model to determine the pathway of actin filament severing for actin, cofilactin, and actin-cofilactin boundaries under different deformations.

## 2.2 MODEL CONSTRUCTION

Proteins are modeled as rigid ellipsoids. Actin and cofilin dimensions and filament helicity were calculated from PDB files 2ZWH (actin; (Oda, Iwasa, Aihara, Maeda, & Narita, 2009)) and 3J0S (cofilactin; (V. E. Galkin et al., 2011)). Protein contact interfaces (filament longitudinal, lateral, cofilin-actin) are defined by a series of elastic bonds (Figure 2.1), which resist compression/extension, but bend and rotate freely.

These elastic bonds have a constant resting length and stiffness values obtained from MD model parameters (Table 2.1), as follows. Periodic structures of actin filaments were constructed and simulated as described (Fan et al., 2013) using the molecular dynamics code NAMD (Phillips et al., 2005). Actin subunits contained bound ADP for both bare and cofilactin (cofilin-decorated actin) structures. The systems were allowed to relax for 75 ns (actin) or 175 ns (cofilactin) until the RMSD (root mean squared deviation

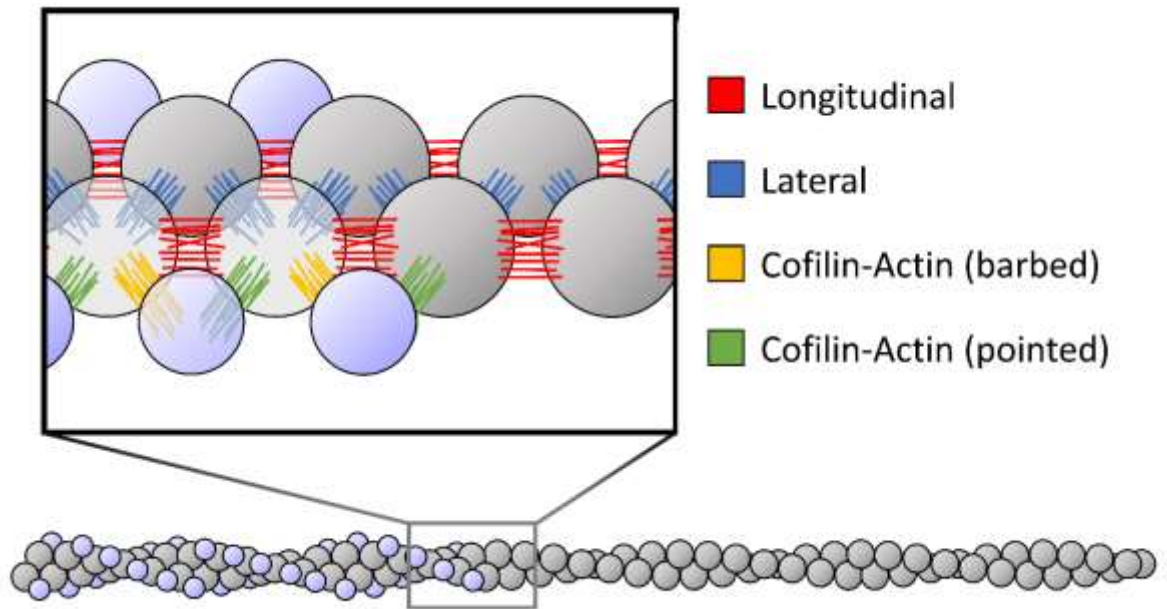


FIGURE 2.1 Cofilactin filament model. A) Actin (grey) and cofilin (blue) are modeled as rigid ellipsoids with interface types distinguished by color. B) Schematic of cantilever bending used to measure bending rigidity ( $L_B$ ). C) Schematic of filament end twisting used to measure  $C_{fil}$ . D) Single subunit twisting used to measure  $C_{sub}$ . Subunits held in their initial, resting positions and orientations are colored red. The external force (direction depicted by orange arrows) is applied to proteins colored blue.

**TABLE 2.1 Model filament parameters**

<b>Actin filament</b>	<b>Value</b>
Filament period	71.2 nm <sup>a</sup>
Number of actin subunits in one period	26 <sup>a</sup>
Rotation per subunit	166.1° <sup>a</sup>
Rise per actin subunit (same strand)	5.52 nm <sup>a</sup>
Actin filament interaction radius	1.8 nm <sup>a</sup>
Actin subunit dimensions	5.1 x 5.1 x 3.3 nm <sup>a</sup>
Actin-actin longitudinal interface stiffness	582 k <sub>B</sub> T/nm <sup>2 a</sup>
Actin-actin lateral interface stiffness	392 k <sub>B</sub> T/nm <sup>2 a</sup>
Actin-actin longitudinal interface area	11.2 nm <sup>2 a,c</sup>
Actin-actin lateral interface area	3.9 nm <sup>2 a,c</sup>
Bond density	12 bonds/nm <sup>2</sup>
<b>Cofilactin filament</b>	
Filament period	55.2 nm <sup>b</sup>
Number of actin subunits in one period	20.1 <sup>b</sup>
Rotation per subunit	162.1° <sup>b</sup>
Rise per actin subunit (same strand)	5.49 nm <sup>b</sup>
Actin filament interaction radius	1.7 nm <sup>b</sup>
Cofilin radius (distance from filament centerline)	3.7 nm <sup>b</sup>
Actin subunit dimensions	5.1 x 5.1 x 3.3 nm <sup>a</sup>
Cofilin subunit dimensions	3.1 x 3.3 x 1.8 nm <sup>b</sup>
Actin-actin longitudinal interface stiffness	169 k <sub>B</sub> T/nm <sup>2 b</sup>
Actin-actin lateral interface stiffness	429 k <sub>B</sub> T/nm <sup>2 b</sup>
Actin-actin longitudinal interface area	4.3 nm <sup>2 b,c</sup>
Actin-actin lateral interface area	3.7 nm <sup>2 b,c</sup>
Actin-cofilin interface stiffness, towards pointed end	157 k <sub>B</sub> T/nm <sup>2 b</sup>
Actin-cofilin interface stiffness, towards barbed end	204 k <sub>B</sub> T/nm <sup>2 b</sup>
Actin-cofilin interface area, towards pointed end	10.3 nm <sup>2 b,c</sup>
Actin-cofilin interface area, towards barbed end	7.4 nm <sup>2 b,c</sup>
Bond density	12 bonds/nm <sup>2</sup>
<b>Severing parameters</b>	
Filament severing rate (actin and cofilactin)	500e-9 s <sup>-1</sup> monomer <sup>-1</sup>
Bond rupture distance (actin)	0.24 nm
Bond rupture distance (cofilactin)	0.29 nm

<sup>a</sup> Measured from PDB file 3J8I.

<sup>b</sup> Measured from PDB file 3JOS.

<sup>c</sup> NIH Supercomputing resource, <http://helixweb.nih.gov/structbio/basic.html>

of backbone atom positions) stabilized. Elastic network models were generated from the next 50 ns (collected every 50 ps), but coarse-graining the filament to one “bead” per subunit instead of 4. The center of mass of each protein (actin or cofilactin) was connected to all adjacent proteins (up to four actin subunits and two cofilin subunits). The bond stiffness of each was iteratively adjusted until the fluctuations in the harmonic network model best matched the atomistic MD simulation fluctuation projected along the distance between the coarse-grained sites (as in (Lyman, Pfaendtner, & Voth, 2008), but with one bead per protein instead of multiple), where it was enforced that the bond stiffness of every “identical bond” (i.e. between two beads of the same type and the same distance away in the filament structure) also be the same for symmetry reasons.

The elastic bonds were incorporated into the meso-scale model by placing bonds randomly, with a uniform density, over an area defined by the buried solvent accessible surface area (calculated using the calc-surface program accessed using the National Institutes of Health scientific supercomputing resource at <http://helixweb.nih.gov/structbio/basic.html> for all atoms but water using a 1.4 Angstrom probe size).

Protein components are defined by their 3D position ( $\mathbf{G}^{(k)}$ ) and its local frame ( $\mathbf{a}^{(k)}_1, \mathbf{a}^{(k)}_2, \mathbf{a}^{(k)}_3$ ); designated by  $R(\boldsymbol{\psi}^{(k)})$ , the rotation that maps the fixed frame ( $\mathbf{e}_1, \mathbf{e}_2, \mathbf{e}_3$ ) to ( $\mathbf{a}^{(k)}_1, \mathbf{a}^{(k)}_2, \mathbf{a}^{(k)}_3$ ) (Figure 2.2A). The coordinates of any elastic bond attachment point ( $\mathbf{M}^{(k)}$ ) on the surface of protein ( $k$ ) are defined by the mass center ( $\mathbf{G}^{(k)}$ ) and a vector ( $\mathbf{X}^{(k)}$ ), which connects the mass center to  $\mathbf{M}^{(k)}$  and thus yields the position coordinates in the local reference frame denoted ( $\mathbf{a}^{(k)}_1, \mathbf{a}^{(k)}_2, \mathbf{a}^{(k)}_3$ ) (Figure 2.2A). The position of  $\mathbf{M}^{(k)}$  on protein  $k$  is given by (De La Cruz et al., 2010):

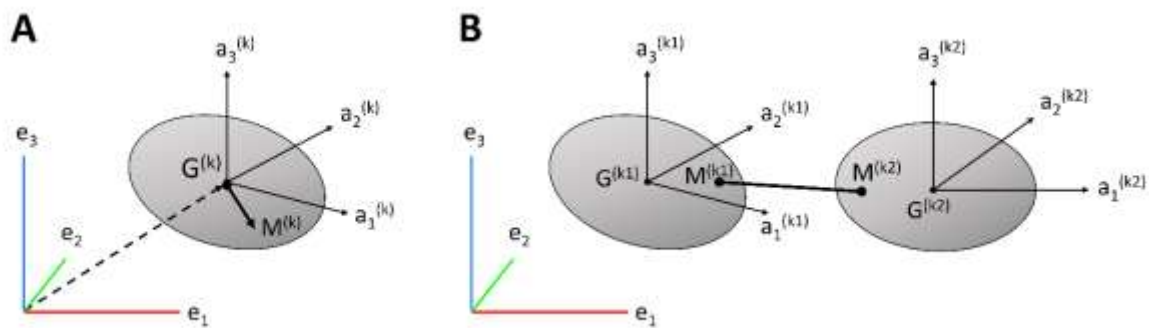


FIGURE 2.2 A) Depiction of the center of mass vector (dashed line,  $\mathbf{G}^{(k)}$ ), local reference frame vectors ( $\mathbf{a}^{(k)}$ ), and the vector from the mass center to an attachment point on protein  $k$  ( $\mathbf{M}^{(k)}$ ). B) Diagram showing an example of a bond connecting two proteins  $k_1$  and  $k_2$ .

$$\mathbf{M} = \mathbf{G} + R(\boldsymbol{\psi}) \cdot \mathbf{X} \quad (2.1)$$

Global filament deformations are applied by relative displacements and/or rotations of a subset of the constituent proteins. Filaments, either resting or deformed with imposed external forces, represent a static equilibrium. Inertial and damping forces are neglected in the model, as these are negligible in comparison to elastic forces at this length scale.

Each elastic bond linking two proteins (Figure 2.2B) at an interface is described by a harmonic potential with energy  $E$  with a magnitude that depends on the stiffness ( $S^{(k_1, k_2, j)}$ ), resting length ( $\lambda^{(k_1, k_2, j)}$ ), and the distance ( $|\mathbf{M}^{(k_1, j)} - \mathbf{M}^{(k_2, j)}|$ ) between the attachment points of bond  $j$  between proteins  $k_1$  and  $k_2$  according to:

$$E_{elastic, j}^{(k_1, k_2)} = S^{(k_1, k_2, j)} / 2 \left( |\mathbf{M}^{(k_1, j)} - \mathbf{M}^{(k_2, j)}| - \lambda^{(k_1, k_2, j)} \right)^2 \quad (2.2)$$

The elastic energy associated with each interface is given by the sum of all bond energies connecting two proteins  $k_1$  and  $k_2$  at this interface:

$$G_{elastic, int}^{(k_1, k_2)} = \sum_j G_{elastic, j}^{(k_1, k_2)} \quad (2.3)$$

The total elastic energy is given by the sum of all interface energies throughout the filament:

$$G_{fil} = \sum_{k_1, k_2} G_{elastic, int}^{(k_1, k_2)} \quad (2.4)$$

We emphasize that  $G_{fil}$  represents an elastic strain energy, and  $G_{fil} = 0$  for filaments in their resting positions (i.e.  $|\mathbf{M}^{(k_1, j)} - \mathbf{M}^{(k_2, j)}| = \lambda^{(k_1, k_2, j)}$  for all bonds).

### *Application of external load*

Simulations of filament shape deformation were carried out as described in detail (De La Cruz et al., 2010). The external, applied force ( $\mathbf{F}_{\text{ext}}$ ) or torque ( $\mathbf{T}_{\text{ext}}$ ) is coded via  $3 \times N$  vectors, where  $N$  is the number of proteins with an imposed force or torque. The internal forces and torques ( $F_{\text{int}}$  and  $T_{\text{int}}$ ) are computed by summing the elementary forces and torques of all elastic bonds adjoining protein components. Forces are balanced such that at equilibrium the internal forces and torques are equal to the applied external load ( $F_{\text{int}} + F_{\text{ext}} = 0$  and  $T_{\text{int}} + T_{\text{ext}} = 0$ ).

Filaments (500 or 100 nm, with or without cofilin clusters sizes predicted to exist over a range of cofilin occupancies (De La Cruz, 2005; Gressin et al., 2015)) were deformed with external compressive or torsional loads in a series of small steps to maintain force balance equilibrium throughout the simulation. Buckling was imposed by compressing until the end-to-end length reached 70% of the contour length. The filament curvature under these buckling conditions compare to the radius of curvature for severing (McCullough et al., 2011), and this specific condition was chosen to match deformations evaluated previously with the continuum mechanics model (De La Cruz et al., 2015). Filament end orientations were constrained to prevent rotation. Twisting loads were applied for a stated number of rotations in either direction (e.g. over-twisting or under-twisting) while constraining the filament end-to-end distance.

The contribution of elastic strain energy to filament severing was calculated relative to the spontaneous (i.e. thermally driven) severing rate constant  $k_{\text{sev}}$  according to (Dudko, Hummer, & Szabo, 2006):

$$\frac{k_{sev}(strained)}{k_{sev}} = \left(1 - \frac{2 \Delta G_{elastic}^{\circ'}}{3 \Delta G^{\ddagger'}}$$

where  $\Delta G_{elastic}^{\circ'}$  is the sum of elastic strain energies of the interfaces whose rupture is associated with filament fragmentation (e.g. two longitudinal and one lateral interface for bare actin, plus two additional cofilin-actin interfaces for cofilactin severing), and  $\Delta G^{\ddagger'}$  is the transition state energy barrier to filament severing that governs the value of  $k_{sev}$  (Table 2.2). The effect of strain on cofilin dissociation was calculated in a similar manner with corresponding rate constants and activation free energies.

#### *Severing parameters and transition state energies*

In chapter 4, rather than simply estimate fragmentation enhancement, I implement fragmentation at a sub-interface level. Equation 2.5 only applies to sufficiently high kinetic barriers, and this would break down under conditions of partial bond rupture, so I chose to use a simplified model to calculate fragmentation rates for this section, which I describe below.

The filament fragmentation rate constant varies with experimental conditions (salt concentration, buffer conditions, etc.). Here, we use an averaged filament fragmentation rate ( $k_{frag}$ ) of  $5 \times 10^{-7} \text{ s}^{-1} \text{ subunit}^{-1}$ , as measured *in vitro* under physiological solution conditions (Kinosian et al., 1993; Schmoller, Niedermayer, Zensen, Wurm, & Bausch, 2011). We assume the fragmentation rate constant of cofilactin is comparable to that of bare actin (McCullough et al., 2011).

**TABLE 2.2 Filament severing and cofilin dissociation rate constants and transition state energies**

Filament severing site	$k_{sev}$ (s <sup>-1</sup> )	$\Delta G^\ddagger$ (k <sub>B</sub> T)
Actin-Actin <sup>a,b</sup>	$1 \times 10^{-6}$	43.3
Cofilactin-Cofilactin <sup>a,b</sup>	$1 \times 10^{-6}$	43.3
Actin-Cofilactin boundary <sup>a,c</sup>	$8.3 \times 10^{-6}$	41.2
Cofilin binding mode	$k_{diss}$ (s <sup>-1</sup> )	$\Delta G^\ddagger$ (k <sub>B</sub> T)
Isolated <sup>a,d</sup> ( $k_{diss} = k.$ )	0.18	31.2
Singly contiguous <sup>a,d</sup> ( $k_{diss} = k.\omega.$ )	0.11	31.7
Doubly contiguous <sup>a,d</sup> ( $k_{diss} = k.\omega.^2$ )	0.07	32.2

<sup>a</sup> Severing and dissociation rates are converted to free energies of severing/rupture via the Eyring equation:

$$k_{diss} \text{ or } k_{sev} = \frac{k_B T}{h} e^{-\Delta G^\ddagger / k_B T}$$

<sup>b</sup> (McCullough et al., 2011) We note that a range exists in the literature (e.g. a site-specific value of  $\sim 10^{-7}$  s<sup>-1</sup> can be estimated from the data in (Andrianantoandro & Pollard, 2006; Suarez et al., 2011)), but the relative enhancements vary much less.

<sup>c</sup>(Kang et al., 2014)

<sup>d</sup>  $k.$  is the native dissociation rate of an isolated cofilin from actin filaments.  $\omega.$  is the cooperativity of cofilin dissociation with adjacent cofilin proteins bound. (Cao, Goodarzi, & De La Cruz, 2006)

Using the Arrhenius equation of transition state theory (Eq. 2.6),

$$k_{frag(native)} = \kappa \frac{k_B T}{h} e^{-\Delta G_{fil}^\ddagger / k_B T} \quad (2.6)$$

we can relate  $k_{frag}$  to the activation energy for filament fragmentation ( $\Delta G_{fil}^\ddagger$ ), Plank's constant ( $h$ ), Boltzmann's constant ( $k_B$ ), and the temperature ( $T$ ). This equation, assuming the transmission coefficient ( $\kappa$ ) is unity, yields a fragmentation activation energy of  $44 k_B T$ . Note that  $\Delta G_{fil}^\ddagger$  reflects a kinetic barrier (activation energy), and thus is distinct from estimations of equilibrium binding energy (Sept & McCammon, 2001).

We assume that the sum of interface activation energies ( $\Delta G_{int}^\ddagger$ ) across the filament cross section (3 for actin and actin-cofilactin boundaries, 5 for cofilactin) is equal to the total filament fragmentation activation energy (Eq. 2.7):

$$\Delta G_{fil}^\ddagger = \sum_{i=1}^N \Delta G_{int,i}^\ddagger \quad (2.7)$$

and that interface activation energies ( $\Delta G_{int,i}^\ddagger$ ) are proportional to their MD-derived stiffness ( $S_{int}$ ), such that:

$$\frac{\Delta G_{int,1}^\ddagger}{\Delta G_{int,2}^\ddagger} = \frac{S_{int,1}}{S_{int,2}} \quad (2.8)$$

for any given interfaces 1 and 2. The activation energy of each interface is divided equally among that interface's  $N$  total bonds:

$$\Delta G_{int}^\ddagger / N = \Delta G_{bond}^\ddagger \quad (2.9)$$

### *Implementation of filament fragmentation*

In our model, protein-protein contacts and interfaces rupture at two different scales: individual harmonic bonds rupture when extended beyond a critical distance, and the filament fragments spontaneously (due to thermal energy), as dictated by the rate constant and subunit interface strain. For clarity, we refer to the breaking of individual harmonic bonds as “bond rupture”, and the breaking of the filament as “filament fragmentation”, or just fragmentation. These two levels of fragmentation together tend to accelerate fragmentation. Bond rupture alone eventually leads to very flexible interfaces (since the few remaining bonds are free to rotate) that break very slowly when filaments/interfaces are bent. Spontaneous fragmentation alone would be slightly slower as well, as bond rupture lowers the activation energy of fragmentation more than elastic strain would on its own.

We have chosen to implement stochastic filament fragmentation (as opposed to a purely deterministic process) to avoid overanalyzing short lived, low stability, intermediates. Filaments in vitro (or in vivo) are constantly experiencing thermally-induced deformations. In this case, there exists an intrinsic rate constant for filament fragmentation of fluctuating filaments. If forces drive changes in filament shape, as we have modeled here, the strain energy within filament interfaces increases, and the stability of these interfaces is compromised. Interfaces that are highly strained or mostly ruptured will fragment rapidly. Since these strained interfaces have relatively short lifetimes, we implemented a stochastic fragmentation that limits our analysis to a subset of intermediates with partially ruptured interfaces. This approach allows us to estimate the extent of interface disruption required for fragmentation.

Individual interface bonds rupture when they are stretched to their critical bond distance  $R$  (Table 2.1). The critical bond distance for a given interface, i.e. the distance to which all bonds of an interface must be stretched to reach the fragmentation transition state energy ( $\Delta G^\ddagger_{bond}$ ), is defined by Eq. 2.10 (following Hooke's law):

$$R_{bond} = \sqrt{2 * \Delta G^\ddagger_{bond} / S_{bond}} = \sqrt{2 \frac{\Delta G^\ddagger_{bond} * N}{S_{bond} * N}} = \sqrt{2 \Delta G^\ddagger_{int} / S_{int}} \quad (2.10)$$

where  $N$  is the number of bonds in an interface. Individual bonds only rupture when they are extended, not compressed. Broken bonds retain a small resistivity (0.05% of original stiffness) to assist with energy minimization in subsequent deformation steps.

The total strain energy within each interface ( $E_{strain,int}$ ) is the sum of all elastic energy ( $E_{elastic,bond}$ ) and broken energy ( $E_{broken,bond}$ ) across each interface:

$$E_{strain,int} = \sum_j E_{broken,bond,j} + \sum_j E_{elastic,bond,j} \quad (2.11)$$

We assume that the elastic strain energy of the interface ( $E_{strain,int}$ ) destabilizes the ground state and increases the filament fragmentation rate constant by lowering the transition state energy barrier. The elastic energy of any given bond ( $E_{elastic,bond}$ ) is reduced to 0 upon rupture, and its initial resting energy ( $\Delta G^\ddagger_{bond}$ ; Eq. 2.9), assumed to destabilize the ground state because contacts are lost, is expressed as  $E_{broken,bond}$  to indicate that it has been ruptured. An alternative description of this process is that the ruptured bonds do not contribute to the strain energy, but instead lower the transition state energy barrier. Both approaches yield identical results since we monitor energy changes.

The strain energy across each filament cross section (shown in Figure 2.3A) is the sum of the comprising interface strain energies:

$$E_{strain,fil} = \sum_i E_{strain,int,i} \quad (2.12)$$

Filament fragmentation does not require that  $E_{strain,fil}$  reach the level of  $\Delta G_{fil}^\ddagger$  for filament fragmentation. Fragmentation possibly occurs for each interface after every simulation step, according to Kramer's theory:

$$k_{frag(strained)} = \frac{k_B T}{h} e^{-\Delta G_{fil}^\ddagger/k_B T + E_{strain,fil}/k_B T} = k_{frag(native)} e^{E_{strain,fil}/k_B T} \quad (2.13)$$

We convert this rate to a probability  $P$  of rupture for each step (Eq. 2.14), according to the cumulative distribution function of an exponential process. To calculate the time step,  $\Delta t$ , we assume that each simulation, if completed, occurs over one second.

$$P_{fil\ rupture} = 1 - e^{-k_{frag(strained)} * \Delta t} \quad (2.14)$$

After each small deformation we check every filament severing interface for fragmentation according to the strain energy  $E_{strain,fil}$ , and the corresponding fragmentation rate constant. The time step  $\Delta t$  is determined by the rate of deformation (described below) and the distance of that deformation step.

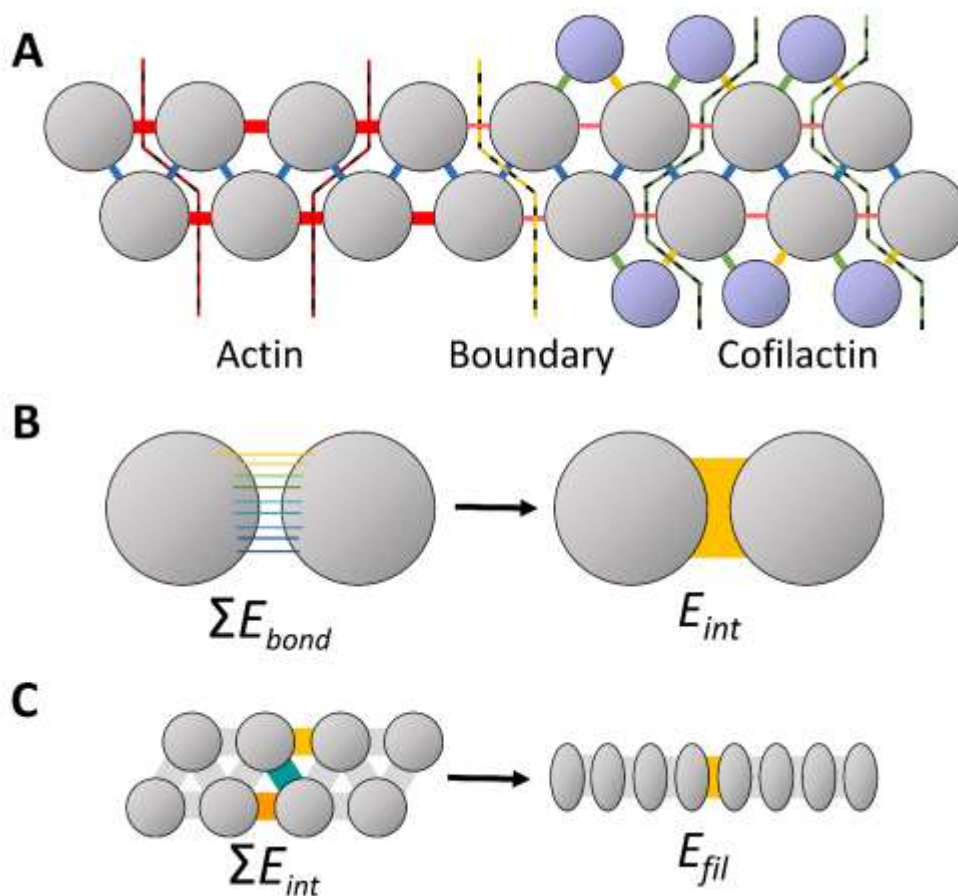


FIGURE 2.3 A) Filament interface diagram. Actin (grey) and cofilin (purple) molecules are shown near an actin-cofilactin interface. Filaments connections include longitudinal (red), lateral (blue), and cofilin-actin interfaces towards the pointed (green) and barbed (yellow) end. The light red, thinner longitudinal bonds shows where the weaker longitudinal interface of cofilactin is applied. Lines show a subset of the filament cross-sections over which the filament energy is calculated for fragmentation rate calculations. For both bare actin and cofilactin there exists a cross-section for each lateral (blue) interface. Within cofilactin, the cross-section goes through one lateral (blue), two longitudinal (red) and two cofilin-actin interfaces. We choose to always go through the cofilin-actin interactions on the barbed side, as these interfaces are weaker (Table 2.1). B) Illustration of Equation 2.9. C) Illustration of Equation 2.8.

### *Summary of simulation flow*

A flowchart of the simulations is shown in Figure 2.4. Simulations are initiated by building a helical filament according to an input filament length and cofilin distribution. There is one equilibration step to calculate the resting position of the filament. To begin each simulation step, a small translation/rotation is applied a subset of proteins (Fig. 2.5, blue subunits). Next, the position and rotation of all other subunits (Fig. 2.5, gray subunits) are iteratively adjusted (checking for bond rupture after each iteration (Eq. 2.14)) until force-balance equilibrium is achieved for all proteins across the filament. If fragmentation is turned on (as in Chapter 4), each filament interface is checked for fragmentation according to the probability defined by Eqs. 2.13 and 2.14. If fragmentation does not occur, the simulation resumes with additional translation/rotation of boundary subunits. If fragmentation occurs, the simulation is concluded. Filaments were deformed in a series of small steps with imposed compressive, extensional, or torsional loads (Figure 2.5). Force balance equilibrium was maintained after each step using the Newton-Raphson method to iteratively minimize the force and torque by adjusting the position and rotation matrices for each protein within the filament until a predefined error tolerance was met. Inertial damping forces are neglected, as these are minor compared to elastic forces at this length scale.

Compression was imposed by bringing the filament ends closer until filament fragmentation. Filament ends were free to rotate. The boundary conditions for compression were chosen to approximate a filament segment within a longer, curved segment. Filaments were extended by moving the filament ends apart until fragmentation; filament ends were not allowed to rotate during extension. Twisting loads were applied

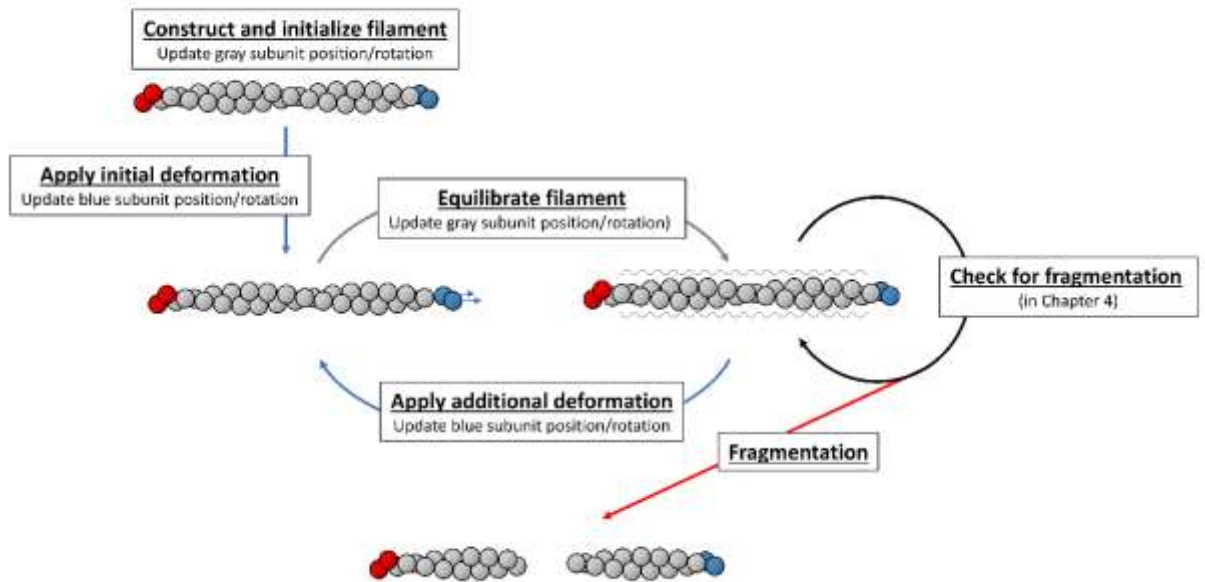


FIGURE 2.4 Flow chart of simulations. Filaments are constructed according to input parameters (length and cofilin distribution). Filaments are allowed to equilibrate for one step while holding boundary subunits. A deformation (a fraction of the total) is applied to the blue subunits while the red subunits are held fixed. The non-held subunits equilibrate (position and rotation is updated). In chapter 4, the strain energy of all interfaces is calculated and there is a check for fragmentation for each fragmentation interface. Chapter 3 skips this check. If there is no fragmentation, additional deformation is applied. The cycle of deformation and equilibration repeats until fragmentation is achieved or a given total deformation is applied to the filament.

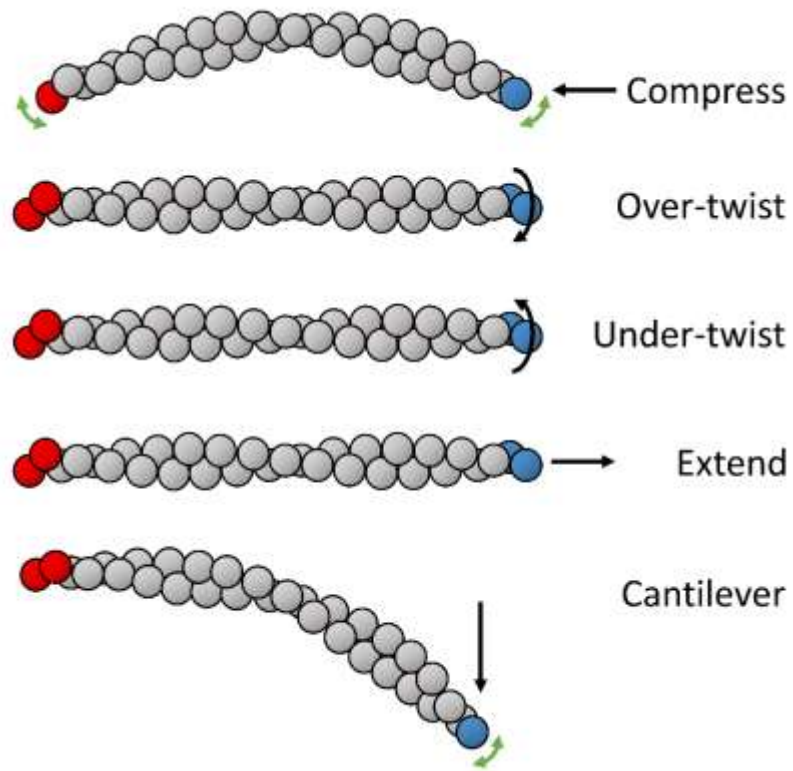


FIGURE 2.5 Applied deformations to filaments. For each given deformation, red monomers are fixed in space. The force shown by the black arrows is applied to the blue subunits for each type of deformation. Green arrows indicate a freedom of rotation for the colored subunits. The grey subunits shown have no external constraints.

by rotating filament ends about the filament axis and preventing axial movement, until filament fragmentation. Filament compression and extension were applied at speeds comparable to that of non-muscle myosin II-B (60 nm s<sup>-1</sup> and 10 nm s<sup>-1</sup>, respectively; (K. Y. Kim, Kawamoto, Bao, Sellers, & Adelstein, 2008). Filament rotation was applied at 720 degrees s<sup>-1</sup>, which is comparable to the rotation rate associated with incorporation of actin subunits to formin-capped filaments under unloaded conditions (Jegou, Carlier, & Romet-Lemonne, 2013).

### 2.3 FILAMENT MECHANICAL PROPERTIES

The bending persistence lengths ( $L_B$ ) were calculated from the perpendicular force ( $F_p$ ) needed to deflect the free end of a tethered filament by distance  $y$ , according to (i.e. a cantilever deformation, Figure 2.5; (Sugawara & Nikaido, 2014)):

$$L_B = \frac{F_p}{y * k_B T} \left( \frac{L^3}{3} \right) \quad (2.15)$$

where  $L$  is the filament contour length,  $k_B$  is Boltzmann's constant and  $T$  is absolute temperature. The filament torsional rigidity, ( $C_{fil}$ ) was calculated from the resulting torque ( $\tau$ ) after applying a defined twist ( $\theta$ , in radians) to a filament end (Figure 2.5) using (Sugawara & Nikaido, 2014):

$$C_{fil} = \frac{\tau * L}{\theta} \quad (2.16)$$

The filament (long-axis) intersubunit torsional rigidity ( $C_{sub}$ ) was measured by applying a torque to a single subunit in the center of the filament and calculated in a similar manner using the actin subunit rise along the same strand ( $r = 5.5$  nm):

$$C_{sub} = \frac{\tau * r}{\theta} \quad (2.17)$$

The filament models developed here capture the actin and cofilactin filament bending and torsional rigidities measured with purified protein components (Table 2.3). The bending persistence lengths ( $L_B$ ) of model actin and cofilactin filaments compare within a factor of 2 of values measured from thermally-driven filament shape fluctuations (McCullough et al., 2008). Similarly, the intersubunit torsional rigidities ( $C_{sub}$ ) of model actin and cofilactin filaments are within a factor of 3 of time-resolved phosphorescence anisotropy measurements (Prochniewicz et al., 2005). The model actin filament torsional rigidity ( $C_{fil}$ ) is also comparable to one (Yasuda, Miyata, & Kinoshita, 1996) but not a second (Tsuda et al., 1996) value measured for individual filaments, which vary by about a factor of three, possibly because of the assays employed.

The value of  $C_{fil}$  depends on the direction of applied twist (Table 2.3). Actin filaments are two-fold more compliant in under-twisting than over-twisting. Cofilactin filaments also under-twist more easily than over-twist, but the asymmetry is less pronounced. The intersubunit torsional rigidity ( $C_{sub}$ ) is symmetrical in both actin and cofilactin filaments (Table 2.3).

**TABLE 2.3 Mechanical properties of model filaments**

<i>Deformation</i>	<i>Actin</i>		<i>Cofilactin</i>	
	<i>Wet-lab</i>	<i>Model</i>	<i>Wet-lab</i>	<i>Model</i>
Bending	$L_B = 9.8 \pm 0.14 \mu\text{m}^a$ $\kappa = 39 \pm 2.0 \times 10^{-27} \text{ N m}^2 \text{ (a)}$	$L_B = 7.0 \pm 0.11 \mu\text{m}$ $\kappa = 29 \pm 0.45 \times 10^{-27} \text{ N m}^2$	$L_B = 2.2 \pm 0.026 \mu\text{m}^a$ $\kappa = 9.4 \pm 2.9 \times 10^{-27} \text{ N m}^2 \text{ (a)}$	$L_B = 1.3 \pm 0.02 \mu\text{m}$ $\kappa = 5.3 \pm 0.08 \times 10^{-27} \text{ N m}^2$
Over-twist, filament subunit	$L_{T,sub} = 0.56 \pm 0.24 \mu\text{m}^b$	$L_{T,sub} = 0.20 \pm 0.01 \mu\text{m}$ $C_{sub} = 0.84 \pm 0.06 \times 10^{-27} \text{ N m}^2 \text{ rad}^{-1}$	$L_{T,sub} = 0.03 \pm 0.01 \mu\text{m}^b$ $C_{sub} = 0.13 \pm 0.06 \times 10^{-27} \text{ N m}^2 \text{ rad}^{-1}$ (b)	$L_{T,sub} = 0.03 \pm 0.02 \mu\text{m}$ $C_{sub} = 0.13 \pm 0.07 \times 10^{-27} \text{ N m}^2 \text{ rad}^{-1}$
Under-twist, filament subunit	$C_{sub} = 2.3 \pm 1.0 \times 10^{-27} \text{ N m}^2 \text{ rad}^{-1} \text{ (b)}$	$L_{T,sub} = 0.20 \pm 0.01 \mu\text{m}$ $C_{sub} = 0.82 \pm 0.04 \times 10^{-27} \text{ N m}^2 \text{ rad}^{-1}$		$L_{T,sub} = 0.03 \pm 0.02 \mu\text{m}$ $C_{sub} = 0.12 \pm 0.08 \times 10^{-27} \text{ N m}^2 \text{ rad}^{-1}$
Over-twist, filament end	$L_{T,fil} = 6.8 \pm 0.7 \mu\text{m}^c$	$L_{T,fil} = 3.2 \pm 0.1 \mu\text{m}$ $C_{fil} = 13 \pm 0.25 \times 10^{-27} \text{ N m}^2 \text{ rad}^{-1}$	N.D. <sup>d</sup>	$L_{T,fil} = 3.2 \pm 0.1 \mu\text{m}$ $C_{fil} = 13 \pm 0.31 \times 10^{-27} \text{ N m}^2 \text{ rad}^{-1}$
Under-twist, filament end	$C_{fil} = 28 \pm 3 \times 10^{-27} \text{ N m}^2 \text{ rad}^{-1} \text{ (c)}$	$L_{T,fil} = 1.2 \pm 0.1 \mu\text{m}$ $C_{fil} = 4.9 \pm 0.28 \times 10^{-27} \text{ N m}^2 \text{ rad}^{-1}$	N.D. <sup>d</sup>	$L_{T,fil} = 2.2 \pm 0.1 \mu\text{m}$ $C_{fil} = 8.9 \pm 0.30 \times 10^{-27} \text{ N m}^2 \text{ rad}^{-1}$

Persistence length ( $L_B$  and  $L_T$ ) and rigidity ( $\kappa$ ) values are converted using the following formulas:  $L_B = \frac{\kappa}{k_B T}$ ,  $L_T = \frac{C}{k_B T}$  @ 25 C

Uncertainties in model measurements represent the standard deviation, N=5.

<sup>a</sup> (McCullough et al., 2008)

<sup>b</sup> (Prochniewicz et al., 2005)

<sup>c</sup> (Yasuda et al., 1996)

<sup>d</sup> Not determined

## Chapter 3: The Effect of Cofilin on Strained Actin Filaments

Published as Schramm AC, Hocky GM, Voth GA, Blanchion L, Martiel JL, De La Cruz EM (2017) Actin Filament Strain Promotes Severing and Cofilin Dissociation *Biophysical Journal*, 112(12), 2624-2633

This manuscript was a collaborative effort. I implemented the model into MATLAB with great assistance from Jean-Louis Martiel. I designed the experiments with Enrique M. De La Cruz. I performed the simulations and analyzed the results. Glen Hocky ran MD simulations to obtain experimental parameters. I wrote the manuscript with Enrique M. De La Cruz. All collaborators assisted with manuscript editing.

### 3.1 INTRODUCTION

Quantitative knowledge of strained filament structure and thermodynamics is necessary for defining the molecular basis of actin filament elasticity and fragmentation mechanism(s). As mentioned in Chapter 1, computational studies spanning a wide range of length and time scales have proven valuable to providing a molecular account of filament structural dynamics and energetics (Berro, Michelot, Blanchoin, Kovar, & Martiel, 2007; Chu & Voth, 2005; De La Cruz et al., 2010; Fan et al., 2013; Fan, Saunders, & Voth, 2012; Hocky et al., 2016; J. I. Kim, Kwon, Baek, Park, & Na, 2015; Saunders & Voth, 2012; Yogurtcu et al., 2012). All-atom molecular dynamics (MD) simulations have revealed key structural elements that influence actin filament bending and twisting stiffness (Chu & Voth, 2005), and the mechanism by which cofilin enhances filament compliance (Fan et al., 2013; Pfaendtner, De La Cruz, & Voth, 2010), but analysis is limited to short filament lengths ( $< 75$  nm) and time scales ( $< 100$  ns) of thermally-driven shape fluctuations. Steered-MD simulations capture behaviors under applied loads (J. I. Kim et al., 2015), but are also restricted to short length scales and, because of the short analysis times, are associated with nanonewton forces that far exceed those exerted by biological motor proteins (De La Cruz & Ostap, 2004). Continuum mechanics modeling permits analysis of long ( $> 1$  micron) filaments under strain with minimal computational cost, but fails to capture pertinent structural information, including that of inter-protein interfaces, and thus is inadequate for determining detailed molecular mechanism(s) of fragmentation (De La Cruz et al., 2015). Accordingly, modeling approaches that bridge the length and time scales of these methods is needed (De La Cruz et al., 2010).

In this chapter I use the model that I outlined in Chapter 2 to determine how filament deformations (including compression, torsion and extension) can differentially strain actin filament interfaces. Results from these model filament simulations indicate that buckling strains longitudinal actin contacts with minimal perturbation of cofilin-actin contacts, and that twisting strongly compromises cofilin-actin interactions which is predicted to accelerate cofilin dissociation from filaments.

## 3.2 RESULTS

### *Strain energy of buckled filaments*

Compressive loads buckle model filaments (Figure 3.1). The strain energy along buckled filaments displays three global maxima, corresponding to regions of highest curvature (Figures 3.1A and 3.1D). Cofilactin filaments are more compliant than bare actin, so the force required for buckling is lower, as is the total work needed to deform them to a similar end to end length. Thus, the total strain energy stored under identical conformations is lower for cofilactin than bare actin (Figures 3.1B and 3.1E).

The overall strain energy profile of model filaments parallels that of continuum mechanics models (De La Cruz et al., 2015) over long (>100 nm) length scales. However, over shorter length scales the local strain energy profiles display a periodicity not captured by continuum models (Figure 3.1B). These differences in sub-micron length-scale energy distribution correspond to the filament helical pitch, where both strands lie in the plane perpendicular to bending (Figure 3.1A). Most of the strain energy (> 85% of the total, Figure 3.1C) localizes in longitudinal bonds, and lateral interfaces are minimally strained by bending.

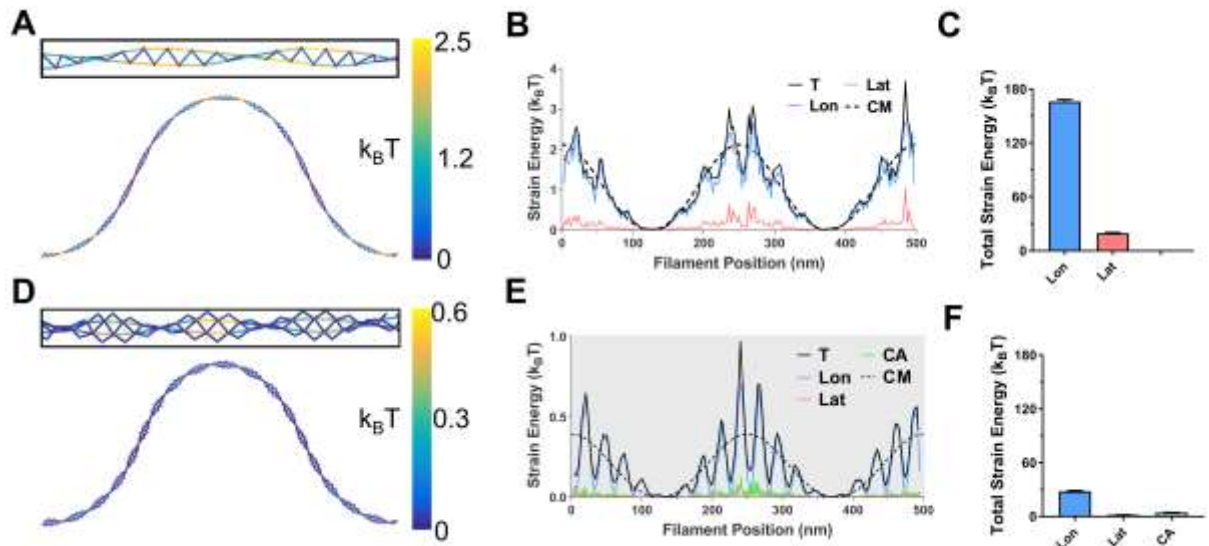


FIGURE 3.1 Shape and strain energy of buckled actin and cofilactin filaments. Skeletonized representation of single A) actin and D) cofilactin filaments (length 500 nm) buckled to a 350-nm end-to-end length with constrained end orientations. Elastic strain energies of protein interfaces are colored according to the scale at the right. Actin and cofilin nodes (i.e. centers of mass) are indicated with red and blue dots, respectively. Distribution of B) actin and E) cofilactin filament interface strain energy along the contour length. Insets are rotated 90 degrees. Grey shading shows where cofilin is present and individual protein interface types are distinguished by color. T: total (longitudinal plus lateral), Lon: longitudinal, Lat: lateral, CA: cofilin-actin, CM: continuum mechanics total energy. The dashed line corresponds to the elastic energy distribution predicted by continuum models (22). C) and F) The total elastic strain energy of each interface type. Uncertainty bars represent the standard deviation,  $N=5$ .

Cofilin changes the (average) filament twist (Figure 3.1D; (V. E. Galkin et al., 2011; V. E. Galkin, Orlova, Vos, Schroder, & Egelman, 2015; McGough et al., 1997)) and introduces a corresponding change in the periodicity of strain energy (Figure 3.1E). Cofilactin filaments are also wider, and thus locally more anisotropic (i.e. more “ribbon”-like), than bare filaments (McCullough et al., 2008; McGough et al., 1997), which enhances the difference between amplitudes of local strain energy maxima and minima. Each cofilactin longitudinal interface is paralleled by two cofilin-actin interfaces. This geometry confers each cofilin-actin interface with more freedom for movement than longitudinal interfaces, thereby straining individual interface bonds less. Because of this, and the tendency for the filament to buckle where filaments are “flat” relative to the bending plane, bending and buckling minimally strain cofilin-actin interfaces.

#### *Strain energy of twisted filaments*

Twisting filament ends in either direction (i.e. over- or under-twist) introduces uniform strain along filaments (Figure 3.2A-C). Over-twisting strains actin longitudinal interfaces more than lateral interfaces. The opposite occurs for under-twisting – lateral contacts are strained more than longitudinal ones. Cofilactin filaments behave similarly, but over-twisting strains longitudinal and lateral contacts equally.

The actin and cofilactin filament torsional rigidities ( $C_{fil}$ ) are comparable (Table 2.3). Accordingly, filaments twisted at their ends deform uniformly (Figure 3.2), and do not display an uneven distribution of strain along actin and cofilactin segments as observed with buckling (Figure 3.1).

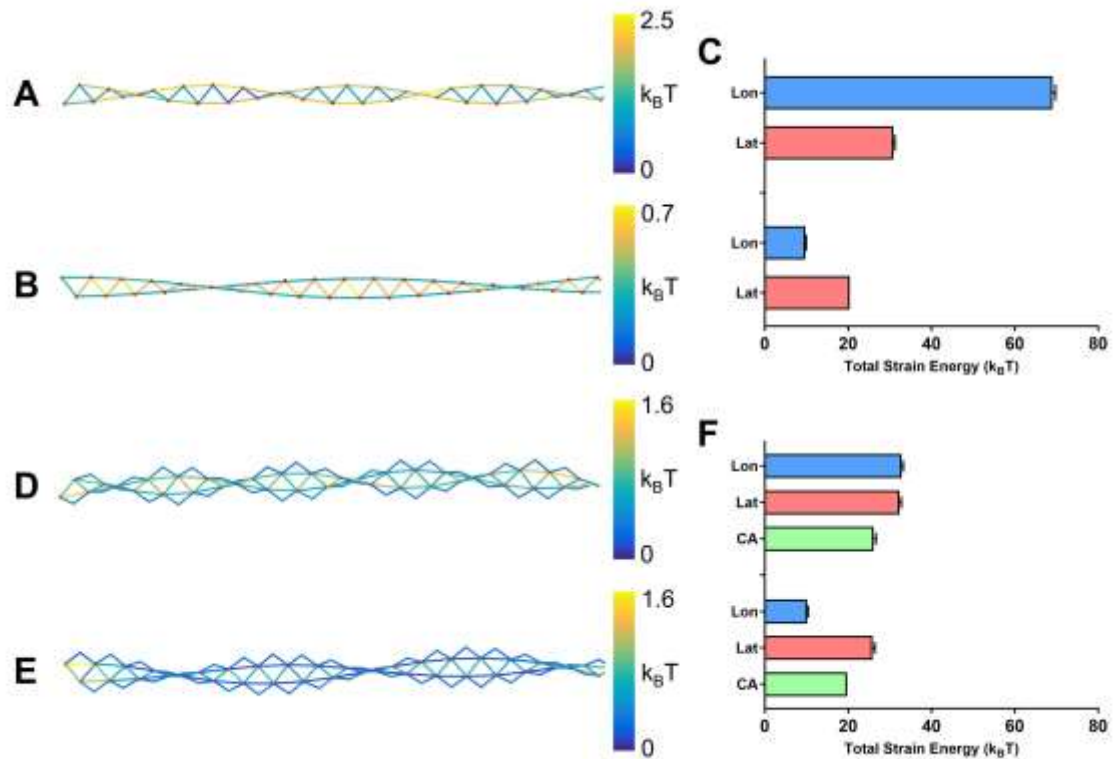


FIGURE 3.2 Shape and strain energy of twisted actin and cofilactin filaments. Skeletonized representation of single actin (A and B) or cofilactin (D and E) filaments (length 100 nm) that have been over-twisted (A and D) or under-twisted (B and E) by one half rotation (i.e. 5 turns per micron) at their ends with end-to-end lengths constrained. Elastic strain energies of protein interfaces are colored according to the scale at the right. Actin and cofilin nodes (i.e. centers of mass) are indicated with red and blue dots, respectively. The total elastic strain energy of each interface type in C) actin and F) cofilactin filaments. Lon: longitudinal, Lat: lateral, CA: cofilin-actin interfaces. Uncertainty bars represent the standard deviation,  $N=5$ .

Twisting filament ends also strains cofilin-actin interfaces and significantly accelerates cofilin dissociation (Figure 3.3). Over-twisting is predicted to have a greater effect than under-twisting. The enhancement is non-linear, and the twisting density exponentially accelerates dissociation.

#### *Strain energy of partially decorated filaments*

Filaments partially decorated with cofilin have a non-uniform elasticity. Cofilactin segments are more compliant in bending than bare actin, introducing a mechanical gradient at boundaries between bare and decorated segments (Kang et al., 2014). The variable stiffness of these filaments causes partially decorated filaments to deform differently from pure actin or cofilactin filaments with uniform elasticity (De La Cruz et al., 2015).

Half-decorated filaments with centered boundaries buckle asymmetrically under compressive loads. The softer, cofilactin segment deforms more than the stiff bare actin segment (Figure 3.4A). As seen with previous continuum models (De La Cruz et al., 2015), the strain energy peaks at regions of highest curvature within the cofilactin segment, at sites distal from the boundary (Figure 3.4B).

Filaments with a small cofilin cluster (~10% of filament length) positioned at the center deform symmetrically (Figure 3.4C). Strain energy localizes within the cofilactin segment, in accordance with continuum models (De La Cruz et al., 2015). However, the local strain energy peaks immediately adjacent to the boundary (Figure 3.4D). This distribution is not captured by continuum mechanics models, which predict a strain

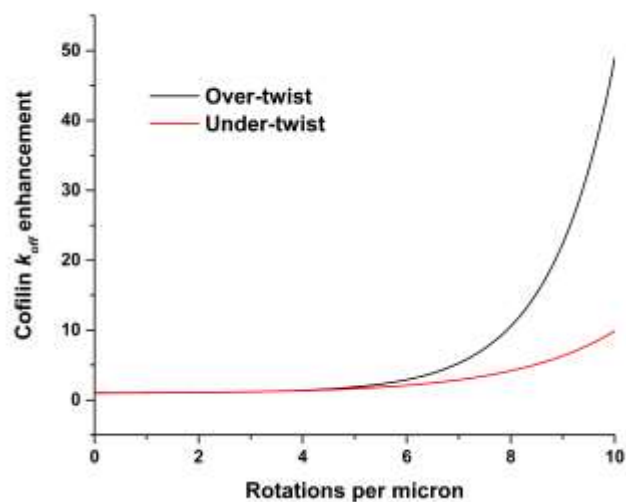


FIGURE 3.3 Filament twisting accelerates cofilin dissociation. The fold-enhancement varies little for all cofilin binding modes, despite the different rate constants (Table 2). Over-twisting (black) has a more pronounced effect on cofilin dissociation than under-twisting (red). We note that in this frame of reference, the x-axis is shifted for bare actin because it is “under-twisted” by 2.5 rotations per micron relative to cofilactin.

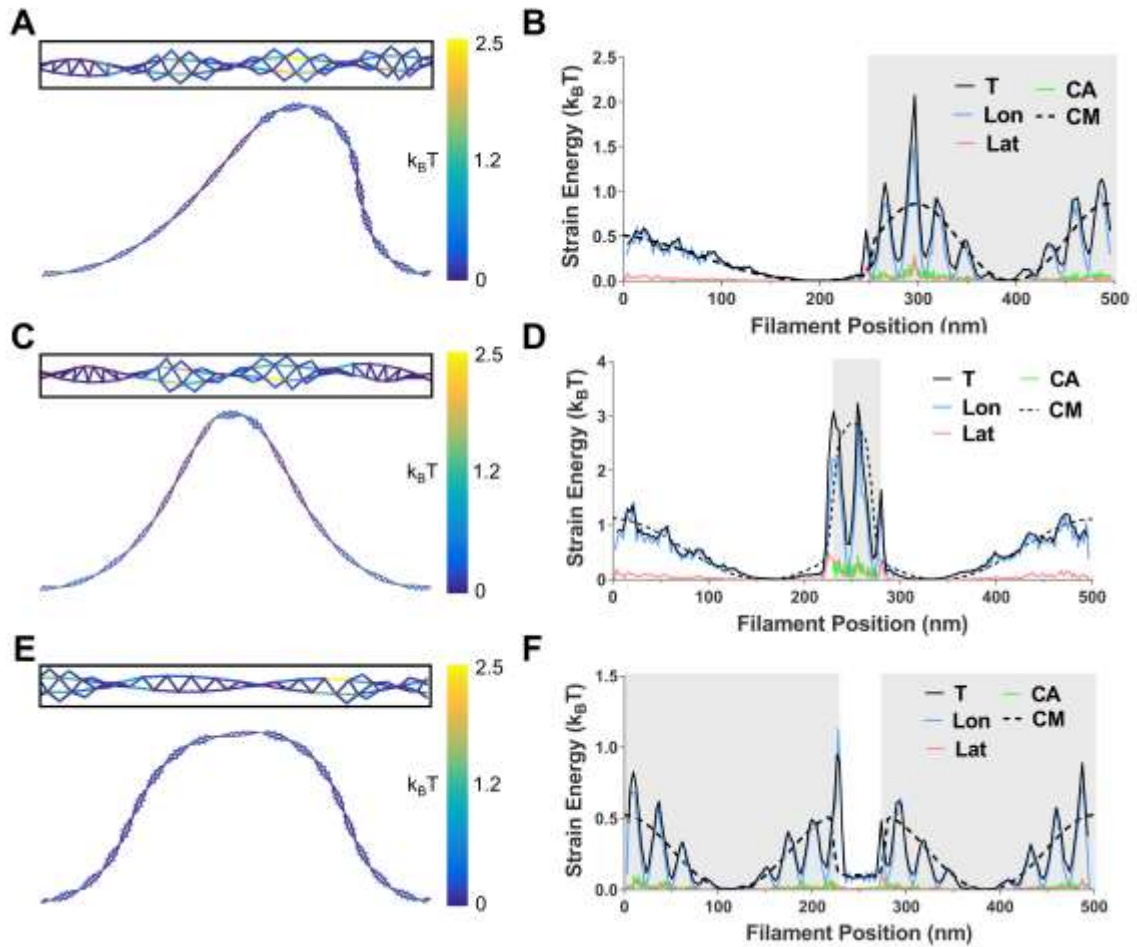


FIGURE 3.4 Shape and strain energy of partially decorated filaments. Skeletonized representation of single filaments (length 500 nm) buckled to a 350-nm end-to-end length with constrained end orientations. Filaments are either A) half-decorated with a single boundary at the center, or contain a small (10% of filament length) C) cofilactin or E) bare segment. Insets are rotated 90 degrees. Elastic strain energies of protein interfaces are colored according to the scale at the right. Actin and cofilin nodes (i.e. centers of mass) are indicated with red and blue dots, respectively. Distribution of filament interface strain energy along the contour length are shown to the right (B, D, and F). Grey shading shows where cofilin is present and individual protein interface types are distinguished by color. T: total (longitudinal plus lateral), Lon: longitudinal, Lat: lateral, CA: cofilin-actin, CM: continuum mechanics total energy. The dashed line corresponds to the elastic energy distribution predicted by continuum models (22).

energy peak at the center of the segment (De La Cruz et al., 2015). Cofilactin filaments with a centered bare segment display similar behaviors (Figures 3.4E-F).

### *Fragmentation of buckled filaments*

The effects of strain on filament fragmentation are interpreted according to a model in which elastic energy destabilizes (i.e. increases  $G$ ) protein interfaces, thereby promoting rupture. We treat filament severing as a two-state (i.e. intact or fragmented) process. This simplified mechanism assumes that the elastic strain energy is stored uniformly throughout the filament cross-section and that fragmentation occurs as a single kinetic transition. Here we consider only the “forward” severing rate constants, since reannealing under load is complicated by filament end repositioning shortly after fragmentation.

Continuum models predict buckled, partially-decorated cofilactin filaments preferentially sever within cofilin clusters because the elastic strain energy distributes preferentially within compliant, cofilactin segments (De La Cruz et al., 2015). The filament models developed here demonstrate that elastic energy peaks adjacent to boundaries, rather than distributing throughout the cofilin-bound segment (Figure 3.4). Consequently, the models predict distinct effects of buckling on filament severing than anticipated from continuum analyses. Not only does severing occur preferentially at boundaries, but it is accelerated by at least an order of magnitude more (Figure 3.5A). The helically-based strain localization captured in this model (Figure 3.1) suggests that the *maximum* strain energy (and therefore maximum severing rate enhancement) will, in most cases, be greater than in the continuum model. However, the average strain energies

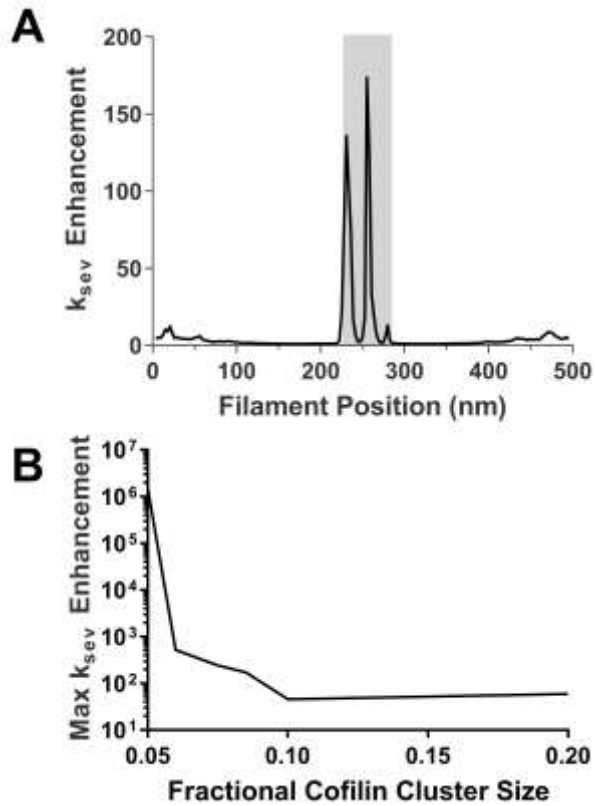


FIGURE 3.5 Compressive loads and buckling accelerate filament severing. A) Severing rate across a 500-nm filament buckled to a 350-nm end-to-end length with a small (10% of total sites) cofilin cluster at the center (shaded in grey). B) Maximum filament severing rate constants across different cluster sizes as predicted by the model.

along the filament are comparable with both models at length scales longer than the filament helical pitch.

### 3.3 DISCUSSION

The mesoscopic length-scale models developed here capture the mechanical (e.g. bending and twisting rigidities) and structural (e.g. topology and protein-protein interfaces) features of (cofil)actin (cofilactin and bare actin) filaments, while maintaining the computational simplicity to investigate physiologically relevant filament shape deformations. The spatial elastic energy distribution within filaments maps local elastic strain to specific protein-protein interfaces, and thus identifies constituent contacts destabilized by filament shape changes. The effects of strain on filament severing and cofilin occupancy are interpreted with a thermodynamic, protein interface rupture model.

#### *Filament severing mechanisms*

Compressive forces driven by contractile motor proteins buckle and fragment actin filaments (Linsmeier et al., 2016; Medeiros et al., 2006; Murrell & Gardel, 2012; C. A. Wilson et al., 2010). Since cofilin renders filaments more compliant in bending (McCullough et al., 2008), occupancy could facilitate myosin-induced buckling (i.e. introduce mechanical instability) and subsequent remodeling of actin networks and bundles (Medeiros et al., 2006). Buckling primarily strains longitudinal actin-actin contacts of actin and cofilactin filaments (Figure 3.1). Hence, these interfaces are likely to be most susceptible to rupture under compressive deformations. Filament interfaces need not be completely ruptured by applied loads. Simply compromising a subset of the

severing interfaces may be adequate to accelerate spontaneous (e.g. thermally-driven) fragmentation.

Filaments partially-decorated with cofilin (which contain boundaries) can sever via at least three distinct pathways (Figure 3.6), depending on the classes of protein interfaces ruptured with severing. Fragmentation can occur within an actin or cofilactin segment, or at a boundary between them. The overall stiffness of these three distinct fragmentation interfaces varies. The boundary interface is least stiff, so an applied compressive force will deform (i.e. strain) boundaries more than cofilactin segments or bare actin. This response applies not only for bending driven by externally applied loads, but also for those that are thermally driven. This low boundary stiffness may contribute to the observed hinging at boundaries within partially-decorated filaments (McCullough et al., 2011).

#### *Influence of filament shape deformations on cofilin binding*

Myosin and formin proteins twist and can also bend and buckle actin filaments (Mizuno et al., 2011; Murrell & Gardel, 2012; Van Goor, Hyland, Schaefer, & Forscher, 2012). Compressive loads and buckling weakly affect cofilin binding, but twisting strains cofilin-actin contacts and is predicted to significantly enhance dissociation (Figure 3.1 and 3.3). This response to applied external load predicts that buckling enhances filament severing without compromising cofilin occupancy, and that twisting accelerates cofilin dissociation while preserving filament integrity. Such a mechanism also predicts that elongating formin-capped filaments anchored at their ends, which would under-twist according to the filament helical pitch (~14 rotations per micron for actin

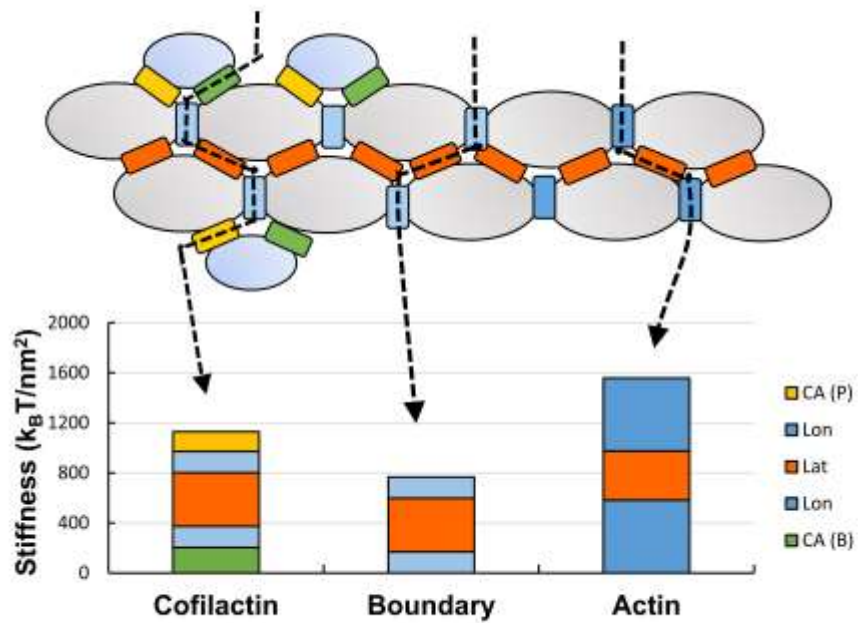


FIGURE 3.6 Multiple severing pathways at cofilactin-actin boundaries in partially decorated filaments. Each column represents a sum of the stiffness values of the interfaces required to sever a filament at the shown location. Lon: longitudinal, Lat: lateral, CA (P): cofilin-actin pointed end, CA (B): cofilin-actin barbed end.

(Mizuno et al., 2011)). This may weaken overall cofilin binding and subsequent severing of formin-nucleated filaments. Torsional stresses induced by myosin motors can have similar effects, though these may be more local in nature.

#### *Limitations of the model and analysis*

Simulations do not consider thermal motion, so entropic contributions from filament shape fluctuations are not captured by our model. However, entropic contributions to the interface stiffness values are considered in the all-atom MD simulations, and are included in the thermodynamic free energy-based Eq. 2.5. A severed filament is expected to have more degrees of freedom than an intact one, which will favor fragmentation. Therefore, the fragmentation probability predicted by our model, which does not consider configurational entropy, represents a lower estimate (i.e. severing will be faster than predicted for a given strain).

Solution salts (180 mM KCl) are explicitly accounted for in the all-atom MD simulations used to define filament interface stiffness parameters, but are not explicitly incorporated into the filament models developed here. Salts bind and stiffen actin filaments (Hocky et al., 2016; Kang et al., 2014; Kang et al., 2012), so the mechanical gradient between bare and cofilin-decorated segments is likely salt-dependent. We only explore a single "solution" condition and neglect potential contributions from filament-associated ion dissociation, as our filaments are non-plastic and the protein interaction strength does not change throughout the simulation.

An advantage of the mesoscopic filament models presented here is that elastic strain energy is discretely mapped within protein interfaces along filaments. This spatial

dispersal of elastic energy facilitates a thermodynamic link between stored elastic free energy, interface destabilization, and rupture probability, namely filament severing and cofilin dissociation. An assumption in this analysis of severing and dissociation enhancement is that the strain energy at each protein interface is distributed uniformly. However, some regions of the interface may experience variable strain, depending on their interface position. Therefore, some regions of a given protein-protein interface are more susceptible to rupture than others. Future modeling efforts will require extending the mesoscopic models to account for interface remodeling and integrating with all-atom MD simulations to evaluate if severing is best determined by such a multi-state pathway with progressive interface rupture, analogous to crack propagation in protein (Miyashita, Onuchic, & Wolynes, 2003) and non-protein materials (S. D. R. Wilson & Hulme, 1983).

## Chapter 4: Fragmentation of Actin Filaments Under Strain

Published as Schramm AC, Hocky, GM, Voth GA, Martiel JL, De La Cruz EM (2019)

Plastic deformation and fragmentation of strained actin filaments *Biophysical Journal*, in  
*press*

This manuscript was a collaborative effort. I implemented new features into the code with great assistance from Jean-Louis Martiel. I designed the experiments with Enrique M. De La Cruz. I performed the simulations and analyzed the results. Glen Hocky ran MD simulations to obtain experimental parameters. I wrote the manuscript with Enrique M. De La Cruz. All collaborators assisted with manuscript editing.

## 4.1 INTRODUCTION

As discussed in Chapter 2, polymerizing actin can generate forces to move cell structures and boundaries, e.g. at the leading edge of a migrating cell (Blanchoin, Boujemaa-Paterski, Sykes, & Plastino, 2014; Pollard & Borisy, 2003; Pollard & Cooper, 2009). Filaments must be mechanically stable and resist fragmentation to generate and sustain the forces that drive movement, but they must also be capable of continuous remodeling. Various families of regulatory proteins fragment actin filaments (e.g. severin, Inf2, gelsolin, twinfilin, and ADF/cofilin; (Blanchoin & Pollard, 1999; Cao et al., 2006; Chhabra & Higgs, 2006; Kinosian et al., 1998; Moseley et al., 2006; Yamamoto, Pardee, Reidler, Stryer, & Spudich, 1982)) act to accelerate this process by increasing the concentration of free filament ends (Blanchoin et al., 2014). Contractile proteins can act synergistically with actin severing proteins to accelerate network turnover (Medeiros et al., 2006; Van Goor et al., 2012). Fragmentation is necessary for the steady state actin dynamics found in biology (Schmoller et al., 2011).

Members of the ADF/cofilin family of severing proteins accelerate filament rupture (Elam, Kang, & De la Cruz, 2013). Cofilin changes the average helical pitch of actin filaments and renders them more compliant in bending and twisting (McCullough et al., 2008; McGough et al., 1997; Prochniewicz et al., 2005). Cofilin binding is cooperative, and clusters of bound cofilin form along filaments (Cao et al., 2006). Severing occurs at or near the junctions between bare and cofilin-decorated regions (i.e. boundaries) where there is a change in filament structure and mechanical properties (De La Cruz et al., 2015; Huehn et al., 2018; McCullough et al., 2011; Suarez et al., 2011). The cofilin N-terminus plays a

critical role in binding, alteration of filament mechanics, and fragmentation (Elam et al., 2017).

Computational and mathematical studies of bare and cofilin-decorated actin (cofilactin) filament fragmentation span broad force regimes and length- and time-scales, and have been valuable for understanding filament dynamics, mechanics, stability, and fragmentation by regulatory proteins (Berro et al., 2007; Berro et al., 2010; Yogurtcu et al., 2012). Molecular dynamics (MD) simulations of actin and cofilactin filaments explain why cofilin binding alters filament bending and twisting mechanics (Chu & Voth, 2005, 2006; Fan et al., 2013; Fan et al., 2012; Hocky et al., 2016), but are restricted to relatively short filaments and time scales that do not allow for the application of forces of a physiologically relevant magnitude (Ackbarow, Chen, Keten, & Buehler, 2007). Continuum mechanics treatments allow the simulation of (relatively) large-scale filament deformations of long filaments (multiple helical pitches). These simulations show that heterogenous filament bending mechanics localizes filament strain energy and accelerates boundary severing (De La Cruz et al., 2015). However, continuum modeling provides little molecular insight into the process.

The model discussed in Chapter 2 fills the gap between MD and continuum mechanics. The predictions made in Chapter 3 presuppose a two-state system (broken and unbroken). However, this is unlikely to be true for a filament of appreciable width, where strain distributes unevenly over the filament cross-section. The non-uniform strain suggests filaments are likely to fragment in multiple, distinguishable phases, as opposed to the simultaneous rupture of all protein-protein interfaces comprising the filament cross-

section. Accordingly, the pathway of strained filament fragmentation remains an open question.

The results of the proceeding chapter show that partial interface rupture and remodeling is a necessary precursor to complete fragmentation of bent and twisted (but not extended) bare and fully cofilin-decorated filaments. Actin-cofilactin boundaries are brittle and fragment at small deformations and without partial interface rupture. Comparing the effects of deformation on fragmentation to the available experimental data suggests that high filament curvature destabilizes actin D-loop docking, which may kinetically favor localized cofilin binding (Muhlrad et al., 2004). Partial interface rupture, resulting from the uneven application of load or other means (e.g. cofilin binding), may be a generally applicable mechanism for destabilizing otherwise stable macromolecule interfaces.

## 4.2 RESULTS

### *Fragmentation of compressed/bent filaments*

We simulated the compressive fragmentation of bare actin, cofilactin, and boundary-containing filaments. Filaments (100 nm) with freely-rotating ends were compressed until fragmentation. During these simulations the filament ends are brought closer together until filament fragmentation occurs (at which point the simulation is stopped). Cofilin occupancy affects the magnitude and location of strain (Figure 4.1), and thus the deformation at which rupture occurs.

At low curvature, elastic energy accumulates primarily in longitudinal (long-axis) actin-actin interfaces (Schramm et al., 2017). Further compression leads to the partial

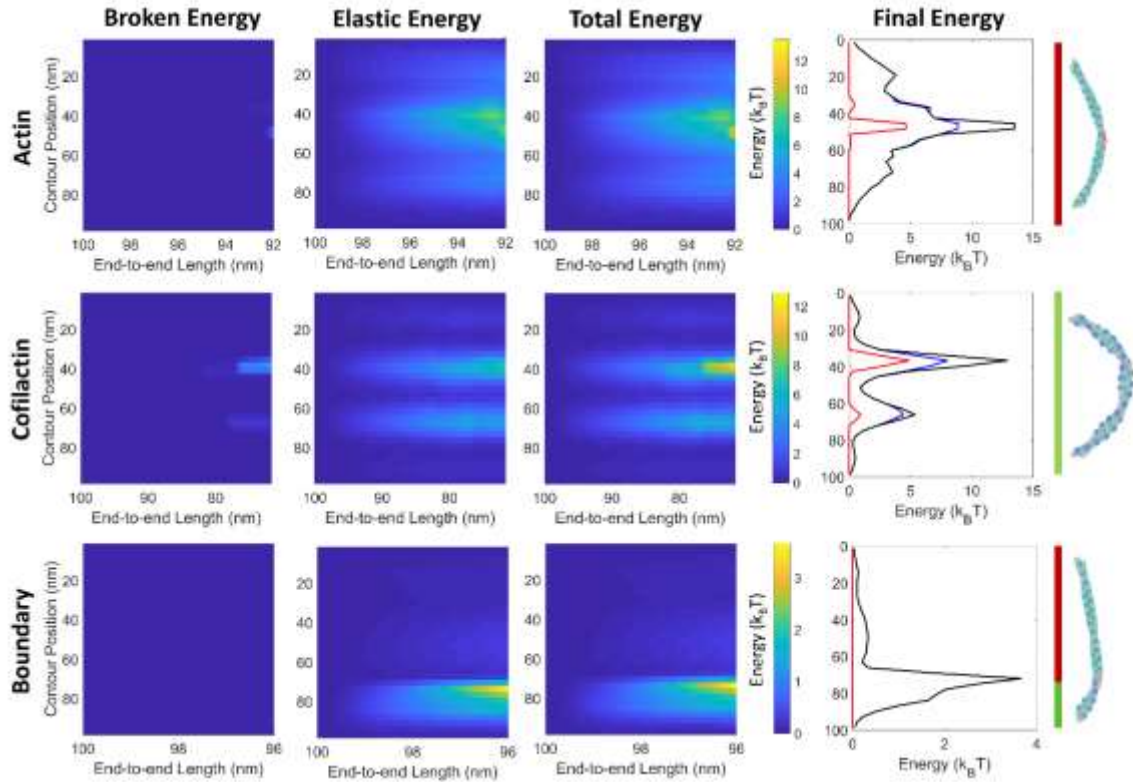


FIGURE 4.1 Filament energy (broken, elastic, and total) of compressed filaments. 100 nm filaments are compressed with freely rotating ends. The first row shows a simulation of bare actin, the second, cofilactin, and the third, a boundary. Lines on the right edge of the figure show the location of actin (red) and cofilactin (green) for each distribution. Final energy corresponds to the energy immediately prior to rupture (and the rightmost column of the kymographs).  $E_{broken,fil}$  – red,  $E_{elastic,fil}$  – blue,  $E_{strain,fil}$  – black. These traces show a single rupture event. Note that the x-axis and energies for each row are a different scale.

**TABLE 4.1 Pre-fragmentation interface energies**

Deformation	Filament Type	Interface Type	$E_{\text{elastic,int}}/\Delta G_{\text{int,native}}^{\ddagger}$ (pre-fragmentation)	$E_{\text{broken,int}}/\Delta G_{\text{int,native}}^{\ddagger}$ (pre-fragmentation)
<b>Compression (N = 50)</b>	Actin	Longitudinal	$0.33 \pm 0.03$	$0.21 \pm 0.05$
		Lateral	$0.08 \pm 0.05$	$0 \pm 0$
	Cofilactin	Longitudinal	$0.37 \pm 0.09$	$0.42 \pm 0.08$
		Lateral	$0.19 \pm 0.07$	$0.04 \pm 0.06$
		Cofilin-Actin	$0.17 \pm 0.05$	$0.16 \pm 0.08$
	Boundary	Longitudinal	$0.30 \pm 0.05$	$0.063 \pm 0.062$
Lateral		$0.040 \pm 0.015$	$0 \pm 0$	
<b>Extension (N = 20)</b>	Actin	Longitudinal	$0.40 \pm 0.05$	$0 \pm 0$
		Lateral	$0.01 \pm 0.005$	$0 \pm 0$
	Boundary	Longitudinal	$0.26 \pm 0.06$	$0 \pm 0$
		Lateral	$0.008 \pm 0.003$	$0 \pm 0$
<b>Over-twist (N = 20)</b>	Actin	Longitudinal	$0.17 \pm 0.02$	$0.18 \pm 0.11$
		Lateral	$0.22 \pm 0.09$	$0.001 \pm 0.005$
	Boundary	Longitudinal	$0.20 \pm 0.06$	$0.01 \pm 0.02$
		Lateral	$0.06 \pm 0.02$	$0 \pm 0$
<b>Under-twist (N = 20)</b>	Actin	Longitudinal	$0.24 \pm 0.2$	$0.09 \pm 0.03$
		Lateral	$0.35 \pm 0.07$	$0.28 \pm 0.07$
	Boundary	Longitudinal	$0.17 \pm 0.03$	$0.02 \pm 0.03$
		Lateral	$0.09 \pm 0.04$	$0 \pm 0$

interface rupture of highly-strained areas of the filament, again primarily in longitudinal bonds (Table 4.1). The periodic elastic energy along the filament seen in actin and cofilactin filaments corresponds to the half-helical pitch of actin or cofilactin, and can be explained by changes of the bending moment for different helical orientations (Schramm et al., 2017). The strain energy profile for these simulations differs slightly from our previous work due to differences in filament length and boundary conditions (freely rotating instead of clamped ends) that mimic a bent region within a longer filament.

Compression of bare actin filaments unevenly strains longitudinal interfaces, leading to partial interface rupture prior to complete fragmentation (Figure 4.2A). As the bonds at the “edges” of longitudinal interfaces begin to rupture, some of the remaining bonds in that interface compensate by stretching to the level of the recently ruptured bonds. The resulting weakness in the longitudinal interfaces after bond rupture (due to loss of stiffness and interface area) further localizes strain energy at those sites, akin to strain localization at boundaries (De La Cruz et al., 2015; Schramm et al., 2017). This accelerates energy accumulation after the initial onset of bond rupture. In all cases of bare actin fragmentation, a significant fraction of the interface is broken before complete fragmentation occurs (Figure 4.2A & 4.2B, Table 4.2).

Like bare actin filaments, compressed cofilactin filaments most often fragment after significant partial interface rupture (Figure 4.2C, D, Table 4.2). The greater flexibility of cofilactin means the strain energy for a given filament deformation is lower than an equally deformed actin filament. This leads to more gradual fragmentation, both in terms of the amount of deformation required for severing (i.e., a higher critical fragmentation

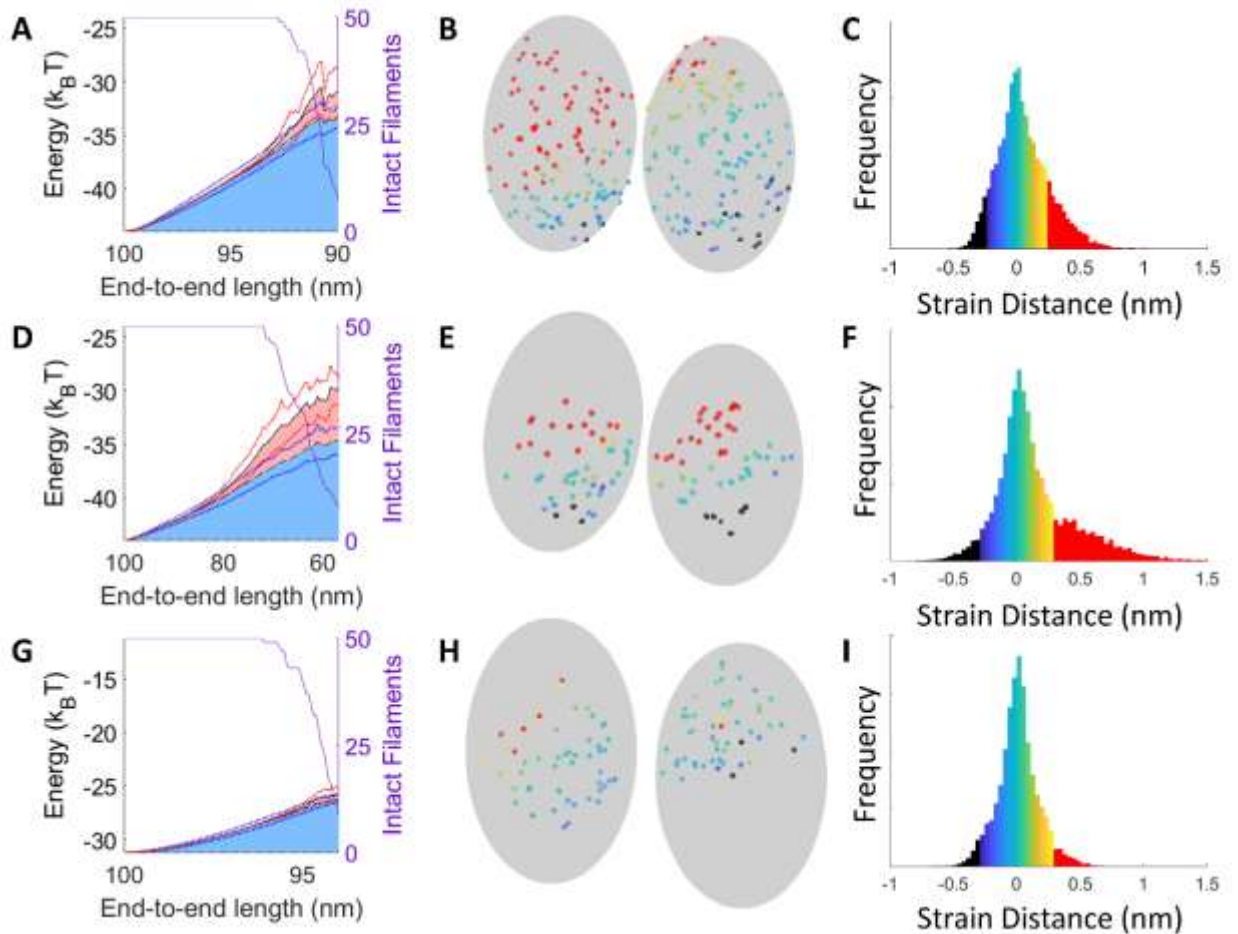


FIGURE 4.2 Strained interfaces of compressed filaments immediately prior to filament fragmentation. A) Elastic (blue) and broken bond (red) energy of the eventually broken interface within a compressed actin filament with freely rotating ends. Blue and red shaded regions correspond to the average elastic energy and broken energy of interface bonds, respectively. Blue and red dotted lines show the standard deviation of elastic and total energy. 50 filaments are simulated, but at larger deformations (smaller end-to-end lengths) only a subset of the overall population still exists (purple line). The energy shown is relative to the activation energy of fragmentation (where  $0 k_B T$  is the energy of rupture). B) Snapshot of the longitudinal interfaces immediately prior to fragmentation. Red dots correspond to broken bonds. C) Histogram of the strain distance for all 50 simulations. The colors shown in the histogram follow the same color scale as in B). Stretched bonds are positive and compressed bonds are negative (i.e. green bonds are at their resting length, yellow bonds are stretched, and blue bonds are compressed). D), E), and F) Same as above for cofilactin. Cofilin molecules and other interfaces are present, but not drawn for ease of viewing. G), H), and I) Same as above for boundaries. Note that the scale for the x-axes in panels A, D, and G differ. The offset for the y-axes in these panels differs, but the scale is the same.

**TABLE 4.2 Pre-fragmentation filament energies and rupture forces**

Deformation	Filament Type	$E_{\text{elastic,fil}}/\Delta G^{\ddagger}_{\text{native}}$	$E_{\text{broken,fil}}/\Delta G^{\ddagger}_{\text{native}}$	Rupture Force (pN)
		(pre-fragmentation)	(pre-fragmentation)	
<b>Compression</b> (N = 50)	Actin	0.26 ± 0.03	0.15 ± 0.03	35.6 ± 0.9
	Cofilactin	0.24 ± 0.03	0.19 ± 0.06	7.2 ± 0.2
	Boundary	0.16 ± 0.02	0.028 ± 0.027	13.6 ± 0.7
<b>Extension</b> (N = 20)	Actin	0.30 ± 0.03	0 ± 0	760 ± 20
	Boundary	0.029 ± 0.007	0 ± 0	290 ± 30
				<b>Rupture Torque (pN nm)</b>
<b>Over-twist</b> (N = 20)	Actin	0.19 ± 0.02	0.13 ± 0.08	460 ± 30
	Boundary	0.12 ± 0.03	0.004 ± 0.008	250 ± 40
<b>Under-twist</b> (N = 20)	Actin	0.27 ± 0.01	0.14 ± 0.03	350 ± 30
	Boundary	0.13 ± 0.03	0.01 ± 0.01	200 ± 50

angle) and the length of time the interfaces across the fragmentation interface are partially broken.

Compressive loads fragment boundaries before any significant bond rupture occurs (Figure 4.2E, F), in contrast to bare or fully-decorated filaments. For these simulations, the boundary is placed off-center to maximize curvature (and severing) at the boundary (as placing it in the center yields maximum curvature within cofilactin), but a filament with a centrally-placed boundary will still preferentially fragment at the boundary (Figure 4.3). The activation energy of fragmentation is considerably lower at boundaries, because the longitudinal actin-actin contacts are weaker (like cofilactin) but they lack the stabilizing cofilin-actin contacts seen in fully-decorated filaments (Kudryashov et al., 2006). Consequently, few bonds rupture before complete filament fragmentation, as a small increase in elastic strain energy at this site is sufficient to promote severing at small deflections. In other words, the boundaries are more brittle than bare or cofilactin filaments.

#### *Fragmentation of extended and twisted filaments*

We next studied the effect of extension on bare actin filaments and actin-cofilactin boundaries. Filaments (100 nm) were stretched by fixing the positions of the molecules on one end of the filament and moving the other end away, while not allowing rotation (Figure 2.5). The strain energy across extended filaments is uniform, aside from a small spike in elastic strain energy at the boundary (Figure 4.4). The rupture location is random for bare actin, but always occurs at the boundary of partially decorated filaments. Very few, if any, individual links rupture prior to fragmentation because the bonds are all evenly strained under filament extension (Figure 4.5, Table 4.2).

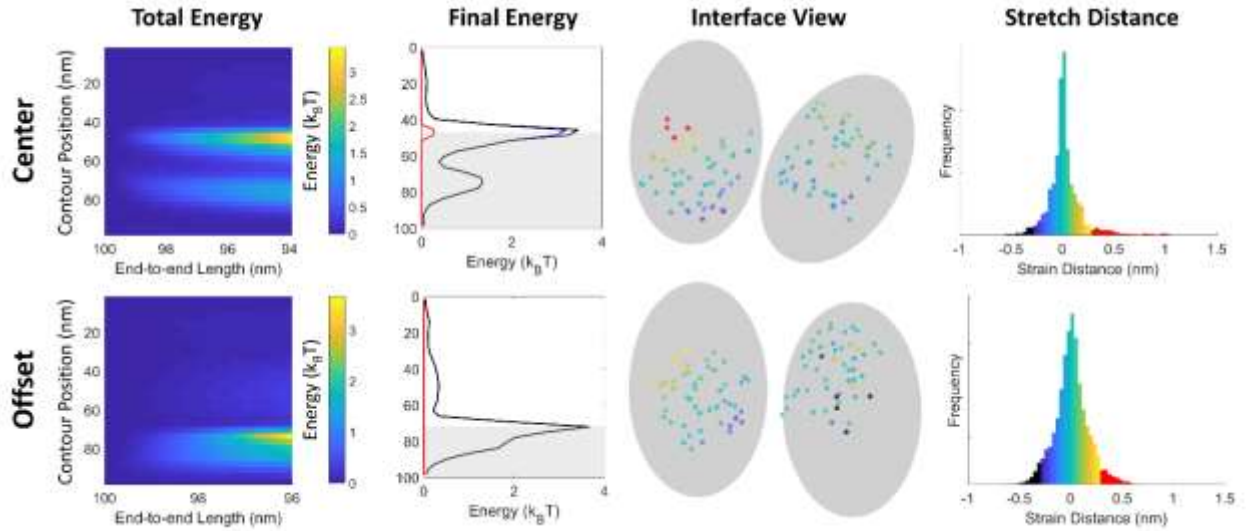


FIGURE 4.3 Effect of the boundary placement of compressed filaments. The total energy column shows the energy across the filament vs the end-to-end displacement. The colors correspond to the adjacent color bar. Final energy is the energy across the filament immediately prior to fragmentation, and the shading shows where cofilin is located.  $E_{broken,fil}$  – red,  $E_{elastic,fil}$  – blue,  $E_{strain,fil}$  – black. The interface view shows the spatial strain on the interface immediately prior to fragmentation for an example simulation. The stretch distance column shows the cumulative histogram across 10 simulations. Positive values are stretched, negative values are compressed. The colors on the stretch distance histogram correspond to the bond colors for the interface view. Red bonds and bars on the histograms are broken bonds.

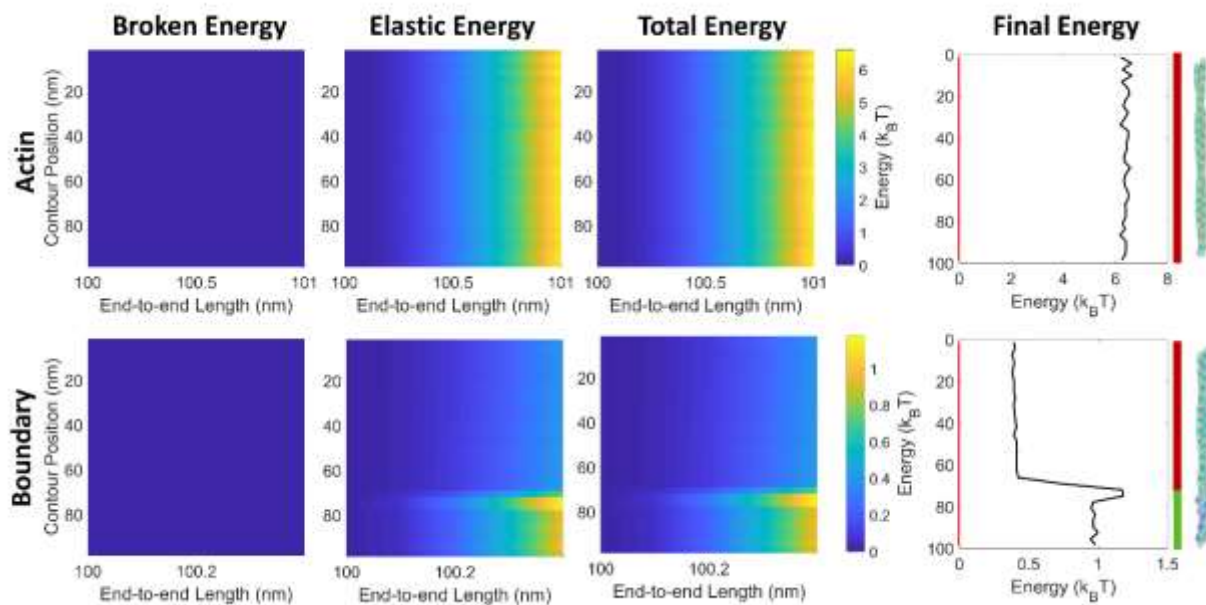


FIGURE 4.4 Simulations of a 100 nm extended bare actin filament (top rows) and a filament with a boundary (bottom rows). Final energy corresponds to the energy just prior to rupture.  $E_{broken,fil}$  – red,  $E_{elastic,fil}$  – blue,  $E_{strain,fil}$  – black. Lines to the right of the final energy show the location of actin (red) and cofilactin (green) for each distribution. The final filament configuration is shown on the right edge of the figure.

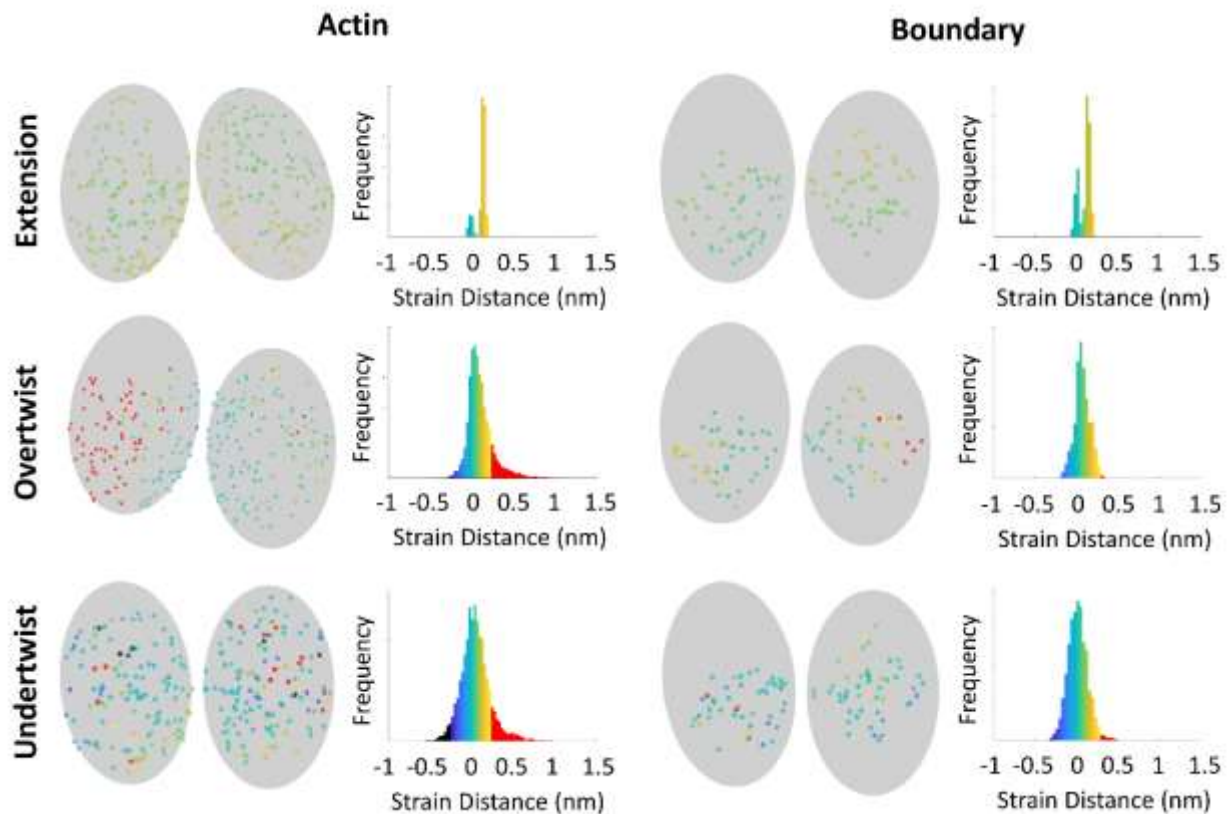


FIGURE 4.5 Strain distribution of extended and twisted filaments (rows) within longitudinal interfaces of the rupture cross section. The histograms show the distribution of strain distance for all bonds in the fragmentation interfaces of actin and actin-cofilactin boundaries (columns, 20 simulations for each). The colors on the histogram correspond to the strain distances for the longitudinal interfaces shown to the left of each histogram (1 example simulation). Red bonds are broken and histogram bars depict broken bonds.

Actin-cofilactin boundaries fragment more rapidly than bare actin, and are more sensitive to tension (Figure 4.6A). Fragmentation rates were calculated for a center (or boundary) interface during twist (Eq. 8). Low tension (less than 100 pN) has minor effects on fragmentation (less than 10-fold), as seen in wet-lab experiments (Wioland, Jegou, & Romet-Lemonne, 2019b). This holds for both bare actin interfaces and boundary interfaces, though boundaries are more affected by tension above this threshold.

We then twisted 100 nm filaments by fixing the positions of both ends and rotating the two actin molecules on each end (Figure 2.5). The strain energy across twisted filaments is uniform, save a small spike in elastic strain energy at boundaries (Figure 4.7). The fragmentation site for twisted filaments is random in bare actin, but is consistently at an actin-cofilactin boundary, if present.

Boundaries are also more susceptible to fragmentation by torsion than bare actin, as when under extensional stress. Under-twisting (i.e., left-handed rotation against actin's natural right-handed twist) filaments promotes fragmentation more than over-twisting (right-handed rotation) by the same number of turns for both bare actin and boundaries (Figure 4.6B). Fragmentation rate constants were calculated for a center (or boundary) interface during extension using Eq. 8. Small torques are predicted to have little effect on bare actin or boundaries.

We also evaluated the effects of simultaneous twist and extension (Figure 4.6C). Over-twisting has a slightly higher effect on filament stability under tension (~15% decrease vs. ~8% for under-twisting 5 rotations/ $\mu\text{m}$ ). Our model suggests that bare actin filament stability under tensile loads is only modestly affected by twist, contrary to previous reports which report a large effect from smaller twists (Tsuda et al., 1996). The

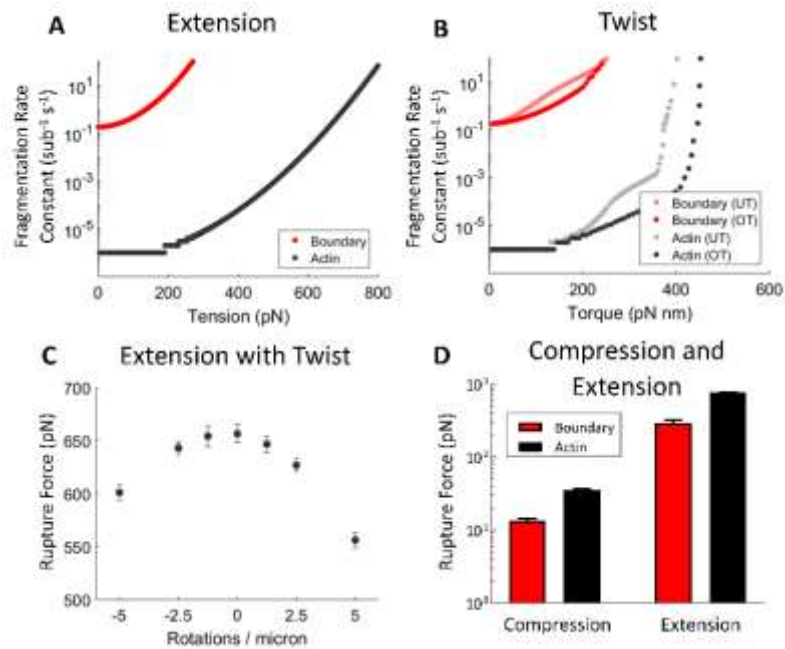


FIGURE 4.6 Comparison of rupture properties between actin and actin-cofilactin boundaries. A) Individual simulation trace of the severing rate constant of a bare actin filament and filament boundary interface under tension (without individual bond rupture). B) Individual simulation trace of the severing rate constant of an interface within a twisted bare actin filament and at a filament boundary, allowing individual bond rupture. Data is shown for both under-twisted (UT) and over-twisted (OT) filaments. C) Effect of twist on extensional rupture force. Positive values refer to over-twist. The rupture force is defined as the force at which the rupture rate constant is  $0.1 \text{ s}^{-1}$ . Uncertainty bars show the standard deviation of extensional rupture force for each twist ( $N=10$ ). D) Compression and extensional rupture forces. Uncertainty bars show the standard deviation of rupture force for compression ( $N=50$ ) and extension ( $N=20$ ). Rupture forces are the maximum force prior to rupture for deformations applied as outlined in the main text. Note that the Y-axis is on a logarithmic scale.

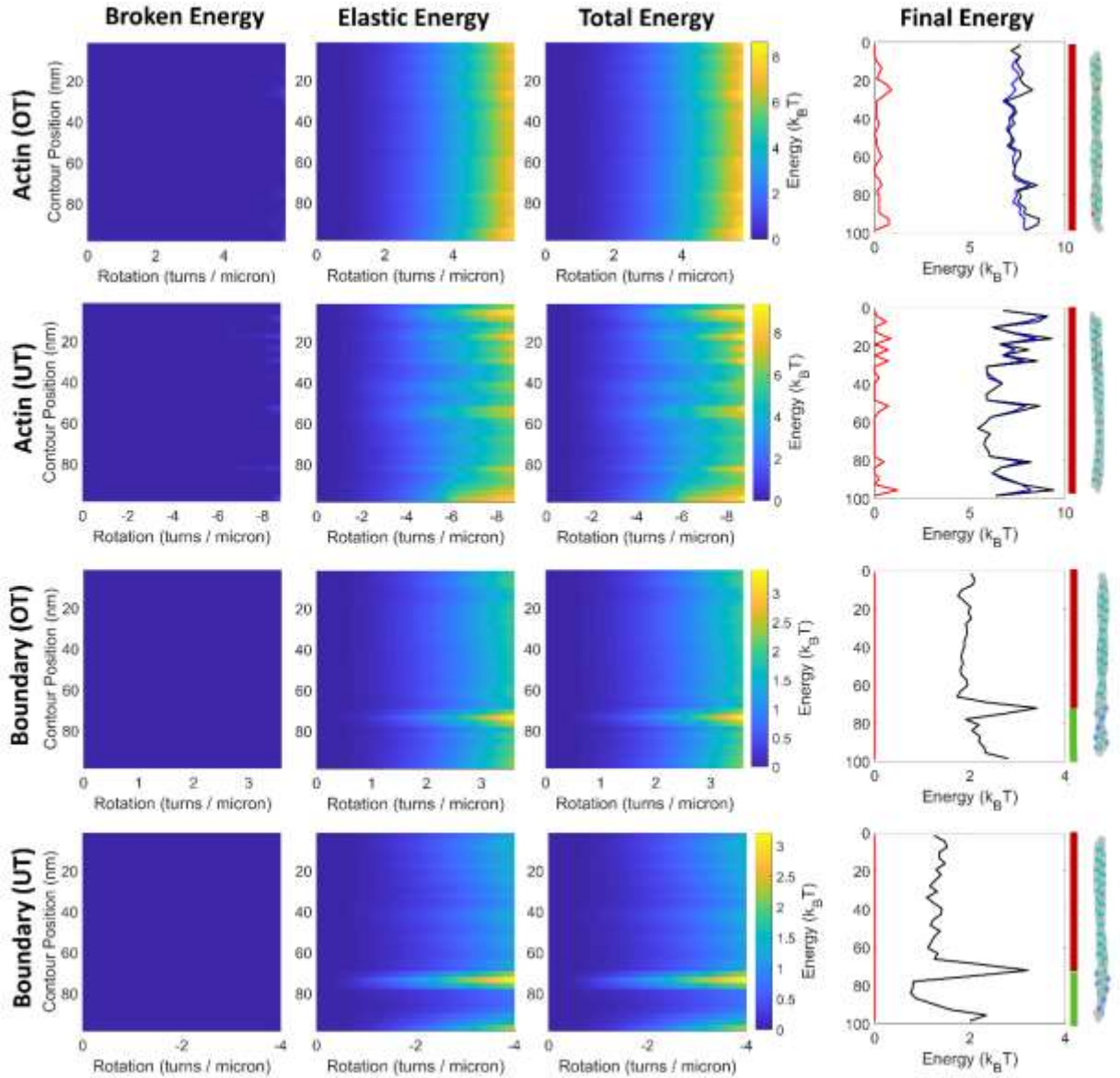


FIGURE 4.7 Simulations of a 100 nm twisted bare actin filament (top two rows) and a filament with a boundary (bottom two rows). Filaments are either over- (rows 1 and 3, OT) or under-twisted (rows 2 and 4, UT). Final energy corresponds to the energy just prior to rupture.  $E_{broken,fil}$  – red,  $E_{elastic,fil}$  – blue,  $E_{strain,fil}$  – black. Lines to the right of the final energy show the location of actin (red) and cofilactin (green) for each distribution. The final filament configuration is shown on the right edge of the figure.

reasons for the discrepancy between the results from this study and those presented here are not clear. However, such the high sensitivity to twist is surprising given the actin filament torsional stiffness which the authors state is  $8 \times 10^{-26} \text{ Nm}^2$ . A twist of one rotation ( $2\pi$ ) on a 10 micron filament (as used in the study) adds  $\sim 1.6 \times 10^{-19} \text{ J}$ , or  $\sim 38 \text{ k}_B\text{T}$  (at 298 K), of energy throughout the entire filament ( $E = \frac{1}{2} \frac{C}{L} \theta^2$ , where C is the torsional rigidity, L is the length of the filament, and  $\theta$  is the twist in radians). If this energy distributes uniformly among the  $>7000$  filament interfaces (longitudinal and lateral) in a 10-micron filament, each would experience  $< 0.01 \text{ k}_B\text{T}$  of strain energy from this twist, which is much smaller than thermal energy. Additionally, this would only add an additional  $0.1^\circ$  twist per subunit rise, far less than the estimated  $2.9^\circ$  degree deviation per subunit for even straightened (and less heterogenous) filaments visualized by cryo-electron microscopy (Vitold E. Galkin, Orlova, Vos, Schröder, & Egelman, 2015).

#### *Critical bending angle of filament fragmentation*

We measured the critical angle of fragmentation for compressed filaments to compare our simulations to previous experiments (McCullough et al., 2011). In these simulations the critical angle was measured by measuring the angle between the ends of a compressed 100 nm filament immediately prior to filament fragmentation (Figure 4.8). The relationship between critical angles is similar to that previously measured ( $\theta_{\text{crit,cofilactin}} > \theta_{\text{crit,actin}} > \theta_{\text{crit,boundary}}$ ) though the curvature required for rupture is about 50-100% greater for boundaries and cofilactin (Figure 4.8). As previously discussed (McCullough et al., 2011), cofilactin filaments are more compliant in bending than bare actin, and thus require

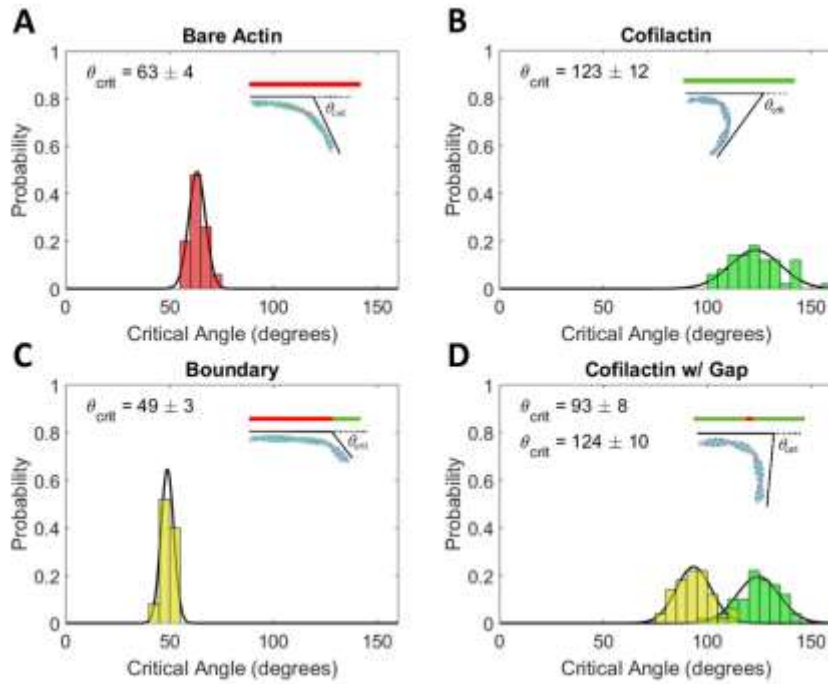


FIGURE 4.8 Critical severing angle distributions of actin and cofilactin filaments. Histograms are shown of the angle between the ends of 100 nm filaments of A) bare, B) fully decorated, C) 25% decorated filaments, and D) fully decorated filaments with a single missing cofilin. Colors in panel D show severing events at the cofilin gap (yellow) and within cofilactin (green). Insets are illustrative of cofilin distribution (green) relative to bare actin (red). Insets also show an example filament at the critical angle (at the gap for panel D). Each distribution is sampled from 50 independent simulations (100 for cofilactin with gap) and critical angles are calculated by a fit to a normal distribution (black lines).

larger bending deformations for an equal amount of strain energy to accumulate and accelerate fragmentation.

### 4.3 DISCUSSION

#### *Filament fragmentation angles*

Measuring the critical fragmentation angle gives us insight into the bimodal distribution of cofilactin rupture angles found in the experiments by McCullough, et al (McCullough et al., 2011). Experiments performed at saturating cofilin concentrations are not truly saturating, but are instead at 90-95% occupancy (Cao et al., 2006). This leaves small gaps in the cofilin distribution along the filament undetectable by fluorescence microscopy. We found that one missing cofilin molecule in the center of an otherwise decorated filament recovered a bimodal distribution (Figure 4.8D). The cofilin gap was the most frequent point of fragmentation and involved in nearly 50% of the total fragmentation events (yellow). The other 50% occurred somewhere else on the filament, most often near the center, similar to cofilactin (green). The relative shift between these peaks is similar in magnitude to the shift between critical fragmentation angles of actin and boundaries. This suggests that the gap resembles a boundary, but the higher flexibility of cofilactin means a larger overall deformation must be applied to reach a similar local strain/fragmentation rate. This effect was originally attributed an alternate binding mode in which cofilactin adopts actin-like mechanical properties, and thus severs at a similar angle to bare actin. While this potential explanation cannot rule out the previous interpretation, it serves as an additional explanation for the observed behavior.

The difference in absolute angles may arise for multiple reasons. Cofilactin filaments may be slightly less stable than actin filaments (we assumed the rate constant of fragmentation was the same), which would lead to a higher critical fragmentation angle in our experiments. In addition, the distance over which the angle is measured for a given radius of curvature affects the value of the critical angle. This value is difficult to determine for optical microscopy, so the 100 nm used here should be considered a rough estimate. Lastly, the previously measured critical angle is for freely fluctuating filaments, meaning that the results are convoluted with the probability of reaching a given angle.

*Actin-cofilactin boundaries are brittle and fragment at low bending angles*

Strained filament boundaries fragment immediately adjacent to sites of cofilin clusters prior to significant interface rupture. The boundary is characterized by a brittleness that leads to quick rupture at a lower bending angle and less interface remodeling than either bare or fully cofilin-decorated. Due to the parameters used in constructing the model, the boundary interfaces fragment more rapidly (lower  $\Delta G^\ddagger$ ) than the adjacent fully-decorated or bare actin segments. The interfaces that do exist (longitudinal and lateral) have the relative weakness of cofilactin (Table 2.1), but lack the additional cofilin-actin bonds (Figure 2.3A). This choice, was not arbitrary, but based on observations of enhanced fragmentation at boundaries (Wioland et al., 2017; Wioland et al., 2019a) and twist propagation into the bare regions adjacent to areas of cofilin decoration (Huehn et al., 2018; Ngo, Koder, Katayama, Ando, & Uyeda, 2015). In addition to the higher intrinsic fragmentation rate of the boundaries, the mechanical weakness of this joint localizes strain to the boundary and further accelerates fragmentation (Figure 3.5).

These simulations show that a propagation of these cofilactin structural changes and the resulting longitudinal interface weakness just 2 subunits into bare actin (1 subunit on each strand, Figure 2.3A) is sufficient to capture the observed enhancement of fragmentation at bare and fully decorated boundaries. The loss of the D-loop interactions in actin adjacent to cofilin clusters is the likely cause of weak boundaries, both in stiffness and stability (Grintsevich et al., 2016; Muhlrads et al., 2004; Umeki et al., 2016). This is implemented in our model with the smaller longitudinal interface area and weaker spring stiffness in cofilactin. While the interface energies of barbed- and pointed-end boundaries are identical in our model, the effect shown here may more closely resemble the weaker, pointed end boundary (Wioland et al., 2017).

*Plastic deformation precedes fragmentation of compressed filaments*

For small deformations, the interface is stressed elastically (elastic regime, Figure 4.9B). In this regime we do not expect any large-scale structural rearrangements, although there may be a shift in the equilibrium between energetically similar configurations (e.g. the D-loop of an actin subunit docking/undocking with the adjacent subunit). For larger deformations, some regions of the protein interface are ruptured/dissociated (plastic regime, Figure 4.9C). This is likely the point of irreversibility for network compression.

Partial interface rupture is also likely to occur due to thermal fluctuations even in the absence of external load, but the broken bonds would reform as the filament relaxes. Under constant load, as applied in this study, these filaments are not allowed to relax (i.e. “heal”).

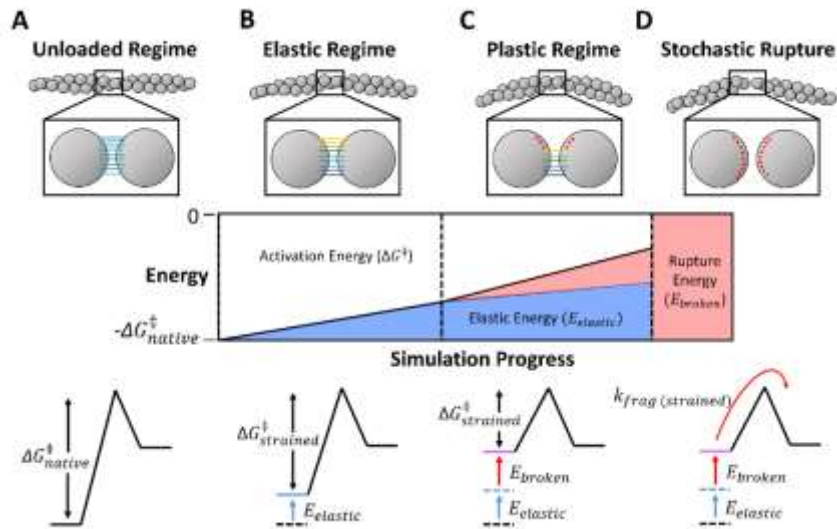


FIGURE 4.9 Schematic of compressed filament fragmentation. Column A shows the interface of a filament under no external load. Column B shows the elastic regime, where bonds within interfaces are strained, decreasing the activation energy of fragmentation ( $\Delta G^\ddagger$ ). Column C shows the plastic regime where bonds rupture and further decreases the activation energy. Column D describes the stochastic fragmentation which occurs at the rate  $k_{frag}$ . Fragmentation can occur at any point during the simulation, but the rate constant increases with reductions in  $\Delta G^\ddagger$ , according to Eq. 8. The energies shown in the bottom two rows refer to the total energy across the filament cross section. These cross-section energies are used to calculate the rate of filament fragmentation at each time step (Eq. 9). The actual values shown in the energy diagrams here are illustrative and not equal to the actual simulation values.

*High filament curvature partially disrupts long-axis actin subunit contacts and could potentially enhance cofilin binding kinetics*

Our results show that bending filaments localizes strain both along the filament (due to the filament helicity) and within the interface, due to the orientation of proteins in a given point along the helix. The two contributions combine to specifically enhance strain in a region that spatially corresponds to contacts between subdomain 1 and subdomain 2 of the adjacent filament subunit (Figure 4.10A, B). That is, these bonds are at the convex edge of the most curved/strained filament regions (Figure 4.1).

This localized strain likely destabilizes contacts in the D-loop region, shifting the equilibrium to more D-loop undocking, even prior to bond rupture in this model (Figure 4.2D). Consequently, we predict that high curvature may accelerate cofilin association kinetics due to the linkage between cofilin binding and D-loop destabilization (Grintsevich et al., 2016; Hocky et al., 2016; Muhlrads et al., 2004; Umeki et al., 2016). In contrast, filament tension uniformly strains actin-actin interfaces, so we do not predict that filament tension affects cofilin affinity, as reported for low tensile loads (Wioland et al., 2019b). Additionally, this observation provides a link between the observed bias for Arp2/3 binding on curved filaments and structural observations of the complex on actin filaments (Pfaendtner et al., 2012; Risca et al., 2012).

One caveat to these findings is that the D-loop is docked in the cryo-EM structures that were used for obtaining the longitudinal interface stiffness. This may have the effect of overestimating the longitudinal bond stiffness, and therefore overestimating the effect that a loss of bonds in the D-loop region may have. In any case, bending deformations are likely to shift the D-loop conformation further to the undocked state.

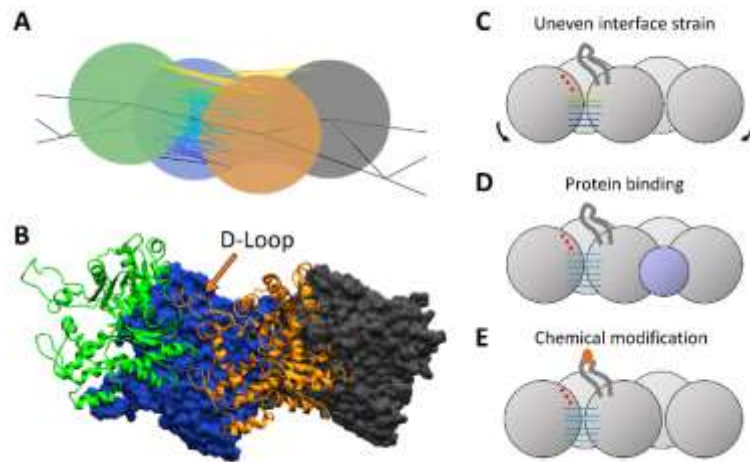


FIGURE 4.10 Strain localization predicts importance of the D-loop for bare actin filament bending rupture. A) Snapshot of the most strained longitudinal interfaces of a compressed actin filament and B) the corresponding structure of the actin filament (PDB ID 2ZWH) oriented with the pointed end to the left. The highest strain in bent filaments is between subdomain 2 and subdomain 1 of the adjacent monomers. This region spatially corresponds to the location of the D-loop. Interface disruption can be caused by C) uneven application of force on an interface, D) protein (cofilin) binding, leading to a structural change, and E) chemical modification of amino acids (as by MICAL).

*Partial rupture of protein interfaces may be a general mechanism to disrupt stable protein-protein interactions.*

For any stable protein-protein interaction, uneven interface strain and partial bond rupture may be necessary to facilitate interface fragmentation at reasonable time scales and forces. This observation is exemplified by actin, where partial interface disruption is used to enhance fragmentation in multiple ways. Filament compression strains the filament interface unevenly, which leads to partial interface fragmentation (Figure 4.2, 7C). In contrast, tension strains the longitudinal interfaces uniformly, which effectively means the entire interface must be stretched nearly to the point of failure before fragmentation (Figure 4.5). Because of the difference in how load is applied to interfaces, the extensional rupture force is over an order of magnitude higher than the force required to fragment compressed filaments (Figure 4.6D, Table 4.2 (Berro et al., 2007; Medeiros et al., 2006; Tsuda et al., 1996; Van Goor et al., 2012)).

Proteins that sever actin filaments also act by weakening long-axis contacts. Cofilin is thought to accelerate fragmentation of actin filaments by disrupting D-loop contacts of a filament subunit with its long-axis neighbor, weakening the interface energy at actin-cofilactin boundaries (Figure 4.10D (Tanaka et al., 2018)). Similarly, the actin destabilizing enzyme MICAL performs its role by reversibly oxidizing methionine residues in the D-loop of F actin monomers to inhibit these contacts (Figure 4.10E) (Grintsevich et al., 2017; Grintsevich et al., 2016; Hung et al., 2011). The similarities between these distinct mechanisms of fragmentation suggest that a similar partial rupture pathway may apply to other actin-related fragmentation events (e.g. forces on the Arp2/3 complex

causing debranching), and that this theme is likely ubiquitous in biology for interactions that require large modulations of stability.

#### *Effect of filament length*

We chose to simulate 100 nm filaments to compromise between longer filaments and quick simulation time. To test whether this choice had an effect on our conclusions we ran simulations of compressed filaments of 50 (75 nm for bare actin), 100, and 150 nm (Figures 4.11-4.13, Table 4.3). We used 75 nm instead of 50 nm filaments for actin because the rigidity of the 50 nm filaments led to artifacts (overlapping subunits) when we compressed them. The strain energy of the fragmented interfaces prior to fragmentation are very similar (Table S4). The fragmentation angle and rupture force scale with the filament length, but the trends between the types of filaments remain the same.

#### *Effect of bond density*

A very low number of bonds between proteins can lead to spurious behavior in our simulations (e.g. actin subunit overlap) because individual links are free to rotate. A single bond in an interface would be free to sample a number of configurations without any energetic cost, as an extreme example of this. To minimize the frequency of such behavior, we chose a relatively high density of bonds between proteins (Figure 4.14, Table 4.4). We ran a series of controls to determine whether this choice had an effect on our experimental results. Low bond density seems to allow filaments to break slightly sooner in the compressive process, with a lower fragmentation angle and pre-fragmentation strain energy. The variance for these measures shown in Table 4.4 also

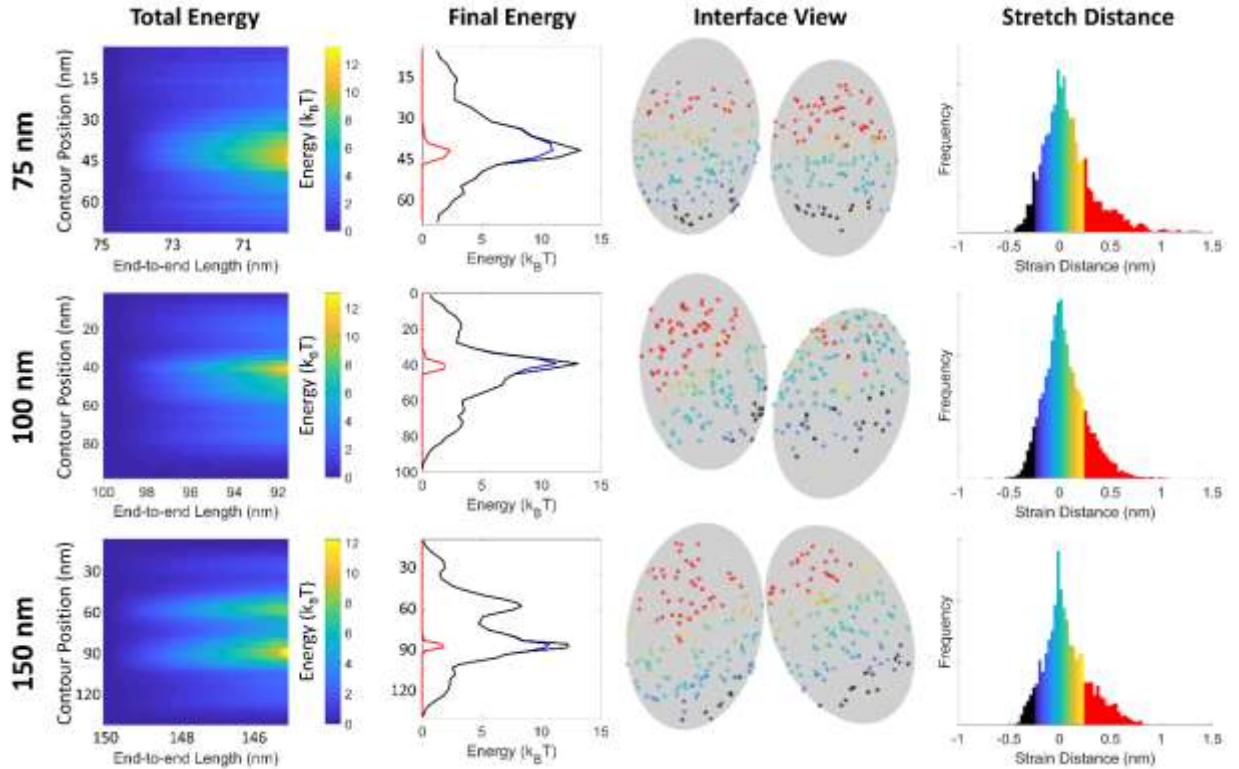


FIGURE 4.11 Effect of filament length (rows) on simulations of compressed actin filaments. The total energy column shows the energy across the filament vs the end-to-end displacement. The colors correspond to the adjacent colorbar. Final energy is the energy across the filament immediately prior to fragmentation.  $E_{broken,fil}$  – red,  $E_{elastic,fil}$  – blue,  $E_{strain,fil}$  – black. The interface view shows the spatial strain on the interface immediately prior to fragmentation for an example simulation. The stretch distance column shows the cumulative histogram across 10 simulations. Positive values are stretched, negative values are compressed. The colors on the stretch distance histogram correspond to the bond colors for the interface view. Red bonds and bars on the histograms are broken bonds.

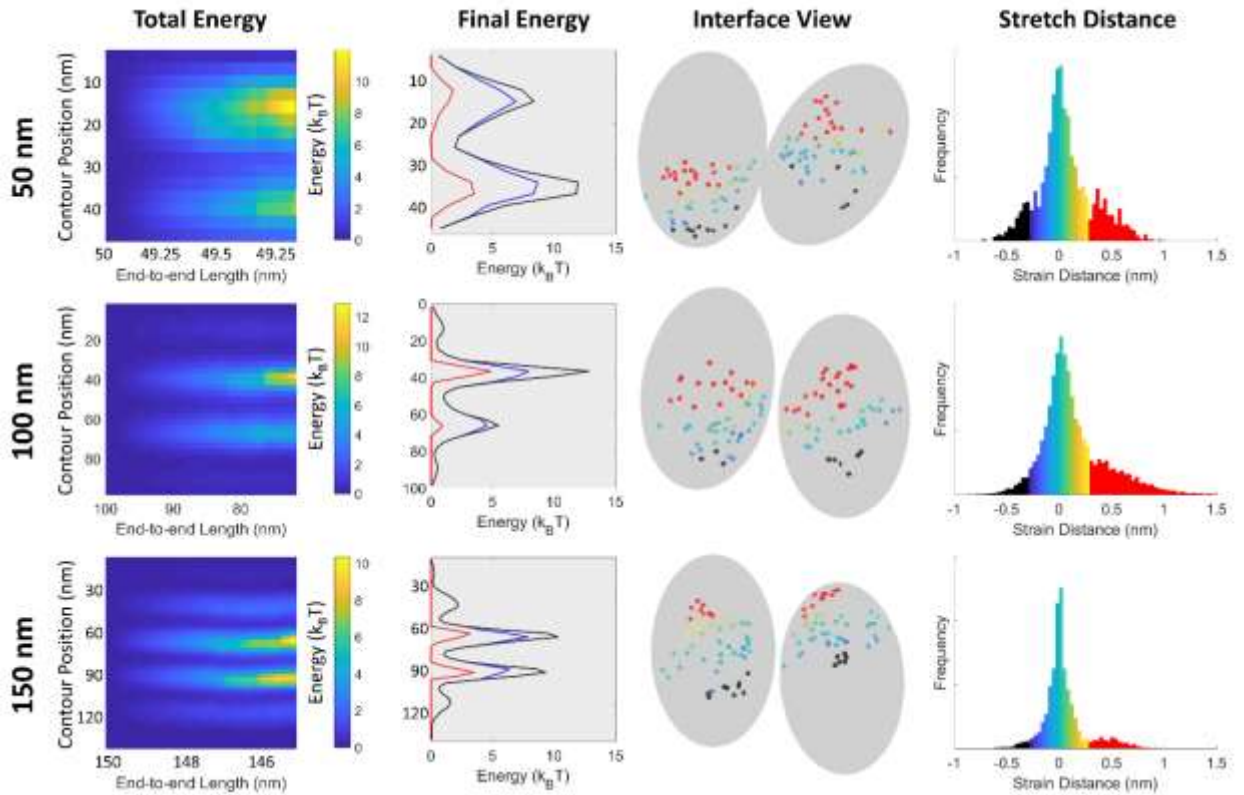


FIGURE 4.12 Effect of filament length (rows) on simulations of compressed cofilactin filaments. The total energy column shows the energy across the filament vs the end-to-end displacement. The colors correspond to the adjacent colorbar. Final energy is the energy across the filament immediately prior to fragmentation.  $E_{broken,fil}$  – red,  $E_{elastic,fil}$  – blue,  $E_{strain,fil}$  – black. The interface view shows the spatial strain on the interface immediately prior to fragmentation for an example simulation. The stretch distance column shows the cumulative histogram across 10 simulations. Positive values are stretched, negative values are compressed. The colors on the stretch distance histogram correspond to the bond colors for the interface view. Red bonds and bars on the histograms are broken bonds.

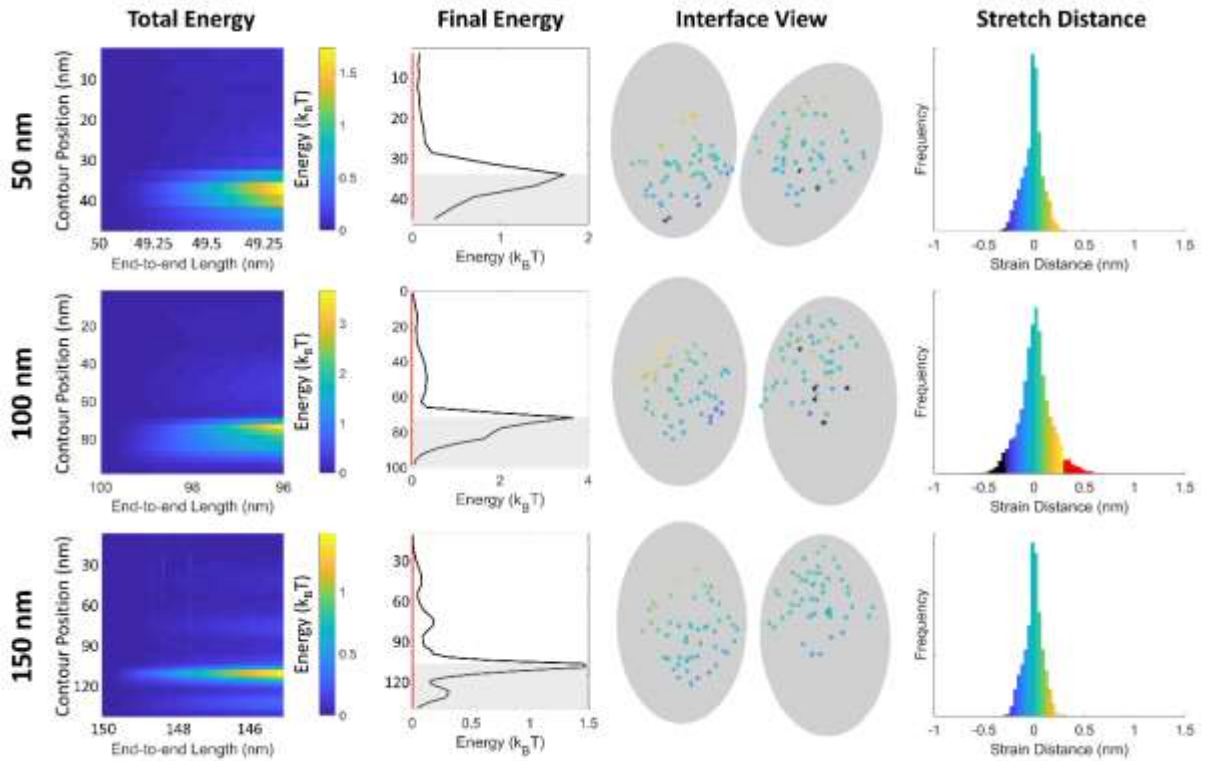


FIGURE 4.13 Effect of filament length (rows) on simulations of compressed filaments with a boundary. The total energy column shows the energy across the filament vs the end-to-end displacement. The colors correspond to the adjacent colorbar. Final energy is the energy across the filament immediately prior to fragmentation, and the shading shows where cofilin is located.  $E_{broken,fil}$  – red,  $E_{elastic,fil}$  – blue,  $E_{strain,fil}$  – black. The interface view shows the spatial strain on the interface immediately prior to fragmentation for an example simulation. The stretch distance column shows the cumulative histogram across 10 simulations. Positive values are stretched, negative values are compressed. The colors on the stretch distance histogram correspond to the bond colors for the interface view. Red bonds and bars on the histograms are broken bonds.

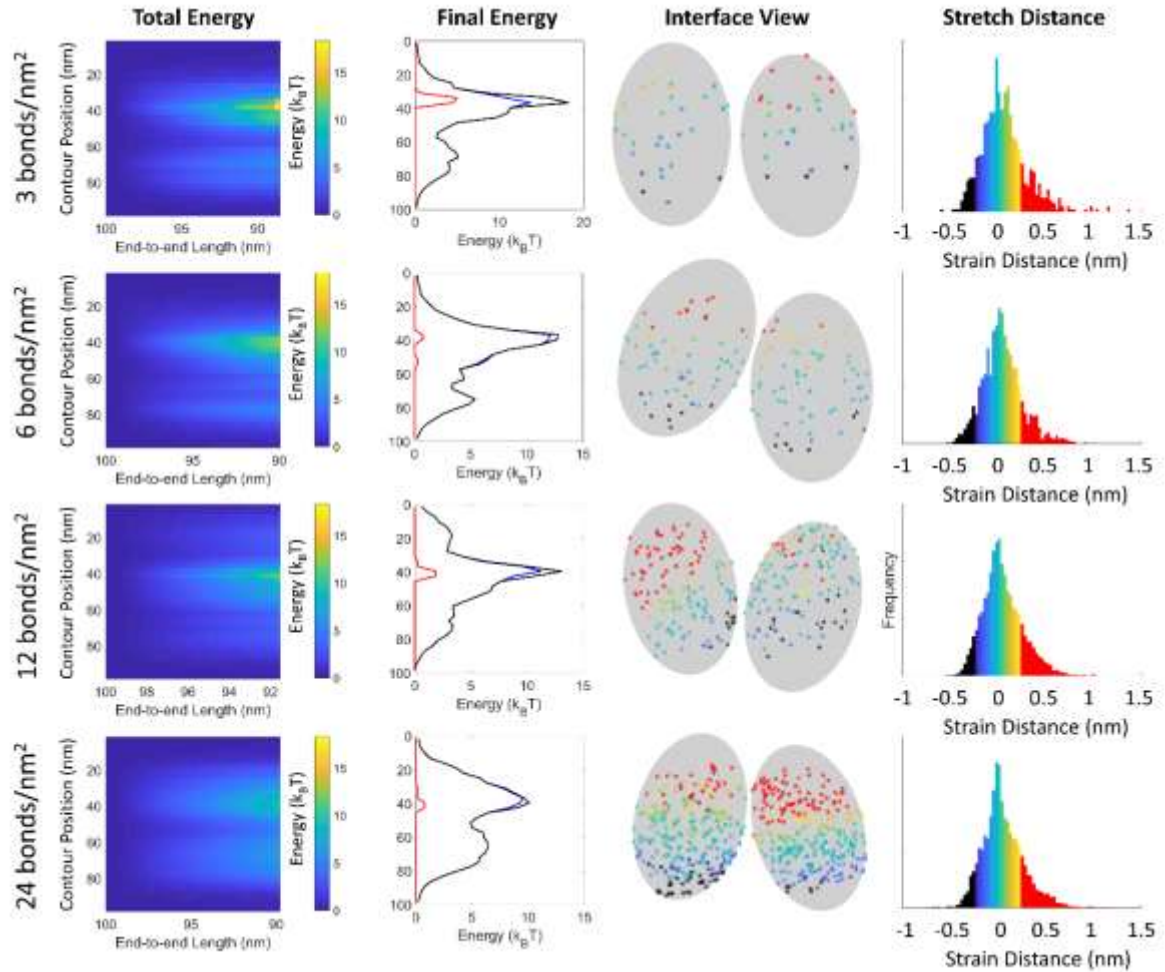


FIGURE 4.14 Effect of bond density (rows) on simulations of compressed actin filaments. The “Total Energy” column shows the energy across the filament vs the end-to-end displacement. The colors correspond to the adjacent colorbar. Final energy is the energy across the filament immediately prior to fragmentation.  $E_{broken,fil}$  – red,  $E_{elastic,fil}$  – blue,  $E_{strain,fil}$  – black. The interface view shows the spatial strain on the interface immediately prior to fragmentation for an example simulation. The stretch distance column shows the cumulative histogram across 10 simulations. Positive values are stretched, negative values are compressed. The colors on the stretch distance histogram correspond to the bond colors for the interface view. Red bonds and bars on the histograms are broken bonds. 12 bonds/nm<sup>2</sup> was the bond density used for simulations in the main text.

**TABLE 4.3 Length effects on compressive simulations**

<b>Filament type (length (nm))</b>	<b>Fragmentation Angle (degrees)</b>	<b><math>E_{\text{elastic,int}}/\Delta G^{\ddagger}_{\text{int,native}}</math> (pre-fragmentation)</b>	<b><math>E_{\text{broken,int}}/\Delta G^{\ddagger}_{\text{int,native}}</math> (pre-fragmentation)</b>	<b>Rupture Force (pN)</b>
<b>Actin (75)</b>	48 ± 3	0.27 ± 0.02	0.18 ± 0.03	53.1 ± 1.4
<b>Actin (100)</b>	63 ± 4	0.26 ± 0.03	0.15 ± 0.03	35.6 ± 0.9
<b>Actin (150)</b>	88 ± 7	0.25 ± 0.01	0.18 ± 0.07	15.4 ± 0.1
<b>Cofilactin (50)</b>	78 ± 9	0.23 ± 0.03	0.11 ± 0.04	21.8 ± 0.7
<b>Cofilactin (100)</b>	123 ± 12	0.24 ± 0.03	0.19 ± 0.06	7.2 ± 0.2
<b>Cofilactin (150)</b>	161 ± 9	0.19 ± 0.03	0.12 ± 0.04	3.7 ± 0.1
<b>Boundary (50)</b>	20 ± 3	0.09 ± 0.02	0.0 ± 0.0	26.4 ± 2.6
<b>Boundary (100)</b>	49 ± 3	0.16 ± 0.02	0.028 ± 0.027	13.6 ± 0.7
<b>Boundary (150)</b>	38 ± 5	0.07 ± 0.02	0.0 ± 0.0	7.2 ± 0.2

**TABLE 4.4 Density effects on compressed actin filaments**

Density	Fragmentation Angle (degrees)	$E_{\text{elastic,int}}/\Delta G_{\text{int,native}}^{\ddagger}$ (pre-fragmentation)	$E_{\text{broken,int}}/\Delta G_{\text{int,native}}^{\ddagger}$ (pre-fragmentation)	Rupture Force (pN)
3 links / nm <sup>2</sup>	59.6 ± 7	0.31 ± 0.5	0.13 ± 0.6	27.7 ± 1.5
6 links / nm <sup>2</sup>	62.9 ± 6	0.30 ± 0.3	0.14 ± 0.5	30.3 ± 0.7
12 links / nm <sup>2</sup>	63 ± 4	0.26 ± 0.03	0.15 ± 0.03	35.6 ± 0.9
24 links / nm <sup>2</sup>	66 ± 4	0.28 ± 0.03	0.16 ± 0.02	32.2 ± 0.3

tend to be higher for the lower bond densities, which is likely due to these interfaces being less uniform. However, the differences in the fragmentation angle and strain energies are much less than between bare actin, cofilactin, and boundaries, so we do not expect this choice of bond density to affect our conclusions.

#### *Effect of actin-cofilactin boundary placement*

We compared simulations where we placed actin-cofilactin boundaries in the center and offset as in the main text (Figure 4.3). Filaments with a center boundary fragment slightly less effectively ( $54 \pm 21$  degrees, for 10 simulations) compared to the offset boundary ( $49 \pm 3$  degrees, for 25 simulations). One reason is because of differences in the filament shape (whether the boundary coincides with an area of high curvature). A second reason is that bare actin is stiffer, so a filament with a higher amount of bare actin (75% of the length, in the offset case) will store more energy for a given deformation. This will lead to the boundary breaking sooner.

#### *Effect of cofilin gap size*

In our discussion of the bimodal distribution of cofilactin fragmentation angles we have implicated small gaps in a fully-decorated filament as the cause of the more easily fragmented population. In Figure 4.8 we simulated cofilactin filaments with a single missing cofilin, but it is possible that larger gaps could exist on the filament. We also ran multiple simulations (25 each) to find the rupture angle of filaments with two or three adjacent missing cofilins to compare to the single gap case. We measured filament rupture for cofilactin with gaps of two or three adjacent missing cofilin molecules and found critical angles of  $45 \pm 14$  degrees and  $42 \pm 13$  degrees, respectively. Both of these are close to the fragmentation angle of boundaries that we measured. This is unsurprising, as the

stiffness and fragmentation rates of these segments are the same as our measured boundaries. A single missing cofilin seems to more closely resemble the experimental result (a difference of ~20 degrees between the two fragmentation populations (McCullough et al., 2011)), but a more confident assessment would require better structural information for these small gaps to inform our model.

## CHAPTER 5: Summary and Conclusions

The effect of force on actin filaments and actin binding proteins has become widely embraced by the actin field in the past decade. Because of actin's involvement in a plethora of force generating processes that often involve visible deformations of the cell membrane, researchers have realized that understanding how these processes are regulated by force is essential. The cellular structures that generate these forces are highly dynamic, and they rely on constant turnover of actin. Unsurprisingly, it is speculated that force plays a role in actin turnover. The effect of force on actin filament fragmentation is a key component of this turnover.

The cofilin/ADF family of proteins has long been implicated in actin filament fragmentation and depolymerization. Until recently, the majority of work to understand cofilin-mediated fragmentation was performed with solutions of purified proteins, or filaments that were affixed to the surface of slides. Since these experiments used the simple system of only purified actin and cofilin, this made it easier to measure intrinsic properties of cofilin such as the binding affinity and severing activity. This prior work showed that cofilin binding was cooperative and fragmentation occurs at boundaries of cofilin-bound and unbound actin. However, like any simplified system, this ignores other contributing factors to the process. In many cases, an additional protein is necessary to understand the system in a biological context, and in this case AIP1 has been shown to enhance cofilin-mediated severing, but force on filaments can be thought of in the same way. In the cell actin usually experiencesr extensional or compressional loads, generated either by the force of polymerization or by myosin. It has been shown that inhibition of myosin II by the small molecule blebbistatin dramatically alters the morphology and

dynamics of lamellipodia-like cellular structures in *Aplysia* bag cell neurons, and that cofilin associates with these structures (Zhang et al., 2019).

These observations taken together show how critical it is to observe and predict the details of fragmentation in the proper force context. This problem is hard to approach traditionally because it requires a means of applying force on individual filaments in a controlled manner, while visualizing the filament along with cofilin. Because of this, computation is a perfect way to explore this phenomenon. The mesoscopic approach I have taken in this dissertation approaches the problem with a blend of computational simplicity and molecular accuracy. Continuum mechanics models, which model filaments as semiflexible (or rigid) rods have been useful for their computational simplicity and relative ease of implementation, but cannot describe molecular details of the severing process. Approaching the problem with all-atom or slightly coarse-grained Brownian dynamics simulations would be ideal, but current computational limits make it difficult to simulate long time scale events such as fragmentation, and it is difficult to accurately apply reasonable magnitudes of force in these models. Additionally, the myriad of interactions in these simulations make it difficult to distinguish relevant changes in these interactions from noise without prior knowledge of which interactions are important.

The model I have developed with my colleague Jean-Louis Martiel for this dissertation has given new insight into the fragmentation of both bare actin and cofilin-mediated actin severing. My model bridges the gap between these two length scales to answer new questions that had yet to be addressed. The helicity of actin filaments was incorporated into this model, and this led to the finding that there is a periodic

enhancement of strain in bent filaments, which is important for strain localization within interfaces, as discussed below (Figure 3.1). Initial predictions showed how a weakness in the actin filament immediately adjacent to the site of cofilin decoration could localize strain at the boundary even more than was previously predicted by continuum mechanics simulations of buckled actin filaments (Figure 3.4). I showed that small patches of cofilin within buckled actin filaments greatly enhanced severing, orders of magnitude more than was previously predicted (Figure 3.5). This model also predicts that cofilin dissociation should be affected by the twist of the filament, but bending exerts little strain on the actin-cofilactin bonds and thus is unlikely to accelerate cofilin dissociation.

Mechanistically, these observations dictate when cofilin will be able to act on filaments. For example, filaments experience small amounts of torque when they are polymerized by formin. This torque will prevent cofilin from binding, which is desirable in this context, where newly formed filaments must be able to grow to exert force. Likewise, it is appropriate that cofilin is unlikely to dissociate from bent filaments because filament bending enhances cofilin severing.

In Chapter 4 I discussed the result of incorporating protein interface bond rupture and filament fragmentation into the model. An important question driving this implementation was how fragmentation progressed in the model. For example, it was unknown if filament would become unstable and completely fragment upon the rupture of a small portion of the interface. We validated our model of fragmentation by comparing the distribution of critical fragmentation angles to experiment (Figure 4.8). Bare and fully-decorated cofilactin filaments undergo plastic deformation (i.e. partial interface rupture) prior to complete fragmentation (Figure 4.2). However, the filaments

get easier to compress as the longitudinal interfaces in the filament begin to rupture and soften, but partial rupture does not necessitate fragmentation at a given bending deformation. Cofilactin-actin boundary interfaces are much more brittle, and fragment at low bending deformations before appreciable partial interface rupture (Figure 4.3, Figure 4.10). This same pattern of partial rupture for homogenous filaments and brittle interfaces holds true for filaments under torsion as well (Figure 4.7). However, stretching filaments strains all interface bonds evenly, and thus leads to the simultaneous rupture of all interface bonds (Figure 4.4). This difference in how strain is applied to interfaces leads to filaments requiring an order of magnitude more force to fragment under tension than compression (Figure 4.6). Critically, I found that the combination of periodic strain (due to filament helicity) and uneven interface strain within bent/compressed actin filaments consistently strains one portion of the actin longitudinal interfaces. Comparison of this highly strained area with actin filament cryo-EM structures shows that its location coincides with the D-loop (Figure 4.10). Consequently, I have proposed that filament bending is likely to affect D-loop docking, and consequently, filament stability. This observation draws parallels with other mechanisms of filament fragmentation, namely filament severing by cofilin and MICAL. Both of these proteins have been shown to affect D-loop docking by either changing the structure of the subunits upon binding (cofilin), or by chemically modifying amino acid residues on the loop (MICAL). Since cofilin binding is linked to changes in the D-loop conformation, this also suggests that high amounts of filament bending strain may lead to a higher rate of cofilin binding to these bent regions. It would be interesting to confirm these findings by all-atom MD

simulations to determine if an application of load leads to enhanced dissociation of the D-loop from the adjacent subunit.

These results suggest a pattern for modulation of binding affinity for actin and actin binding proteins, and possibly for completely different molecules as well. By concentrating strain to a small portion of the protein-protein interface, it becomes relatively easy to fragment actin filaments. Crucially, this may have implications for Arp2/3 complex debranching, as lateral forces on filaments would be likely to apply similar bending deformations to branch points. Similarly, it is possible that so-called “catch bonds” found for some actin binding proteins, which describe binding interactions whose lifetimes increase with force, occur because the interface is put into a more “tension-like” state when under load (and the protein interface is evenly strained), but is free to sample different conformations when relaxed.

## REFERENCES

- Ackbarow, T., Chen, X., Keten, S., & Buehler, M. J. (2007). Hierarchies, multiple energy barriers, and robustness govern the fracture mechanics of alpha-helical and beta-sheet protein domains. *Proc Natl Acad Sci U S A*, *104*(42), 16410-16415. doi: 10.1073/pnas.0705759104
- Agnew, B. J., Minamide, L. S., & Bamburg, J. R. (1995). Reactivation of phosphorylated actin depolymerizing factor and identification of the regulatory site. *J Biol Chem*, *270*(29), 17582-17587. doi: 10.1074/jbc.270.29.17582
- Andrianantoandro, E., & Pollard, T. D. (2006). Mechanism of actin filament turnover by severing and nucleation at different concentrations of ADF/cofilin. *Mol Cell*, *24*(1), 13-23. doi: 10.1016/j.molcel.2006.08.006
- Arber, S., Barbayannis, F. A., Hanser, H., Schneider, C., Stanyon, C. A., Bernard, O., & Caroni, P. (1998). Regulation of actin dynamics through phosphorylation of cofilin by LIM-kinase. *Nature*, *393*(6687), 805-809. doi: 10.1038/31729
- Bamburg, J. R., McGough, A., & Ono, S. (1999). Putting a new twist on actin: ADF/cofilins modulate actin dynamics. *Trends Cell Biol*, *9*(9), 364-370.
- Berro, J., Michelot, A., Blanchoin, L., Kovar, D. R., & Martiel, J. L. (2007). Attachment conditions control actin filament buckling and the production of forces. *Biophys J*, *92*(7), 2546-2558. doi: 10.1529/biophysj.106.094672
- Berro, J., Sirotkin, V., & Pollard, T. D. (2010). Mathematical modeling of endocytic actin patch kinetics in fission yeast: disassembly requires release of actin filament fragments. *Mol Biol Cell*, *21*(16), 2905-2915. doi: 10.1091/mbc.E10-06-0494
- Bieling, P., Li, T. D., Weichsel, J., McGorty, R., Jreij, P., Huang, B., . . . Mullins, R. D. (2016). Force Feedback Controls Motor Activity and Mechanical Properties of Self-Assembling Branched Actin Networks. *Cell*, *164*(1-2), 115-127. doi: 10.1016/j.cell.2015.11.057
- Blanchoin, L., Boujemaa-Paterski, R., Sykes, C., & Plastino, J. (2014). Actin dynamics, architecture, and mechanics in cell motility. *Physiol Rev*, *94*(1), 235-263. doi: 10.1152/physrev.00018.2013
- Blanchoin, L., & Pollard, T. D. (1999). Mechanism of interaction of Acanthamoeba actophorin (ADF/Cofilin) with actin filaments. *J Biol Chem*, *274*(22), 15538-15546. doi: 10.1074/jbc.274.22.15538
- Blanchoin, L., & Pollard, T. D. (2002). Hydrolysis of ATP by polymerized actin depends on the bound divalent cation but not profilin. *Biochemistry*, *41*(2), 597-602.
- Boczkowska, M., Rebowski, G., & Dominguez, R. (2013). Glia maturation factor (GMF) interacts with Arp2/3 complex in a nucleotide state-dependent manner. *J Biol Chem*, *288*(36), 25683-25688. doi: 10.1074/jbc.C113.493338
- Breitsprecher, D., & Goode, B. L. (2013). Formins at a glance. *J Cell Sci*, *126*(Pt 1), 1-7. doi: 10.1242/jcs.107250
- Bretscher, A. (1981). Fimbrin is a cytoskeletal protein that crosslinks F-actin in vitro. *Proc Natl Acad Sci U S A*, *78*(11), 6849-6853. doi: 10.1073/pnas.78.11.6849
- Cao, W., Goodarzi, J. P., & De La Cruz, E. M. (2006). Energetics and kinetics of cooperative cofilin-actin filament interactions. *J Mol Biol*, *361*(2), 257-267. doi: 10.1016/j.jmb.2006.06.019
- Carlier, M. F., & Pantaloni, D. (1986). Direct evidence for ADP-Pi-F-actin as the major intermediate in ATP-actin polymerization. Rate of dissociation of Pi from actin filaments. *Biochemistry*, *25*(24), 7789-7792.

- Castaneda, N., Zheng, T., Rivera-Jacquez, H. J., Lee, H. J., Hyun, J., Balaeff, A., . . . Kang, H. (2018). Cations Modulate Actin Bundle Mechanics, Assembly Dynamics, and Structure. *J Phys Chem B*, *122*(14), 3826-3835. doi: 10.1021/acs.jpcc.8b00663
- Chen, Q., Courtemanche, N., & Pollard, T. D. (2015). Aip1 promotes actin filament severing by cofilin and regulates constriction of the cytokinetic contractile ring. *J Biol Chem*, *290*(4), 2289-2300. doi: 10.1074/jbc.M114.612978
- Chhabra, E. S., & Higgs, H. N. (2006). INF2 Is a WASP homology 2 motif-containing formin that severs actin filaments and accelerates both polymerization and depolymerization. *J Biol Chem*, *281*(36), 26754-26767. doi: 10.1074/jbc.M604666200
- Chu, J. W., & Voth, G. A. (2005). Allostery of actin filaments: molecular dynamics simulations and coarse-grained analysis. *Proc Natl Acad Sci U S A*, *102*(37), 13111-13116. doi: 10.1073/pnas.0503732102
- Chu, J. W., & Voth, G. A. (2006). Coarse-grained modeling of the actin filament derived from atomistic-scale simulations. *Biophys J*, *90*(5), 1572-1582. doi: 10.1529/biophysj.105.073924
- Cooper, J. A., Walker, S. B., & Pollard, T. D. (1983). Pyrene actin: documentation of the validity of a sensitive assay for actin polymerization. *J Muscle Res Cell Motil*, *4*(2), 253-262. doi: 10.1007/BF00712034
- Courtemanche, N., & Pollard, T. D. (2013). Interaction of profilin with the barbed end of actin filaments. *Biochemistry*, *52*(37), 6456-6466. doi: 10.1021/bi400682n
- De La Cruz, E. M. (2005). Cofilin binding to muscle and non-muscle actin filaments: isoform-dependent cooperative interactions. *J Mol Biol*, *346*(2), 557-564. doi: 10.1016/j.jmb.2004.11.065
- De La Cruz, E. M., & Gardel, M. L. (2015). Actin Mechanics and Fragmentation. *J Biol Chem*, *290*(28), 17137-17144. doi: 10.1074/jbc.R115.636472
- De La Cruz, E. M., Martiel, J. L., & Blanchoin, L. (2015). Mechanical heterogeneity favors fragmentation of strained actin filaments. *Biophys J*, *108*(9), 2270-2281. doi: 10.1016/j.bpj.2015.03.058
- De La Cruz, E. M., & Ostap, E. M. (2004). Relating biochemistry and function in the myosin superfamily. *Current Opinion in Cell Biology*, *16*, 61-67. doi: 10.1016/j.ceb.2003.11.011
- De La Cruz, E. M., Roland, J., McCullough, B. R., Blanchoin, L., & Martiel, J. L. (2010). Origin of twist-bend coupling in actin filaments. *Biophys J*, *99*(6), 1852-1860. doi: 10.1016/j.bpj.2010.07.009
- De La Cruz, E. M., & Sept, D. (2010). The kinetics of cooperative cofilin binding reveals two states of the cofilin-actin filament. *Biophys J*, *98*(9), 1893-1901. doi: 10.1016/j.bpj.2010.01.023
- Dominguez, R., & Holmes, K. C. (2011). Actin structure and function. *Annu Rev Biophys*, *40*, 169-186. doi: 10.1146/annurev-biophys-042910-155359
- Dudko, O. K., Hummer, G., & Szabo, A. (2006). Intrinsic rates and activation free energies from single-molecule pulling experiments. *Phys Rev Lett*, *96*(10), 108101. doi: 10.1103/PhysRevLett.96.108101
- Elam, W. A., Cao, W., Kang, H., Huehn, A., Hocky, G. M., Prochniewicz, E., . . . De La Cruz, E. M. (2017). Phosphomimetic S3D cofilin binds but only weakly severs actin filaments. *J Biol Chem*, *292*(48), 19565-19579. doi: 10.1074/jbc.M117.808378
- Elam, W. A., Kang, H., & De la Cruz, E. M. (2013). Biophysics of actin filament severing by cofilin. *FEBS Lett*, *587*(8), 1215-1219. doi: 10.1016/j.febslet.2013.01.062
- Fan, J., Saunders, M. G., Haddadian, E. J., Freed, K. F., De La Cruz, E. M., & Voth, G. A. (2013). Molecular origins of cofilin-linked changes in actin filament mechanics. *J Mol Biol*, *425*(7), 1225-1240. doi: 10.1016/j.jmb.2013.01.020

- Fan, J., Saunders, M. G., & Voth, G. A. (2012). Coarse-graining provides insights on the essential nature of heterogeneity in actin filaments. *Biophys J*, *103*(6), 1334-1342. doi: 10.1016/j.bpj.2012.08.029
- Frieden, C. (1983). Polymerization of actin: mechanism of the Mg<sup>2+</sup>-induced process at pH 8 and 20 degrees C. *Proc Natl Acad Sci U S A*, *80*(21), 6513-6517. doi: 10.1073/pnas.80.21.6513
- Fujiwara, I., Vavylonis, D., & Pollard, T. D. (2007). Polymerization kinetics of ADP- and ADP-Pi-actin determined by fluorescence microscopy. *Proc Natl Acad Sci U S A*, *104*(21), 8827-8832. doi: 10.1073/pnas.0702510104
- Galkin, V. E., Orlova, A., Kudryashov, D. S., Solodukhin, A., Reisler, E., Schroder, G. F., & Egelman, E. H. (2011). Remodeling of actin filaments by ADF/cofilin proteins. *Proc Natl Acad Sci U S A*, *108*(51), 20568-20572. doi: 10.1073/pnas.1110109108
- Galkin, V. E., Orlova, A., Vos, M. R., Schroder, G. F., & Egelman, E. H. (2015). Near-atomic resolution for one state of F-actin. *Structure*, *23*(1), 173-182. doi: 10.1016/j.str.2014.11.006
- Galkin, Vitold E., Orlova, A., Vos, Matthijn R., Schröder, Gunnar F., & Egelman, Edward H. (2015). Near-Atomic Resolution for One State of F-Actin. *Structure*, *23*(1), 173-182. doi: <https://doi.org/10.1016/j.str.2014.11.006>
- Gandhi, M., Smith, B. A., Bovellan, M., Paavilainen, V., Daugherty-Clarke, K., Gelles, J., . . . Goode, B. L. (2010). GMF is a cofilin homolog that binds Arp2/3 complex to stimulate filament debranching and inhibit actin nucleation. *Curr Biol*, *20*(9), 861-867. doi: 10.1016/j.cub.2010.03.026
- Gittes, F., Mickey, B., Nettleton, J., & Howard, J. (1993). Flexural rigidity of microtubules and actin filaments measured from thermal fluctuations in shape. *J Cell Biol*, *120*(4), 923-934. doi: 10.1083/jcb.120.4.923
- Goode, B. L., Eskin, J. A., & Wendland, B. (2015). Actin and endocytosis in budding yeast. *Genetics*, *199*(2), 315-358. doi: 10.1534/genetics.112.145540
- Gressin, L., Guillotin, A., Guerin, C., Blanchoin, L., & Michelot, A. (2015). Architecture dependence of actin filament network disassembly. *Curr Biol*, *25*(11), 1437-1447. doi: 10.1016/j.cub.2015.04.011
- Grintsevich, E. E., Ge, P., Sawaya, M. R., Yesilyurt, H. G., Terman, J. R., Zhou, Z. H., & Reisler, E. (2017). Catastrophic disassembly of actin filaments via Mical-mediated oxidation. *Nat Commun*, *8*(1), 2183. doi: 10.1038/s41467-017-02357-8
- Grintsevich, E. E., Yesilyurt, H. G., Rich, S. K., Hung, R. J., Terman, J. R., & Reisler, E. (2016). F-actin dismantling through a redox-driven synergy between Mical and cofilin. *Nat Cell Biol*, *18*(8), 876-885. doi: 10.1038/ncb3390
- Hayakawa, K., Sakakibara, S., Sokabe, M., & Tatsumi, H. (2014). Single-molecule imaging and kinetic analysis of cooperative cofilin-actin filament interactions. *Proc Natl Acad Sci U S A*, *111*(27), 9810-9815. doi: 10.1073/pnas.1321451111
- Hayakawa, K., Tatsumi, H., & Sokabe, M. (2008). Actin stress fibers transmit and focus force to activate mechanosensitive channels. *J Cell Sci*, *121*(Pt 4), 496-503. doi: 10.1242/jcs.022053
- Hayakawa, K., Tatsumi, H., & Sokabe, M. (2011). Actin filaments function as a tension sensor by tension-dependent binding of cofilin to the filament. *J Cell Biol*, *195*(5), 721-727. doi: 10.1083/jcb.201102039
- Hocky, G. M., Baker, J. L., Bradley, M. J., Sinitskiy, A. V., De La Cruz, E. M., & Voth, G. A. (2016). Cations Stiffen Actin Filaments by Adhering a Key Structural Element to Adjacent Subunits. *J Phys Chem B*, *120*(20), 4558-4567. doi: 10.1021/acs.jpccb.6b02741

- Howard, J. (2001). *Mechanics of motor proteins and the cytoskeleton*. Sunderland, Mass.: Sinauer Associates, Publishers.
- Huang, D. L., Bax, N. A., Buckley, C. D., Weis, W. I., & Dunn, A. R. (2017). Vinculin forms a directionally asymmetric catch bond with F-actin. *Science*, *357*(6352), 703-706. doi: 10.1126/science.aan2556
- Huehn, A., Cao, W., Elam, W. A., Liu, X., De La Cruz, E. M., & Sindelar, C. V. (2018). The actin filament twist changes abruptly at boundaries between bare and cofilin-decorated segments. *J Biol Chem*, *293*(15), 5377-5383. doi: 10.1074/jbc.AC118.001843
- Hung, R. J., Pak, C. W., & Terman, J. R. (2011). Direct redox regulation of F-actin assembly and disassembly by Mical. *Science*, *334*(6063), 1710-1713. doi: 10.1126/science.1211956
- Huxley, H. E. (1963). Electron Microscope Studies on the Structure of Natural and Synthetic Protein Filaments from Striated Muscle. *J Mol Biol*, *7*, 281-308.
- Isambert, H., Venier, P., Maggs, A. C., Fattoum, A., Kassab, R., Pantaloni, D., & Carlier, M. F. (1995). Flexibility of actin filaments derived from thermal fluctuations. Effect of bound nucleotide, phalloidin, and muscle regulatory proteins. *J Biol Chem*, *270*(19), 11437-11444. doi: 10.1074/jbc.270.19.11437
- Janmey, P. A., & Stossel, T. P. (1989). Gelsolin-polyphosphoinositide interaction. Full expression of gelsolin-inhibiting function by polyphosphoinositides in vesicular form and inactivation by dilution, aggregation, or masking of the inositol head group. *J Biol Chem*, *264*(9), 4825-4831.
- Jegou, A., Carlier, M. F., & Romet-Lemonne, G. (2013). Formin mDia1 senses and generates mechanical forces on actin filaments. *Nat Commun*, *4*, 1883. doi: 10.1038/ncomms2888
- Kang, H., Bradley, M. J., Cao, W., Zhou, K., Grintsevich, E. E., Michelot, A., . . . De La Cruz, E. M. (2014). Site-specific cation release drives actin filament severing by vertebrate cofilin. *Proc Natl Acad Sci U S A*, *111*(50), 17821-17826. doi: 10.1073/pnas.1413397111
- Kang, H., Bradley, M. J., McCullough, B. R., Pierre, A., Grintsevich, E. E., Reisler, E., & De La Cruz, E. M. (2012). Identification of cation-binding sites on actin that drive polymerization and modulate bending stiffness. *Proc Natl Acad Sci U S A*, *109*(42), 16923-16927. doi: 10.1073/pnas.1211078109
- Kim, J. I., Kwon, J., Baek, I., Park, H. S., & Na, S. (2015). Cofilin reduces the mechanical properties of actin filaments: approach with coarse-grained methods. *Phys Chem Chem Phys*, *17*(12), 8148-8158. doi: 10.1039/c4cp06100d
- Kim, K. Y., Kawamoto, S., Bao, J., Sellers, J. R., & Adelstein, R. S. (2008). The B2 alternatively spliced isoform of nonmuscle myosin II-B lacks actin-activated MgATPase activity and in vitro motility. *Biochem Biophys Res Commun*, *369*(1), 124-134. doi: 10.1016/j.bbrc.2007.11.108
- Kinosian, H. J., Newman, J., Lincoln, B., Selden, L. A., Gershman, L. C., & Estes, J. E. (1998). Ca<sup>2+</sup> regulation of gelsolin activity: binding and severing of F-actin. *Biophys J*, *75*(6), 3101-3109. doi: 10.1016/S0006-3495(98)77751-3
- Kinosian, H. J., Selden, L. A., Estes, J. E., & Gershman, L. C. (1993). Actin filament annealing in the presence of ATP and phalloidin. *Biochemistry*, *32*(46), 12353-12357. doi: 10.1021/bi00097a011
- Kudryashov, D. S., Galkin, V. E., Orlova, A., Phan, M., Egelman, E. H., & Reisler, E. (2006). Cofilin cross-bridges adjacent actin protomers and replaces part of the longitudinal F-actin interface. *J Mol Biol*, *358*(3), 785-797. doi: 10.1016/j.jmb.2006.02.029
- Landau, L. D., Lifshits, E. M., Kosevich, A. d. M., & Pitaevskii, L. P. (1986). *Theory of elasticity* (3rd English ed.). Oxford Oxfordshire ; New York: Pergamon Press.

- Lee, B. C., Peterfi, Z., Hoffmann, F. W., Moore, R. E., Kaya, A., Avanesov, A., . . . Gladyshev, V. N. (2013). MsrB1 and MICALs regulate actin assembly and macrophage function via reversible stereoselective methionine oxidation. *Mol Cell*, *51*(3), 397-404. doi: 10.1016/j.molcel.2013.06.019
- Linsmeier, I., Banerjee, S., Oakes, P. W., Jung, W., Kim, T., & Murrell, M. P. (2016). Disordered actomyosin networks are sufficient to produce cooperative and telescopic contractility. *Nat Commun*, *7*, 12615. doi: 10.1038/ncomms12615
- Lohman, T. M., & Mascotti, D. P. (1992). Thermodynamics of ligand-nucleic acid interactions. *Methods Enzymol*, *212*, 400-424.
- Lyman, E., Pfaendtner, J., & Voth, G. A. (2008). Systematic multiscale parameterization of heterogeneous elastic network models of proteins. *Biophys J*, *95*(9), 4183-4192. doi: 10.1529/biophysj.108.139733
- Manhart, A., Icheva, T. A., Guerin, C., Klar, T., Boujemaa-Paterski, R., Thery, M., . . . Mogilner, A. (2019). Quantitative regulation of the dynamic steady state of actin networks. *Elife*, *8*. doi: 10.7554/eLife.42413
- Mattila, P. K., & Lappalainen, P. (2008). Filopodia: molecular architecture and cellular functions. *Nat Rev Mol Cell Biol*, *9*(6), 446-454. doi: 10.1038/nrm2406
- McCullough, B. R., Blanchoin, L., Martiel, J. L., & De la Cruz, E. M. (2008). Cofilin increases the bending flexibility of actin filaments: implications for severing and cell mechanics. *J Mol Biol*, *381*(3), 550-558. doi: 10.1016/j.jmb.2008.05.055
- McCullough, B. R., Grintsevich, E. E., Chen, C. K., Kang, H., Hutchison, A. L., Henn, A., . . . De La Cruz, E. M. (2011). Cofilin-linked changes in actin filament flexibility promote severing. *Biophys J*, *101*(1), 151-159. doi: 10.1016/j.bpj.2011.05.049
- McGhee, J. D., & von Hippel, P. H. (1974). Theoretical aspects of DNA-protein interactions: cooperative and non-co-operative binding of large ligands to a one-dimensional homogeneous lattice. *J Mol Biol*, *86*(2), 469-489. doi: 10.1016/0022-2836(74)90031-x
- McGough, A., Chiu, W., & Way, M. (1998). Determination of the gelsolin binding site on F-actin: implications for severing and capping. *Biophys J*, *74*(2 Pt 1), 764-772. doi: 10.1016/S0006-3495(98)74001-9
- McGough, A., Pope, B., Chiu, W., & Weeds, A. (1997). Cofilin changes the twist of F-actin: implications for actin filament dynamics and cellular function. *J Cell Biol*, *138*(4), 771-781. doi: 10.1083/jcb.138.4.771
- Medeiros, N. A., Burnette, D. T., & Forscher, P. (2006). Myosin II functions in actin-bundle turnover in neuronal growth cones. *Nat Cell Biol*, *8*(3), 215-226. doi: 10.1038/ncb1367
- Miyashita, O., Onuchic, J. N., & Wolynes, P. G. (2003). Nonlinear elasticity, proteinquakes, and the energy landscapes of functional transitions in proteins. *Proceedings of the National Academy of Sciences*, *100*(22), 12570-12575. doi: 10.1073/pnas.2135471100
- Mizuno, H., Higashida, C., Yuan, Y., Ishizaki, T., Narumiya, S., & Watanabe, N. (2011). Rotational movement of the formin mDia1 along the double helical strand of an actin filament. *Science*, *331*(6013), 80-83. doi: 10.1126/science.1197692
- Mizuno, H., Tanaka, K., Yamashiro, S., Narita, A., & Watanabe, N. (2018). Helical rotation of the diaphanous-related formin mDia1 generates actin filaments resistant to cofilin. *Proceedings of the National Academy of Sciences of the United States of America*, *115*(22), E5000-E5007. doi: 10.1073/pnas.1803415115
- Mizuno, H., & Watanabe, N. (2012). mDia1 and formins: screw cap of the actin filament. *Biophysics (Nagoya-shi)*, *8*, 95-102. doi: 10.2142/biophysics.8.95

- Mogilner, A., & Oster, G. (2003). Force generation by actin polymerization II: the elastic ratchet and tethered filaments. *Biophys J*, *84*(3), 1591-1605. doi: 10.1016/S0006-3495(03)74969-8
- Moriyama, K., Iida, K., & Yahara, I. (1996). Phosphorylation of Ser-3 of cofilin regulates its essential function on actin. *Genes Cells*, *1*(1), 73-86. doi: 10.1046/j.1365-2443.1996.05005.x
- Moseley, J. B., Okada, K., Balcer, H. I., Kovar, D. R., Pollard, T. D., & Goode, B. L. (2006). Twinfilin is an actin-filament-severing protein and promotes rapid turnover of actin structures in vivo. *J Cell Sci*, *119*(Pt 8), 1547-1557. doi: 10.1242/jcs.02860
- Muhlrad, A., Kudryashov, D., Michael Peyser, Y., Bobkov, A. A., Almo, S. C., & Reisler, E. (2004). Cofilin induced conformational changes in F-actin expose subdomain 2 to proteolysis. *J Mol Biol*, *342*(5), 1559-1567. doi: 10.1016/j.jmb.2004.08.010
- Muhlrad, A., Pavlov, D., Peyser, Y. M., & Reisler, E. (2006). Inorganic phosphate regulates the binding of cofilin to actin filaments. *FEBS J*, *273*(7), 1488-1496. doi: 10.1111/j.1742-4658.2006.05169.x
- Murrell, M. P., & Gardel, M. L. (2012). F-actin buckling coordinates contractility and severing in a biomimetic actomyosin cortex. *Proc Natl Acad Sci U S A*, *109*(51), 20820-20825. doi: 10.1073/pnas.1214753109
- Ngo, K. X., Kodera, N., Katayama, E., Ando, T., & Uyeda, T. Q. (2015). Cofilin-induced unidirectional cooperative conformational changes in actin filaments revealed by high-speed atomic force microscopy. *Elife*, *4*, 1-22. doi: 10.7554/eLife.04806
- Oda, T., Iwasa, M., Aihara, T., Maeda, Y., & Narita, A. (2009). The nature of the globular- to fibrous-actin transition. *Nature*, *457*(7228), 441-445. doi: 10.1038/nature07685
- Pfaendtner, J., De La Cruz, E. M., & Voth, G. A. (2010). Actin filament remodeling by actin depolymerization factor/cofilin. *Proc Natl Acad Sci U S A*, *107*(16), 7299-7304. doi: 10.1073/pnas.0911675107
- Pfaendtner, J., Volkmann, N., Hanein, D., Dalhaimer, P., Pollard, T. D., & Voth, G. A. (2012). Key structural features of the actin filament Arp2/3 complex branch junction revealed by molecular simulation. *J Mol Biol*, *416*(1), 148-161. doi: 10.1016/j.jmb.2011.12.025
- Phillips, J. C., Braun, R., Wang, W., Gumbart, J., Tajkhorshid, E., Villa, E., . . . Schulten, K. (2005). Scalable molecular dynamics with NAMD. *Journal of Computational Chemistry*, *26*(16), 1781-1802. doi: 10.1002/jcc.20289
- Pollard, T. D. (2016). Actin and Actin-Binding Proteins. *Cold Spring Harb Perspect Biol*, *8*(8), a018226. doi: 10.1101/cshperspect.a018226
- Pollard, T. D., & Borisy, G. G. (2003). Cellular motility driven by assembly and disassembly of actin filaments. *Cell*, *112*(4), 453-465. doi: 10.1016/S0092-8674(03)00120-X
- Pollard, T. D., & Cooper, J. A. (2009). Actin, a central player in cell shape and movement. *Science*, *326*(5957), 1208-1212. doi: 10.1126/science.1175862
- Pope, B. J., Gonsior, S. M., Yeoh, S., McGough, A., & Weeds, A. G. (2000). Uncoupling actin filament fragmentation by cofilin from increased subunit turnover. *J Mol Biol*, *298*(4), 649-661. doi: 10.1006/jmbi.2000.3688
- Prochniewicz, E., Janson, N., Thomas, D. D., & De La Cruz, E. M. (2005). Cofilin increases the torsional flexibility and dynamics of actin filaments. *J Mol Biol*, *353*(5), 990-1000. doi: 10.1016/j.jmb.2005.09.021
- Razinia, Z., Makela, T., Ylanne, J., & Calderwood, D. A. (2012). Filamins in mechanosensing and signaling. *Annu Rev Biophys*, *41*, 227-246. doi: 10.1146/annurev-biophys-050511-102252

- Risca, V. I., Wang, E. B., Chaudhuri, O., Chia, J. J., Geissler, P. L., & Fletcher, D. A. (2012). Actin filament curvature biases branching direction. *Proc Natl Acad Sci U S A*, *109*(8), 2913-2918. doi: 10.1073/pnas.1114292109
- Rottner, K., Faix, J., Bogdan, S., Linder, S., & Kerkhoff, E. (2017). Actin assembly mechanisms at a glance. *J Cell Sci*, *130*(20), 3427-3435. doi: 10.1242/jcs.206433
- Rouayrenc, J. F., & Travers, F. (1981). The first step in the polymerisation of actin. *Eur J Biochem*, *116*(1), 73-77.
- Rould, M. A., Wan, Q., Joel, P. B., Lowey, S., & Trybus, K. M. (2006). Crystal structures of expressed non-polymerizable monomeric actin in the ADP and ATP states. *J Biol Chem*, *281*(42), 31909-31919. doi: 10.1074/jbc.M601973200
- Saunders, M. G., & Voth, G. A. (2012). Comparison between actin filament models: coarse-graining reveals essential differences. *Structure*, *20*(4), 641-653. doi: 10.1016/j.str.2012.02.008
- Schmoller, K. M., Niedermayer, T., Zensen, C., Wurm, C., & Bausch, A. R. (2011). Fragmentation is crucial for the steady-state dynamics of actin filaments. *Biophys J*, *101*(4), 803-808. doi: 10.1016/j.bpj.2011.07.009
- Schramm, A. C., Hocky, G. M., Voth, G. A., Blanchoin, L., Martiel, J. L., & De La Cruz, E. M. (2017). Actin Filament Strain Promotes Severing and Cofilin Dissociation. *Biophys J*, *112*(12), 2624-2633. doi: 10.1016/j.bpj.2017.05.016
- Sept, D., & McCammon, J. A. (2001). Thermodynamics and kinetics of actin filament nucleation. *Biophys J*, *81*(2), 667-674. doi: 10.1016/S0006-3495(01)75731-1
- Sjoblom, B., Salmazo, A., & Djinovic-Carugo, K. (2008). Alpha-actinin structure and regulation. *Cell Mol Life Sci*, *65*(17), 2688-2701. doi: 10.1007/s00018-008-8080-8
- Suarez, C., Roland, J., Boujemaa-Paterski, R., Kang, H., McCullough, B. R., Reymann, A. C., . . . Blanchoin, L. (2011). Cofilin tunes the nucleotide state of actin filaments and severs at bare and decorated segment boundaries. *Curr Biol*, *21*(10), 862-868. doi: 10.1016/j.cub.2011.03.064
- Sugawara, E., & Nikaido, H. (2014). Properties of AdeABC and AdeIJK efflux systems of *Acinetobacter baumannii* compared with those of the AcrAB-TolC system of *Escherichia coli*. *Antimicrob Agents Chemother*, *58*(12), 7250-7257. doi: 10.1128/AAC.03728-14
- Tanaka, K., Takeda, S., Mitsuoka, K., Oda, T., Kimura-Sakiyama, C., Maeda, Y., & Narita, A. (2018). Structural basis for cofilin binding and actin filament disassembly. *Nat Commun*, *9*(1), 1860. doi: 10.1038/s41467-018-04290-w
- Tang, J. X., & Janmey, P. A. (1996). The polyelectrolyte nature of F-actin and the mechanism of actin bundle formation. *J Biol Chem*, *271*(15), 8556-8563. doi: 10.1074/jbc.271.15.8556
- Tsuda, Y., Yasutake, H., Ishijima, A., & Yanagida, T. (1996). Torsional rigidity of single actin filaments and actin-actin bond breaking force under torsion measured directly by in vitro micromanipulation. *Proc Natl Acad Sci U S A*, *93*(23), 12937-12942. doi: 10.1073/pnas.93.23.12937
- Umeki, N., Hirose, K., & Uyeda, T. Q. (2016). Cofilin-induced cooperative conformational changes of actin subunits revealed using cofilin-actin fusion protein. *Sci Rep*, *6*, 20406. doi: 10.1038/srep20406
- Van Goor, D., Hyland, C., Schaefer, A. W., & Forscher, P. (2012). The role of actin turnover in retrograde actin network flow in neuronal growth cones. *PLoS One*, *7*(2), e30959. doi: 10.1371/journal.pone.0030959
- Vavylonis, D., Yang, Q., & O'Shaughnessy, B. (2005). Actin polymerization kinetics, cap structure, and fluctuations. *Proc Natl Acad Sci U S A*, *102*(24), 8543-8548. doi: 10.1073/pnas.0501435102

- Vignjevic, D., Kojima, S., Aratyn, Y., Danciu, O., Svitkina, T., & Borisy, G. G. (2006). Role of fascin in filopodial protrusion. *J Cell Biol*, *174*(6), 863-875. doi: 10.1083/jcb.200603013
- Vogel, S. K., Petrasek, Z., Heinemann, F., & Schwille, P. (2013). Myosin motors fragment and compact membrane-bound actin filaments. *Elife*, *2*, e00116. doi: 10.7554/eLife.00116
- Wear, M. A., Yamashita, A., Kim, K., Maeda, Y., & Cooper, J. A. (2003). How capping protein binds the barbed end of the actin filament. *Curr Biol*, *13*(17), 1531-1537.
- Wegner, A. (1976). Head to tail polymerization of actin. *J Mol Biol*, *108*(1), 139-150.
- Wilson, C. A., Tsuchida, M. A., Allen, G. M., Barnhart, E. L., Applegate, K. T., Yam, P. T., . . . Theriot, J. A. (2010). Myosin II contributes to cell-scale actin network treadmilling through network disassembly. *Nature*, *465*(7296), 373-377. doi: 10.1038/nature08994
- Wilson, S. D. R., & Hulme, A. (1983). The Effect of Bubbles Attached to an Electrode on Electrical Resistance and Dissolved Gas Concentration. *Proceedings of the Royal Society A: Mathematical, Physical and Engineering Sciences*, *387*(1792), 133-146. doi: 10.1098/rspa.1983.0054
- Wioland, H., Guichard, B., Senju, Y., Myram, S., Lappalainen, P., Jegou, A., & Romet-Lemonne, G. (2017). ADF/Cofilin Accelerates Actin Dynamics by Severing Filaments and Promoting Their Depolymerization at Both Ends. *Curr Biol*, *27*(13), 1956-1967 e1957. doi: 10.1016/j.cub.2017.05.048
- Wioland, H., Jegou, A., & Romet-Lemonne, G. (2019a). Torsional stress generated by ADF/cofilin on cross-linked actin filaments boosts their severing. *Proc Natl Acad Sci U S A*, *116*(7), 2595-2602. doi: 10.1073/pnas.1812053116
- Wioland, H., Jegou, A., & Romet-Lemonne, G. (2019b). Torsional stress generated by ADF/cofilin on cross-linked actin filaments boosts their severing. *Proc Natl Acad Sci U S A*. doi: 10.1073/pnas.1812053116
- Witke, W. (2004). The role of profilin complexes in cell motility and other cellular processes. *Trends Cell Biol*, *14*(8), 461-469. doi: 10.1016/j.tcb.2004.07.003
- Yamamoto, K., Pardee, J. D., Reidler, J., Stryer, L., & Spudich, J. A. (1982). Mechanism of interaction of Dictyostelium severin with actin filaments. *J Cell Biol*, *95*(3), 711-719. doi: 10.1083/jcb.95.3.711
- Yang, N., Higuchi, O., Ohashi, K., Nagata, K., Wada, A., Kangawa, K., . . . Mizuno, K. (1998). Cofilin phosphorylation by LIM-kinase 1 and its role in Rac-mediated actin reorganization. *Nature*, *393*(6687), 809-812. doi: 10.1038/31735
- Yasuda, R., Miyata, H., & Kinoshita, K., Jr. (1996). Direct measurement of the torsional rigidity of single actin filaments. *J Mol Biol*, *263*(2), 227-236. doi: 10.1006/jmbi.1996.0571
- Yogurtcu, O. N., Kim, J. S., & Sun, S. X. (2012). A mechanochemical model of actin filaments. *Biophys J*, *103*(4), 719-727. doi: 10.1016/j.bpj.2012.07.020
- Zhang, X. F., Ajeti, V., Tsai, N., Fereydooni, A., Burns, W., Murrell, M., . . . Forscher, P. (2019). Regulation of axon growth by myosin II-dependent mechanocatalysis of cofilin activity. *J Cell Biol*, *218*(7), 2329-2349. doi: 10.1083/jcb.201810054